UNIVERSITY OF OKLAHOMA
GRADUATE COLLEGE

HARNESSING NATURAL HISTORY COLLECTIONS TO TRACK MAMMALIAN RESPONSES TO GLOBAL CHANGE IN THE ANTHROPOCENE

A DISSERTATION
SUBMITTED TO THE GRADUATE FACULTY
in partial fulfillment of the requirements for the
Degree of
DOCTOR OF PHILOSOPHY

By
MIRANDA KALI THERIOT
Norman, Oklahoma
2026

Downloaded from SHAREOK. Persistent Handle URL: https://hdl.handle.net/11244/342438

HARNESSING NATURAL HISTORY COLLECTIONS TO TRACK MAMMALIAN RESPONSES TO GLOBAL CHANGE IN THE ANTHROPOCENE

A DISSERTATION APPROVED FOR THE
SCHOOL OF BIOLOGICAL SCIENCES

BY THE COMMITTEE CONSISTING OF

Dr. Hayley Lanier, Chair

Dr. Daniel Becker

Dr. Michael Kaspari

Dr. Jeffrey Kelly

Dr. Jacqueline Lungmus

©Copyright by MIRANDA KALI THERIOT 2026
All Rights Reserved.

It takes a village to produce a dissertation, and properly thanking all the people who had some part in this could be its own dissertation. For the sake of brevity, I will content myself with extending especial gratitude to:

My advisor, Hayley, for her unwavering dedication and optimism through the many phases and seasons of these past six years.

My former advisor, Link Olson, for impressing upon me the importance of detailed rigor, repeatability, and the proper use of en and em dashes.

My committee, for giving me feedback, ideas, and patience.

My labmates—past, present, and honorary—for laughing at my goofs and shaping me into a better mentor, scientist, and friend.

The innumerable contributors and stewards of natural history collections, without whom this work would not be possible.

My high school sciences teachers, for pushing us small-town kids to aim big.

My family, for keeping my academic dreams afloat and embracing my deep love for critters and creatures, especially the weird ones.

Finally, Duncan, my best friend and partner in life.

TABLE OF CONTENTS

TABLE OF CONTENTS v
LIST OF TABLES viii
LIST OF FIGURES xiii
ABSTRACT xiv
INTRODUCTION 1
CHAPTER 1 5
Abstract 5
Introduction 5
Materials and methods 7
Specimens and measurements 7
Age determination 8
Other predictors of size: predicted harvest and growing season conditions 9
Statistical analyses 10
Results 12
Individual age and skull size 12
Age is a significant predictor of size variation 12
Skull size increases nonlinearly with age 13
Change in mean size and the proportion of younger individuals over time 15
Discussion 16
Shifts in age structure influence body-size changes 17
Age structure shifts as a response to climate change 18
The feasibility of testing for age effects 19
Implications for studying responses to global change 19
References 21
Supplementary Material 26
CHAPTER 2 59
Abstract 59
Introduction 59
Materials and Methods 62
Specimens and skull measurements 62
Hair sampling 63
Stable isotope analysis 63

Hair cortisol concentration 63
Broadscale body-side trends in cottontails 64
Statistical analyses 64
Results 65
Repeatability and PCA of cranial measurements 65
Size, stable isotopes, and stress 65
Body-size trends in three widespread, cottontail species 66
Discussion 67
Small mammals may compensate for nutrient dilution through forage selection 68
Despite potential buffers against nutrient dilution, declines in mean body size are range-wide 70
Future Directions 71
References 73
Supplementary Material 77
CHAPTER 3 97
Abstract 97
Introduction 97
Materials and Methods 99
Focal species 99
Specimen photography 99
Landmarking 100
Age determination in raccoons 100
Assigning habitat category 101
Statistical analyses 101
Results 102
Geography and climate 103
Urban versus rural habitat 105
Age 105
Discussion 109
No evidence for widespread domestication syndrome in urban mammals 109
Age distribution is a key component of morphological trends 110
Evolution and phenotypic plasticity 111
The untapped potential of natural history collections in urban ecology 111
Conclusions 111
References 113

Supplementary Material 118
CONCLUSION 142
REFERENCES 143

LIST OF TABLES

Chapter 1

Table 1 13

Chapter 1 Supplementary Material

Table S3.1 30
Table S3.2 30
Table S3.3 32
Table S3.4 32
Table S3.5 33
Table S3.6 34
Table S3.7 35
Table S3.8 35
Table S3.9 36
Table S3.10 36
Table S3.11 37
Table S3.12 38
Table S3.13 39
Table S3.14 39
Table S3.15 40
Table S3.16 41
Table S3.17 42
Table S3.18 42
Table S3.19 43
Table S3.20 44
Table S3.21 44
Table S3.22 45
Table S3.23 46
Table S3.24 46
Table S3.25 47
Table S3.26 48
Table S3.27 49
Table S3.28 50

Table S3.29 51
Table S3.30 51
Table S3.31 52
Table S3.32 52
Table S3.33 53
Table S3.34 54
Table S3.35 54
Table S3.36 55
Table S3.37 55
Table S3.38 56
Table S3.39 56
Table S3.40 57

Chapter 2

Table 1 65
Table 2 66
Table 3 67
Table 4 68

Chapter 2 Supplementary Material

Table S1 79
Table S2 80
Table S3 81
Table S4 81
Table S5 82
Table S6 82
Table S7 83
Table S8 83
Table S9 84
Table S10 84
Table S11 85
Table S12 85
Table S13 86

Table S14 86
Table S15 87
Table S16 87
Table S17 88
Table S18 88
Table S19 88
Table S20 89
Table S21 89
Table S22 90
Table S23 90
Table S24 91
Table S25 91
Table S26 92
Table S27 92
Table S28 93
Table S29 93
Table S30 94
Table S31 94
Table S32 95
Table S33 95
Table S34 95
Table S35 96
Table S36 96

Chapter 3

Table 1 101
Table 2 104

Chapter 3 Supplementary Material

Table S1 118
Table S2 125
Table S3 125
Table S4 125

Table S5 126
Table S6 126
Table S7 126
Table S8 127
Table S9 127
Table S10 127
Table S11 128
Table S12 128
Table S13 128
Table S14 131
Table S15 131
Table S16 132
Table S17 132
Table S18 133
Table S19 133
Table S20 134
Table S21 134
Table S22 135
Table S23 135
Table S24 136
Table S25 136
Table S26 137
Table S27 137
Table S28 137
Table S29 137
Table S30 138
Table S31 138
Table S32 138
Table S33 138
Table S34 138
Table S35 138
Table S36 139
Table S37 139

Table S38 139
Table S39 139
Table S40 139
Table S41 140
Table S42 140
Table S43 140

LIST OF FIGURES

Chapter 1

Figure 1 9
Figure 2 14
Figure 3 15
Figure 4 16

Chapter 1 Supplementary Material

Figure S3.1 29

Chapter 2

Figure 1 62
Figure 2 67
Figure 3 69
Figure 4 70

Chapter 2 Supplementary Material

Figure S1 77
Figure S2 79
Figure S3 80

Chapter 3

Figure 1 100
Figure 2 106
Figure 3 107
Figure 4 108

Chapter 3 Supplementary Material

Figure S1 120
Figure S2 121
Figure S3 130

ABSTRACT

In the current era of rapid global change—the Anthropocene—understanding and predicting the varied responses among wild animal populations hinges on identifying the drivers underlying these complex patterns. Morphological trends, particularly in body size, are a key facet of these patterns; size is linked to many aspects of physiology (maintaining body temperature, energy requirements, etc.), ecology (dietary niche, inter- and intraspecific interactions, etc.), and life history (litter size, growth and development, etc.) and can thus both mediate and signal the nature and pace of global-change responses. Moreover, morphological change can be readily assessed over broad spatial and temporal scales thanks to the wealth of biodiversity data stored in natural history collections. My dissertation leverages these robust datasets to evaluate mammalian responses to global change over space and time, with a focus on the effects of shifting population age structure, reduced diet quality, and urbanization. My first chapter shows that population age distribution—despite often being overlooked in mammal research due to the traditional assumption of constant adult size—is a key factor that can help us refine models of morphological variation and unlock insights into demographic responses to climate change. My second chapter demonstrates how multiple forms of specimen-derived data can be used to understand climate-driven reductions in diet quality, or nutrient dilution. Results suggest that small mammalian herbivores, such as cottontail rabbits, may have some ability to buffer against widespread nutrient dilution through diet or habitat selection, but this may be a limited stopgap, as museum data spanning over seventy years indicate range-wide declines in mean body length. Finally, my third chapter evaluates the potential for domestication syndrome—the suite of physical characteristics thought to coincide with close association with humans—among four common, urban-dwelling mammals. Findings indicate that there are no shared, domestication-like trends among these ecologically and taxonomically disparate species, emphasizing the importance of other aspects of responses to urbanization, like local environmental context and population age structure. This research provides further support for the multifaceted nature of body size and shape, targeting key contributors to variation that have not yet been extensively studied in mammals, and underscores the value of natural history collections in unraveling these nuanced trends to construct a more holistic understanding of global-change responses.

INTRODUCTION

Humans have direct and profound impacts on ecosystems worldwide, recognition of which has led to the proposal of a new geological epoch, the Anthropocene (Lewis and Maslin 2015; Crutzen and Stoermer 2021). This recent phase of Earth's history is characterized by accelerating increases in global mean temperatures, shifts in weather regimes, alterations to global nutrient cycles, and land use changes (Vitousek *et al.* 1997; LeBauer and Treseder 2008; van Vilet 2019; IPCC 2023). These interwoven and reinforcing threats are driving habitat loss and biodiversity decline (Jantz *et al.* 2015; Habibullah *et al.* 2022), which in turn directly and negatively affect human health and well-being, including in nutrition (IPCC 2023, Ter Haar *et al.* 2025) and the risk of emerging zoonoses (Keesing *et al.* 2010, IPCC 2023). Therefore, 21st century conservation efforts center on identifying and mitigating these effects of global change.

An essential component of preserving and stewarding healthy ecosystems into the future is tracking organismal responses to global change, which researchers broadly categorize into three main forms: move, adapt, or die. First, animals can respond to environmental change by moving away from advancing adverse conditions. Over recent decades, climate-driven range expansions and contractions have become increasingly common across taxa (MacLean and Beissinger 2017). These spatial shifts have widespread consequences for local and regional community assemblages and, when paired with the increasing size and density of human populations, exacerbate human-wildlife conflict (Abrahms *et al.* 2023; Ma *et al.* 2024). Opportunities for movement are limited or disadvantageous for populations that are hemmed in by physical barriers—both natural, e.g., rivers, and artificial, e.g., roadways—or large swathes of unsuitable habitat that are difficult to traverse. When movement is not viable, organisms must adjust to new conditions *in situ*. Thus, the second major class of response is to adapt, which encompasses a broad spectrum of phenotypic shifts, either through plasticity or true adaptation by selection. For example, persisting in place may elicit behavioral responses, such as alterations to daily activity timing to avoid intolerable temperatures, human disturbance, or other adverse conditions (Gaynor *et al.* 2018; Gilbert *et al.* 2023). Climate-driven shifts in seasonality (e.g., earlier onset of spring), often produce shifts in phenology—or the timing of yearly events such as breeding or migration—potentially causing temporal mismatches in interspecific interactions (Cohen 2003; Parmesan 2006; Thackeray *et al.* 2016). Additionally, climate change is also associated with alterations to physiology (Rodriguez-Dominguez *et al.* 2019; Names *et al.* 2024) as well as life history and demographic rates (Sepp *et al.* 2018; Paniw *et al.* 2019; Paniw *et al.* 2021) across taxa, further impacting community structure and species vulnerability. Finally, when the pace and nature of environmental change outstrip the capacity for mitigation via movement or adaptation, the eventual outcome is death, at the level of individuals, populations, or entire species. Rates of extirpation and extinction are projected to continue to rise across taxa (Thomas *et al.* 2004, Urban 2015, Cowie *et al.* 2022), therefore the efficacy of conservation efforts depends on understanding environmental factors, traits, and responses that favor persistence and resilience, i.e., those associated with species that (seemingly) can successfully move or adapt, so that we may devise targeted interventions for those that cannot.

A significant challenge in this endeavor lies in tracking patterns over broad spatial and temporal scales, for which the extensive biodiversity data provided by natural history collections is an indispensable resource. Museum specimens provide long-term data on population sizes, genetic diversity, geographic ranges, species interactions, and changing phenotypes (Sanders et al. 2023). Additionally, collections are ever expanding, and the emergence of novel and more

efficient methodologies for obtaining and analyzing data allow us to continually build on and refine specimen-based research for tracking global change (Lendemer *et al.* 2020; Nakahama 2021). One of the most accessible and informative forms of specimen-derived data is morphology; body size in particular is a key facet of global change responses, as it is a complex trait that, on a gross scale, mediates the manner and speed at which organisms can respond to changing environmental conditions, and, on a finer scale, is sensitive to the pressures of those changes, serving as a readily measurable indicator of changing environmental pressures.

First, size can influence how and to what extent organisms are exposed to adverse environmental conditions as well as the suite of available mitigation strategies. For instance, small animals have access to microhabitats—such as burrows, the space under leaf litter or snow, etc.—that can offer a buffer against climate conditions (Liow *et al.* 2009; Pauli *et al.* 2013), whereas larger animals may be better equipped to endure temporary periods of low food availability (Peters 1983). However, among mammals, climate-driven shifts in range, abundance, phenology, morphology, and/or genetic diversity have been more frequently detected in larger species than smaller ones, suggesting that the shortage of opportunities to behaviorally buffer against environmental conditions is a key determinant of climate change vulnerability (McCain and King 2014). Moreover, slower reproductive rates and longer generation times confer a reduced capacity for rapid adaptive responses to environmental change, thus larger animals suffer higher extirpation and extinction rates, particularly under anthropogenic threats (Cardillo et al. 2005).

In addition to mediating other forms of global change responses, body size as a trait is sensitive to environmental shifts. Warming climates have been predicted to drive reductions in body size in accordance with Bergmann's rule, a biogeographic pattern describing the tendency towards smaller body sizes at lower (warmer) latitudes (Bergmann, 1847). While the causes and broad applicability of this trend have been debated at length (McNab 1971; Teplitsky *et al.* 2008; Watt *et al.* 2010), a commonly evoked mechanism is that, all else being equal, a greater surface-area-to-volume ratio confers a thermoregulatory advantage in hotter environments, which we could reasonably expect to also apply under climate change. Daufresne et al. (2009) proposed declining body size as a "universal response to warming," though notably their focus was on aquatic ecosystems; a great deal of variability has since been revealed among vertebrates—both aquatic and terrestrial—with increases, decreases, and stasis in size reported across taxa (Gardner et al. 2011). Moreover, opposing trends have been documented among populations of the same species (Meiri et al. 2009), suggesting an important role of local conditions. As such, a prevailing alternative explanation posits resource availability as the primary driver of body-size trends over space and time (McNab 2010; Huston and Wolverton 2011). As climate change extends the growing season (Linderholm 2006) and attenuates winter cold (Williams et al. 2015) across many ecosystems, a common result is improved year-round food availability. Additionally, human activity can provide supplementary resources—through refuse, agriculture, etc.—that are both abundant and calorically dense (Curtis et al. 2018). This provides animals with more energy to invest towards growth, possibly driving increases in body size over time (Hantak et al. 2021). However, climate warming does not always improve resource availability. For instance, warmer winters can reduce snow cover, thus exposing small animals—and their winter food sources—to harsher conditions (Pauli et al. 2013). Food and water scarcity has also become a greater challenge, particularly in arid habitats, with increasing drought severity and frequency (Fuller et al. 2021). Finally, while increasing temperatures and elevated atmospheric CO_2 can spur plant growth, producing a larger volume of forage, this coincides with lower concentrations of

essential nutrients in plant tissues, thus herbivores may experience a greater quantity of food at the expense of nutritional quality (Welti *et al.* 2020, Kaspari and Welti 2024; Ter Haar *et al.* 2025).

Although thermoregulatory pressures according to Bergmann's rule and shifts in resources have often been presented as alternative hypotheses—explaining decreases and increases in body size, respectively—these effects can act simultaneously (e.g., Correll *et al.* 2016; Jirinec *et al.* 2021) along with myriad other factors influencing morphology. For example, body-size trends have been linked to landscape changes, such as urbanization (Guralnick et al. 2020) and habitat fragmentation (Schmidt and Jensen 2003, 2005; Lomolino and Perault 2007). Morphological changes can also result from—or interact with—other classes of climate-change response, particularly shifts in population structure and dynamics. On the individual level, increased size comes with tradeoffs, including development time (larger bodies generally take longer to develop, potentially impacting time to reproductive maturity and longevity; Peters 1983; Kruuk 2017) and fecundity (allocating more energy to the self leaves less available to invest in offspring; Peters 1983). On the population level, this can produce shifts in abundance and demographic rates. Although the effects of global change on demography have not yet been extensively studied (Paniw et al. 2021), tracking changes in body size can offer insights into population age structure, as size and shape changes throughout life in many taxa. Much of the work on this topic has been focused on ectotherms, particularly those of economic or conservation concern. For instance, declines in the mean size of Pacific salmon (*Oncorhynchus* spp.) has been linked to a younger age—and therefore smaller size—at which fish mature and return to freshwater breeding sites, as opposed to reduced growth (Oke *et al.* 2020; Manishin *et al.* 2021). Similarly, in sea turtles, declining mean size was found to coincide with increasing population size, mediated by higher reproductive success rate of younger, smaller individuals (Hays et al. 2025). In general, shifts in population structure can increase vulnerability to disease, drought, and other environmental pressures (Scheele et al. 2016, Rouyer et al. 2012), so linking age structure to morphological trends can serve as an important means to identify at-risk populations.

Understanding responses to global change through this lens of morphology is only possible due to natural history collections; however, museum specimens hold a wealth of other data—ecological, genetic, physiological—that we can use to construct a more holistic view of the drivers and mechanisms of major patterns. Here, I leveraged this network of data, the extended specimen (Webster 2017), to address knowledge gaps in global change research. My first chapter uses age data derived from dental characteristics to challenge the traditional assumption of static adult size/shape in mammals and elucidate the role of demography in population-level body-size trends (Theriot et al. 2024). My second chapter combines data on body size (craniodental measurements), diet composition (stable isotope analysis), and physiological stress (hormone concentrations) to assess the effects of nutrient dilution, the first such investigation in a small, mammalian herbivore. Finally, my third chapter employs shape analysis (geometric morphometrics) to test the hypothesis that urban-dwelling mammals respond to human disturbance in a manner mirroring domesticated animals (i.e., "domestication syndrome") which has garnered recent interest in urban ecology but has yet to be extensively evaluated.

My work contributes to the growing body of research underscoring the importance of natural history collections as a key resource for study biodiversity in a changing world. Applying

museum-specimen-derived data to the fullest extent provides a powerful tool that enables us to detect global-change responses and their underlying mechanisms, offering critical insights toward identifying climate-threatened species and conserving ecosystems into the future.

CHAPTER 1

ACCOUNTING FOR AGE: UNCOVERING THE NUANCED DRIVERS OF MAMMAL BODY-SIZE RESPONSES TO CLIMATE CHANGE

Published in: *Journal of Mammalogy* 07 March 2024

https://doi.org/10.1093/jmammal/gyae005

Miranda K. Theriot[1,2], Link E. Olson[2], and Hayley C. Lanier[1]

[1]*Sam Noble Oklahoma Museum of Natural History, School of Biological Sciences, University of Oklahoma, Norman, OK 73072, United States*

[2]*University of Alaska Museum, University of Alaska Fairbanks, Fairbanks, AK 99775, United States*

Abstract

Shifts in mean body size coinciding with environmental change are well documented across animal species and populations, serving as a widespread and complex indicator of climate-change response. In mammal research, identifying and disentangling the potential drivers of these trends (e.g., thermoregulation, resource availability) is hindered by treating adult size as fixed, ignoring morphological changes that occur throughout life in many species. However, observed population-level size trends may reflect underlying shifts in age structure (i.e., change in the proportion of older, potentially larger individuals in the population). Here, we assessed the role of age structure by explicitly evaluating age as a contributor to temporal variation in skull size (a proxy for body size) in two carnivorans, Canadian Lynx (*Lynx canadensis*) and American Marten (*Martes americana*). Using a series of linear and nonlinear models, we tested age in years (determined by cementum-layer analysis) as a predictor of skull size alongside other factors previously proposed to be important drivers of body-size trends including population density for lynx, growing season conditions for martens. In both species, age was a significant predictor of skull size indicating a rapid year-to-year increase in young adult size that diminished in later adulthood. However, temporal shifts in age structure alone did not explain the observed changes in size over time, indicating that age structure acts in concert with other as-yet unidentified factors to drive body-size change. By explicitly evaluating the role of age, we can both refine models of temporal body-size trends and gain insights into size change as a signal of underlying demographic shifts—such as age-specific survivorship—providing a more holistic understanding into how mammals are responding to climate change.

Introduction

As global change intensifies, understanding and predicting organismal responses depends not only on detecting trends, but identifying their underlying drivers. Many varied and complex

responses to climate change have become evident including marked shifts in phenology, geographic range, and morphology (Parmesan 2006; Pacifici et al. 2017). Changes in body size—one commonly documented response—may be particularly important, because size is linked to many aspects of physiology, ecology, and life history (Peters 1983; Woodward et al. 2005) and can influence how organisms cope with ongoing climate change (Weeks et al. 2020; Peralta-Maraver and Rezende 2021) or other anthropogenic stressors including human harvest (Coltman et al. 2003). However, in part because there are multiple interacting factors that affect size, there are often varied responses across taxa (Gardner et al. 2011) and among populations of the same species (e.g., Meiri et al. 2009). Understanding the contributions of these factors is necessary to advance our ability to characterize and predict biotic responses to global change.

Climate-related morphological change has been linked to a variety of explanatory factors, such as the effects of elevated temperatures or shifts in resource availability (McNab 2010; Gardner et al. 2011; Teplitsky and Millien 2014). For instance, many authors have ascribed declining size—particularly in endotherms—to higher average ambient temperatures (see review in Gardner et al. 2011) consistent with Bergmann's rule (Bergmann 1847), an ecogeographical pattern in which warmer, lower-latitude (and/or lower-elevation) environments appear to favor smaller individuals, possibly due to the greater surface-area-to-volume ratio that allows individuals to shed excess heat more effectively (Mayr 1956; James 1970; Watt et al. 2010). In contrast, when species or populations show temporal increases in mean body size, many authors have focused on the role of resource availability (e.g., McNab 2010; Little et al. 2017), because longer summers (Linderholm 2006) or milder winters (Williams et al. 2015) resulting from climate change may alter year-round food availability. Beyond the effects of temperature and resources, many other drivers of size variation have been explored such as urbanization and habitat fragmentation (Martin and Sheridan 2022), precipitation (Sheridan et al. 2022), and interspecific competition (Zalewski et al. 2022; Ohlberger et al. 2023). This growing body of research clearly indicates that temporal size trends are influenced by many complementary factors. Simultaneously assessing multiple potential drivers is necessary to advance our understanding of how body size may be shifting in response to climate change or other anthropogenic stressors.

One important, yet often overlooked, aspect in the study of body-size responses to climate change is the role of population age structure (i.e., the relative abundance of individuals of different ages at a given point in time). The relationship between age structure and size structure is well established in some ectotherms, with authors drawing a distinction between changes in body size among individuals at the same age or stage (i.e., size-at-age shift) and changes in reproduction or juvenile recruitment (i.e., age-structure shift) as two possible mechanisms of population-level size trends (Daufresne et al. 2009; Ohlberger et al. 2023); however, such considerations are lacking for endotherms. In mammals, most studies that report significant body-size trends do not account for age beyond excluding juveniles (Theriot et al. 2023), which is often at least partly based on the presumed attainment of a fixed, species-specific threshold of "adult size" (see review by Yom-Tov and Geffen 2011). However, changes in size and shape continue to occur throughout life for many species, since bone is living tissue that can be remodeled by wear and muscle action (Elbroch 2006; Law 2020). If the size of individuals varies by age (at least in some dimensions) and environmental changes alter age-specific survivorship, then observed temporal body-size trends may reflect shifts in age distribution over time. In other words, a change in average size over time may actually indicate a change in the relative number of older (and potentially larger) individuals in the population or sample. Thus,

population age structure may play a key role in driving temporal body-size trends linked to climate change, yet this has not been explicitly tested in endotherms to the best of our knowledge.

Evaluating demographic effects may be especially important for taxa in which changes in size or shape throughout adulthood are particularly pronounced. For instance, skull size and shape are known to change throughout ontogeny in some carnivorans (Elbroch 2006; Law 2020); however, few (if any) studies on temporal body-size change in these species account for age of adults, despite using potentially age-sensitive skull measurements (Theriot et al. 2023). Reassessing such studies offers an opportunity to test the effects of age on temporal body-size trends. Additionally, comparing results using potentially age-sensitive measurements to measurements that are less likely to change significantly in adulthood (due to functional constraints) can help identify approaches to control for age. To that end, we replicated and expanded on 2 studies on American Marten (*Martes americana*, hereafter martens; Yom-Tov et al. 2008) and Canadian Lynx (*Lynx canadensis*, hereafter lynx; Yom-Tov et al. 2007). Significant changes in body size over time were reported in populations of both species (an increase in martens and decrease in lynx), which the authors ascribed to changes in resource availability. However, neither study accounted for the effects of age on skull size and shape, which have been documented in these species (Andersen and Wiig 1984; Flynn and Schumacher 2016) but can often be difficult to estimate (Theriot et al. 2023). Therefore, age may present a confounding variable when body-size approximations include potentially age-sensitive measurements, as in Yom-Tov et al. (2007, 2008).

Here, we expanded on Yom-Tov et al. (2007, 2008) to evaluate whether changes in body size over time may reflect changes in demographic structure (hereafter the age structure hypothesis). We tested four predictions under the age structure hypothesis: 1) some skull dimensions can increase significantly with age, while others are more constant throughout life; 2) skull dimensions that are not expected to change significantly in adulthood (e.g., due to functional constraints) have not changed significantly over time, on average; 3) age explains a significant portion of body-size variation over time (i.e., age is a significant predictor in models of temporal trends); and 4) a change in age structure (i.e., the relative proportion of individuals of different ages in the sample) over time coincides with observed temporal trends in mean body size. It is important to note that the age structure hypothesis complements, but does not necessarily replace, other explanations for body-size change over time (e.g., thermoregulation and resource availability). However, by focusing on age structure, we can evaluate how characterizing changes in size and shape throughout life can offer insights into links between morphological and demographic responses to global change.

Materials and methods

Specimens and measurements

Here, we expand on two previous studies that examined temporal trends in body size to explore the additional insights added by an age component. This approach enables us to directly assess how the inclusion of age data influences detection and interpretation of body-size changes over time. We included 434 marten and 543 lynx specimens of known sex collected primarily in interior Alaska (latitude range 58.00 to 68.92 and longitude -164.6 to -133.0 for lynx; latitude 61.35 to 68.00 and longitude -155.5 to -142.2 for martens) from 1950-2000. The majority of

specimens were carcasses from fur trappers (donated to the museum directly or obtained through the Alaska Department of Fish and Game); therefore, the sample is limited to specimens collected during the winter and early spring (November–March). All specimens are housed in the University of Alaska Museum (Supplementary Data SD1 and Supplementary Data SD2 for catalog numbers and additional data).

Consistent with the original publications (Yom-Tov et al. 2007, 2008), we used 2 different but overlapping sets of measurements for each species (Fig. 1). For martens, the original authors made their measurements available: greatest total length of the skull (hereafter "greatest length"); greatest width of the skull ("skull width"); width of the upper canine ("canine width"); and width of the fourth upper premolar ("premolar width"). For lynx, the data were not published, so one of us (MKT) took the full set of measurements, which included: greatest skull length; greatest skull width; upper canine width; and minimum width between the orbits ("interorbital width"). All measurements were recorded by the first author using digital calipers reading to the nearest 0.01 mm. Assessing and comparing multiple measurements is important for accurate size estimation (Damuth and MacFadden 2005). To that end, and to repeat methods used by the original authors, principal component analysis was conducted to reduce each set of log-transformed (natural logarithm) measurements to a single variable, hereafter size PC1, using the R stats package function *prcomp* (R Core Team 2022).

For both species, we also collected and analyzed an alternative measure of skull length, condylopremaxillary length ("constrained length"). In martens, constrained length was recorded by E. Moeller, while in lynx this measurement was taken by MKT as described above. Greatest length and constrained length differ in the posterior anchor point—the lambdoidal ridge (a ridge extending from the posterior of the skull) and the occipital condyle, respectively (Fig. 1). This is an important distinction, as skull ridges are prone to remodeling throughout life to support the attached muscles (Elbroch 2006; Law 2020), while we expect the occipital condyles to be more functionally constrained due to their articulation with the atlas and exhibit little to no variation throughout adulthood. Contrasting these 2 differing skull lengths provides the opportunity to identify whether such purportedly "constrained" measurements are indeed less age sensitive, and to assess whether they reveal different trends over time. Skull length is highly correlated with body mass among carnivorans (Van Valkenburgh 2005), making these measurements an apt choice for assessing the role of age in size estimation. Similarly, we expect the dental measurements to be constant with age after eruption; thus, these measurements may provide a means of avoiding age as a confounding factor in assessing body-size trends.

Age determination

Excluding juveniles from analyses based on cranioskeletal characteristics is a common approach to minimize age bias in studies of mammal body size. Following this convention, Yom-Tov et al. (2007, 2008) identified adult specimens based on closure of cranial sutures and eruption of adult dentition, and subsequently excluded juveniles from the sample.

Here, age in years was determined by cementum-layer analysis, a technique in which layers of deposited tooth material are mapped to years in the life of an individual (Morris 1972). We extracted teeth from all 434 martens and 475 lynx (68 lynx specimens were aged previously by the same method). Teeth were prepared (decalcified, stained, sectioned, and mounted onto slides) and age analysis was conducted (counting of cementum layers, or annuli) by technicians

at Matson's Laboratory (Manhattan, MT) following the methods described by Hiller et al. (2022). The resulting slides are housed at the University of Alaska Museum.

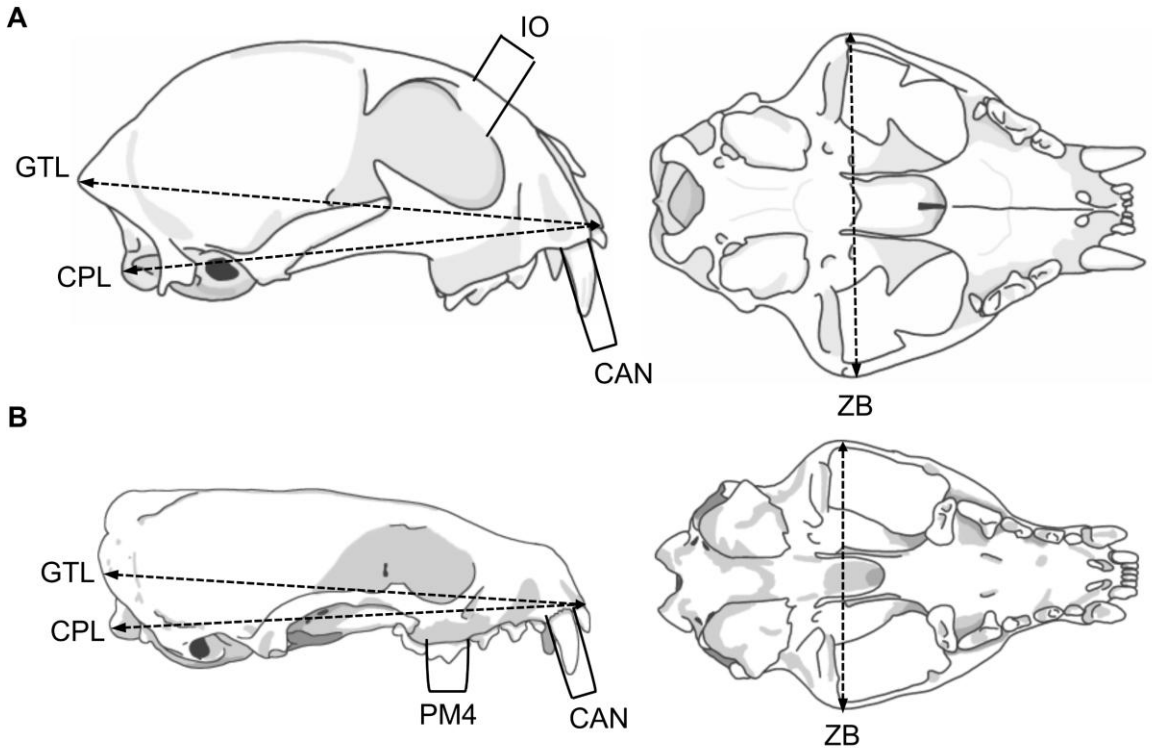


Figure 1. Measurements used to represent size in (A) Canadian Lynx (*Lynx canadensis*) and (B) American Marten (*Martes americana).* Skull length was measured in two ways: greatest total length of the skull (GTL, defined as the maximum distance from the anterior margin of the premaxilla to the posterior margin of the lambdoidal ridge) and condylopremaxillary length (CPL, defined as the maximum distance from the anterior margin of the premaxilla to the posterior margin of the occipital condyle). The other measurements are greatest skull width (i.e., zygomatic breadth, ZB, defined as the maximum width of the skull), interorbital width (i.e., interorbital constriction, IO, defined as the minimum distance between the orbits, lynx only), upper canine width (CAN, defined as anteroposterior width of the upper canine tooth closest to the socket, or when the tooth is absent, the inner width of the socket itself), and fourth upper premolar width (PM4, defined as the anteroposterior width of the fourth upper premolar, martens only). Lynx and marten skull diagrams are not to scale with respect to each other.

Other predictors of size: predicted harvest and growing season conditions

We used Yom-Tov et al.'s (2007, 2008) methods as a launching point to assess age in the context of other factors previously hypothesized to drive body-size variation, specifically growing season conditions in martens (Yom-Tov et al. 2008) and population density in lynx (Yom-Tov et al. 2007). Below, we briefly discuss how we obtained similar data for the present study. For a full account of our interpretation and attempted replication of Yom-Tov et al. (2007, 2008), see

Supplementary Data SD3.

To represent lynx population density—which is known to correlate with mean body size in some small mammals in highly seasonal environments (Oli 1999)—we calculated estimated harvest using the published equation of Yom-Tov et al. (2007), which they developed using trapping records reported to the Alaska Department of Fish and Game (these data were not published), to which they fit a sinusoidal function representing the well-established cyclicity of lynx populations (Elton and Nicholson 1942):

$$\text{Predicted harvest} = \sin((\text{year} - 1974) \times 6 \times 3.1415/27 - 2.89) \times 727.5 + 2{,}176.8$$

The original authors found that predicted harvest 3 years prior to the year of collection (with 3 years thus being their estimated average age in the sample) was most strongly correlated with body size (compared with 0 to 4 years prior). Here, we calculated predicted harvest for the year of collection and estimated year of birth based on age (estimated year of birth = collection year – estimated age) determined by cementum analysis.

For martens, Yom-Tov et al. (2008) included net primary productivity (NPP) in their models to test the role of resource availability in body-size trends. However, those data were not published, and we were unable to locate a similar dataset covering the same temporal and spatial scope. As a proxy for NPP (and resource availability), we calculated the first principal component of average spring temperature, average summer temperature, spring precipitation, and summer precipitation, using data from ClimateWNA (Wang et al. 2016), hereafter referred to as climate PC1. These climate variables—temperature and precipitation during the growing season—have been shown to be significantly correlated with NPP in forest ecosystems (Del Grosso et al. 2008; Tang et al. 2010). For each specimen, we obtained these data for the collection locality (reported as decimal coordinates) in both year of collection and estimated year of birth (estimated as described above) and used this joint dataset to calculate climate PC1 to contrast the relative contributions of NPP at these two timepoints in models of marten body size.

Statistical analyses

For both species, statistical analysis consisted of three approaches: 1) building on the Yom-Tov et al. (2007, 2008) linear model structure to contrast relative contribution of age to other variables; 2) evaluating nonlinear age-size relationships; and 3) testing for changes in the ratio of different ages over time. All analyses were conducted using R version 4.2.2 (R Core Team 2022).

There are 2 primary ways in which age might play a role in explaining body-size variation. First, conditions during a critical growth period may limit adult size (which is assumed to be fixed once attained); thus year of birth, compared to year of collection, may be a better predictor of size trends (Yom-Tov and Geffen 2011). This is what Yom-Tov et al. (2007, 2008) hypothesized in both papers (although they were not able to conduct a direct test), the conditions of interest being population density for lynx and resource availability (here, approximated with growing season conditions) for martens. Second, individuals can change in size and shape throughout adulthood, in which case observed population-level trends in size over time may actually reflect temporal changes in age distribution. In an attempt to tease apart these 2 potential contributors to size variation, we fit the following 3 linear model structures (note that all models include sex, latitude, and longitude as covariates) to each univariate measurement and size PC1:

1. Conditions model: testing only conditions in the estimated year of birth:

$$\text{Log(measurement)} \sim \text{Year}_{\text{birth}} + \text{Sex} + \text{Lat} + \text{Long} + \text{Conditions}_{\text{birth}}$$

2. Age-growth model: testing only variables related to the year of collection (the most similar model structure to that used by the original authors, Supplementary Data SD3) with age included as a predictor:

$$\text{Log (measurement)} \sim \text{Year}_{\text{collection}} + \text{Sex} + \text{Lat} + \text{Long} + \text{Conditions}_{\text{collection}} + \text{Age}$$

3. Combination model: testing how conditions in the year of birth and age influence size variation simultaneously:

$$\text{Log(measurement)} \sim \text{Year}_{\text{birth}} + \text{Sex} + \text{Lat} + \text{Long} + \text{Conditions}_{\text{birth}} + \text{Age}$$

Sex-based differences in skull ontogeny due to muscle development are well known for species in the genus *Martes* (Elbroch 2006; Flynn and Schumacher 2016); therefore, in martens we tested the models detailed above with the addition of an age*sex interaction. Measurements were log-transformed to constrain the distribution of the response variable to positive values. Model fit was compared using the Akaike Information Criterion (AIC) and those with a difference in AIC (ΔAIC) < 2 were considered to fit the data equally well (Burnham and Anderson 2002).

To clarify nonlinear trends in size (as morphological changes throughout life are unlikely to be strictly linear, and temporal trends may also be more complex), we fit generalized additive models (GAMs) using the R package *mgcv* (Wood 2011) to each log-transformed univariate measurement and size PC1. Predictors were selected based on the best-fitting linear model structure identified in approach 1 (the age-growth model for lynx and the combination model for martens; see Results). Year, age, and conditions (predicted harvest for lynx, climate PC1 for martens) were fit using thin plate regression splines and an initial seven knots to limit overfitting. Latitude and longitude were fit using the splines on the sphere smooth function with a penalty order of 2 (m=2). For both species, sex was included as a factor, and for martens, separate smoothers for age were fit for each sex (i.e., an age-sex interaction). All GAMs were fit using a Gaussian distribution and restricted maximum likelihood (REML) with $\gamma = 1.4$ to further limit overfitting (Kim and Gu 2004). As these models cannot effectively estimate a curved relationship from a single point, the oldest specimens in the samples (one lynx age 14, and two martens age 9 and 13) were treated as outliers and omitted from these analyses. Thus, the age range represented in these models was 0 (< 1 year) to 10 in lynx and 0 (< 1 year) to 8 in martens.

Finally, to test for changes in age distribution over time, we used the results from approach 2 to differentiate adult age categories and compared specimen counts within those categories across 2 time periods. We took this approach because in both species age distributions of the samples were skewed towards younger individuals and specimens of advanced ages were rare, thus assigning these categories allows greater statistical power for discerning trends. We divided the samples into categories based on the observed nonlinear age-size relationship detailed above; we characterized young adults as those falling within a period of rapid increase in mean size with increasing age (< 3 years in lynx and < 2 years in martens) and older adults as those with a larger overall size on average, falling in a period of a generally more gradual increase.

For each species, we selected time bins from earlier and later in the study period that included the greatest number of specimens collected over the same number of years—1963-1973 (297 specimens) and 1990-2000 (173 specimens) for lynx, and 1950-1958 (296 specimens) and

1990-1998 (79 specimens) for martens. For both species, we used chi-squared tests to compare the relative proportions of younger and older individuals across time periods in the full samples as well as for males and females separately.

Results

Individual age and skull size

Although all individuals were originally classified and analyzed as adults based on cranial sutures and tooth characteristics (Yom-Tov et al. 2007, 2008), there was considerable variation in age based on cementum analysis. Individuals that were one year old or younger were the most abundant in the sample, comprising 47.0% and 84.1% for lynx and martens, respectively (Fig. 4). In general, age and representation were inversely correlated, with the oldest individuals (14 for lynx, 13 for martens) being the rarest.

The proportion of variance explained by size PC1 was 71.6% for lynx and 72.6% for martens.

Age is a significant predictor of size variation

Age was assessed alongside conditions previously hypothesized to have a strong influence on body size: population density for lynx, and resource availability for martens. Lynx predicted harvest (proxy for population density) calculated according to the methods of Yom-Tov et al. (2007) oscillated between 1,451 and 2,878 individuals, with 9 years between peaks. For martens, climate PC1 was negatively correlated with average spring and summer temperature and positively correlated with spring and summer precipitation (i.e., high climate PC1 represents cold and wet conditions, while low values indicate hot and dry conditions), and the proportion of variance explained was 51.0% (Supplementary Data SD3).

Including age generally produced better-fitting linear models in both lynx and martens, but the relative importance of other factors differed between species. In lynx, the age-growth model fit the data best across all univariate measurements and size PC1 (Table 1); however, the combination model fit equally well for canine width (ΔAIC = 1.93; Table 1). In all cases, age was positively and significantly related to size, as was predicted harvest in the year of collection (except for canine width). In contrast, for martens, the best-fitting model differed by measurement. For size PC1 and the cranial dimensions—greatest length, constrained length, and skull width —the combination model fit the data best. However, for skull width and constrained length in martens the age-growth model fit equally well (ΔAIC = 1.47 and 1.23, respectively; Table 1). Age was a significant predictor of skull length (both measurements), skull width, and size PC1 in male martens, but only skull width in females. Climate PC1 in the year of birth was not a significant predictor for any skull dimension or size PC1. For dental measurements (width of the canine and fourth upper premolar), although the conditions model structure was the best fitting, climate PC1 in the year of birth was not a significant predictor in these models for either tooth measurement. In other words, climate PC1 generally did not explain a significant portion of variation in any measurement or size PC1 in martens and adding age improved model fit for cranial measurements (and size PC1) but not tooth measurements. For full linear model results, see Supplementary Data SD3.

		Conditions		Age-growth		Combination	
	Measurement	AIC	ΔAIC	AIC	ΔAIC	AIC	ΔAIC
Lynx	Greatest length	-2283.89	64.77	**-2348.66**	**0.00**	-2330.68	17.98
	Constrained length	-2256.03	56.43	**-2312.46**	**0.00**	-2304.89	7.57
	Skull width	-1944.79	167.01	**-2111.79**	**0.00**	-2091.57	20.22
	Interorbital width	-1635.62	187.47	**-1823.08**	**0.00**	-1807.34	15.74
	Canine width	-1360.51	43.82	**-1404.32**	**0.00**	-1402.39	1.93
	Size PC1	1623.28	165.78	**1457.50**	**0.00**	1469.81	12.32
Martens	Greatest length	-1849.46	24.64	-1871.89	2.21	**-1874.10**	**0.00**
	Constrained length	-1872.85	4.18	-1875.80	1.23	**-1877.03**	**0.00**
	Skull width	-1357.34	143.98	-1499.85	1.47	**-1501.32**	**0.00**
	Premolar width	**-891.74**	**0.00**	-886.93	4.82	-888.89	2.86
	Canine width	**-328.48**	**0.00**	-326.10	2.39	-325.02	3.46
	Size PC1	1140.08	17.75	1125.27	2.94	**1122.33**	**0.00**

Table 1. Comparison of three linear model structures by AIC for Canadian Lynx (*Lynx canadensis*) and American Marten (*Martes americana*) skull measurements: Conditions (includes year of birth and conditions in the year of birth), Age-growth (includes year of collection and age), and Combination (includes year of birth, age, and conditions in the year of birth). The tested conditions are population density (predicted harvest) for lynx and growing season climatic conditions (climate PC1) for martens. All responses are log-transformed, and all models also include sex, latitude, and longitude as covariates. ΔAIC represents the difference in AIC between a given model for a given measurement and the corresponding best-fitting model (i.e., lowest AIC, bolded). For expanded tables including Akaike weights, see Supplementary Data SD3, Tables S3.24 and S3.28).

Skull size increases nonlinearly with age

To better characterize patterns of size increase throughout life, we fit generalized additive models (GAMs), following a similar structure as the best-fitting linear models described above: the age-growth model for lynx, and the combination model for martens, which we fit across all measurements for ease of comparison. Key results are summarized here; for detailed model outputs, see Supplementary Data SD3.

In lynx, there were significant, positive relationships between age and size in both skull length measurements, interorbital width, and size PC1. There was evidence of nonlinearity in these trends; in all cases, the effective degrees of freedom (or EDF, which denotes the degree of nonlinearity in the estimated model, with higher values indicating greater nonlinearity; Pedersen et al. 2019) was around 3. Specifically, the relationships are generally characterized by a steep increase in size up to around age 3 that diminishes thereafter (Fig. 2). In contrast, canine width

increased significantly and linearly (EDF = 1) with age, an unexpected trend given the prediction that mammal teeth do not grow in size once fully erupted—we tested 2 possible explanations. First, a smaller portion of the canine may be exposed/erupted among younger individuals, thus making the tooth appear smaller. However, re-fitting models after removing individuals less than 2 years old (assigned age 0 or 1) did not negate the statistically significant relationship between

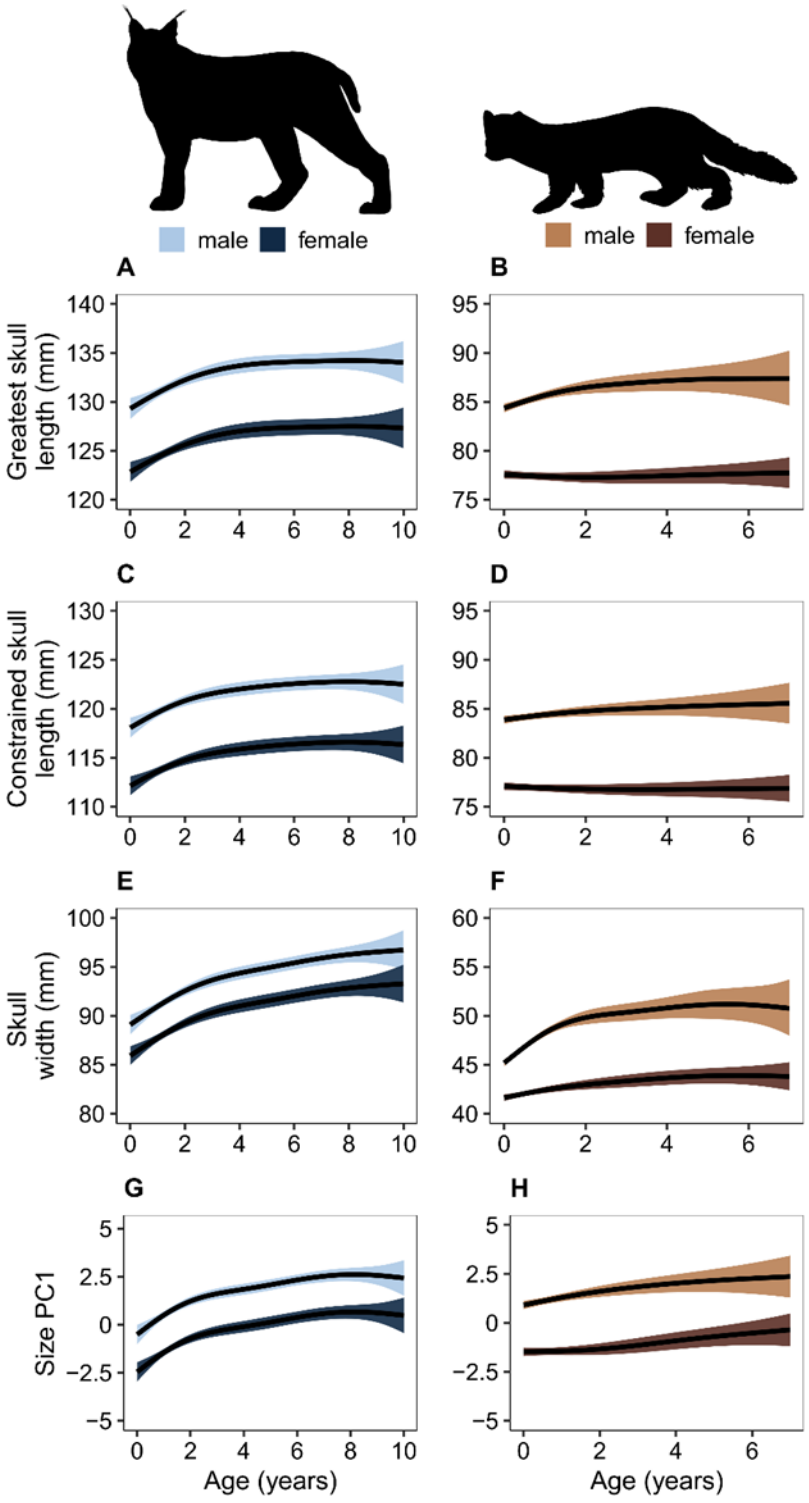


Figure 2. Nonlinear increase in select skull measurements with age. With increasing age, both male and female Canadian Lynx (*Lynx canadensis*) increase significantly in skull length, (A, C), skull width (E) and size PC1 (G), while male American Marten (*Martes americana*) increase significantly in skull length (B, D) but both sexes increase significantly in skull width (F) and size PC1 (H). All models are corrected for latitude, longitude, year, and relevant conditions (predicted harvest for lynx, climate PC1 for martens). Shaded areas represent the 95% confidence interval, with the lighter color denoting males and the darker color females. PhyloPic images by Gabriela Palomo-Munoz (https://creativecommons.org/licenses/by-nc/3.0/).

age and tooth size in the age-growth linear model (age coefficient estimate = 0.007, $t = 3.923$, $P < 0.001$), nor in the nonlinear model (effective degrees of freedom = 3.216, $F_{3.938} = 5.614$, $P < 0.001$). Second, different methods of measuring canine width, i.e., measuring the tooth itself or measuring the interior width of the socket when the canines were absent, may be a confounding variable. We removed specimens measured by the latter method (118, leaving 411 specimens with a canine width measurement) and re-fit the best-fitting linear model and the GAM as above. This change also did not account for the apparently significant effect of age on canine width (linear model age coefficient estimate = 0.009, $t = 8.667$, $P < 0.001$; GAM age effective degrees of freedom = 2.389, $F_{2.959} = 28.440$, $P < 0.001$). Simultaneously removing the youngest individuals and those in which the tooth socket was measured yielded similar results.

In martens, size trends were sex specific (consistent with the linear models described above). In males, there was a significant increase in both skull length measurements but not in females. Skull width, on the other hand, increased significantly with age in both sexes. Canine width increased in females, but premolar width did not change significantly with age in either sex. Finally, size PC1 increased significantly in both sexes with some degree of nonlinearity EDF = 1.7). As with lynx, among the nonlinear relationships, size generally increased rapidly up to a point, then shifted to a more gradual increase; for the martens, this transition occurred around age two (Fig. 2).

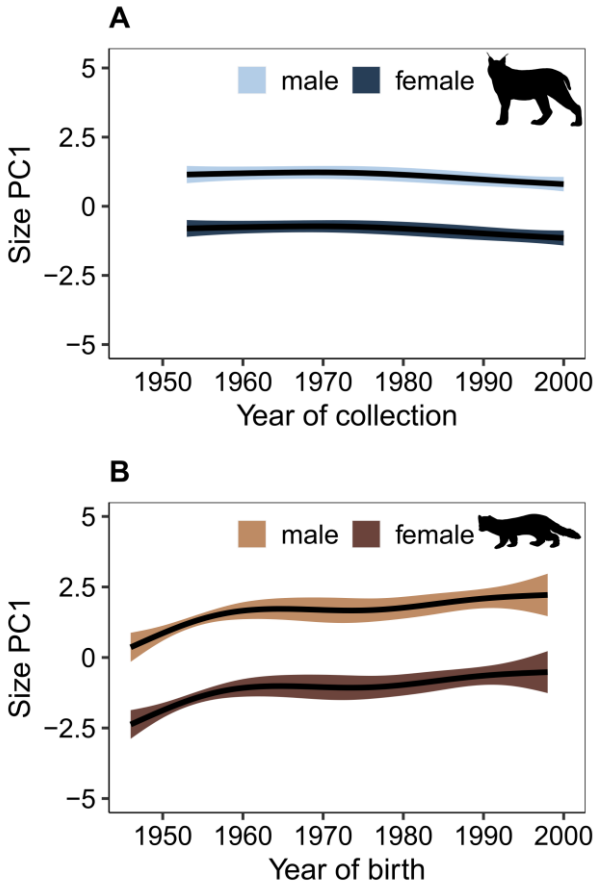


Figure 3. Nonlinear change in mean size PC1 over time in (A) Canadian Lynx (*Lynx canadensis*; significant decrease) and (B) American Marten (*Martes americana*; significant increase). The measure of time (year of collection for lynx, year of birth for martens) included in the generalized additive model is based on the best-fitting linear model structure. All models also include latitude, longitude, age, and relevant conditions (predicted harvest for lynx, climate PC1 for martens). Shaded areas represent the 95% confidence interval, with the lighter color denoting males and the darker color females.

Change in mean size and the proportion of younger individuals over time

Our third and final approach revealed changes in age structure associated with shifts in mean size over time. In both lynx and marten, the GAMs detailed in the previous section provided some evidence for change in size (at least in some dimensions) over time; in lynx, size PC1 declined slightly but significantly over the study period (Fig. 3a) but the only significant temporal trends among univariate models

were a decline in interorbital width and canine width. In martens, on the other hand, all univariate measurements and size PC1 increased significantly over the study period (Supplementary Data SD3; Fig. 3b). Notably, these models included age as a predictor, therefore a change in age distribution cannot fully explain the temporal size trends; however, assessing the proportion of younger individuals over time can indicate whether the effects of age amplify or oppose these shifts.

To test for changes in age structure over time, we compared the relative proportions of different age groups between time periods. In lynx, the proportion of younger individuals (3 or younger) in the sample increased significantly ($\chi^2 = 4.163$, df = 1, $P = 0.041$) from 68.7% (204/297 specimens) in the earlier time period (1963-1973) to 77.5% (134/173) in the more recent time period (1990-2000). Dividing the sample by sex reveals that this is driven by a significant increase in the proportion of younger males ($\chi^2 = 8.340$, df = 1, $P = 0.004$; Fig. 4a). The ratio of younger to older females did not differ significantly. In martens, we found the opposite pattern. Overall, the proportion of younger individuals (1 or younger) decreased significantly ($\chi^2 = 26.799$, df = 1, $P < 0.001$) between time periods, from 89.5% (265/296) in 1950-1958 to 65.8% (52/79) in 1990-1998. However, as with lynx, this trend appears to be largely due to a change in the proportion of younger males ($\chi^2 = 31.306$, df = 1, $P < 0.001$; Fig. 4b), whereas the proportion of younger females did not change.

Additionally, sex ratio also differed by time period in lynx (but not martens), with the proportion of males of any age increasing from 44.4% (132/297) in 1963-1973 to 61.0 % (105/173) in 1990-2000 ($\chi^2 = 11.547$, df = 1, $P = 0.001$).

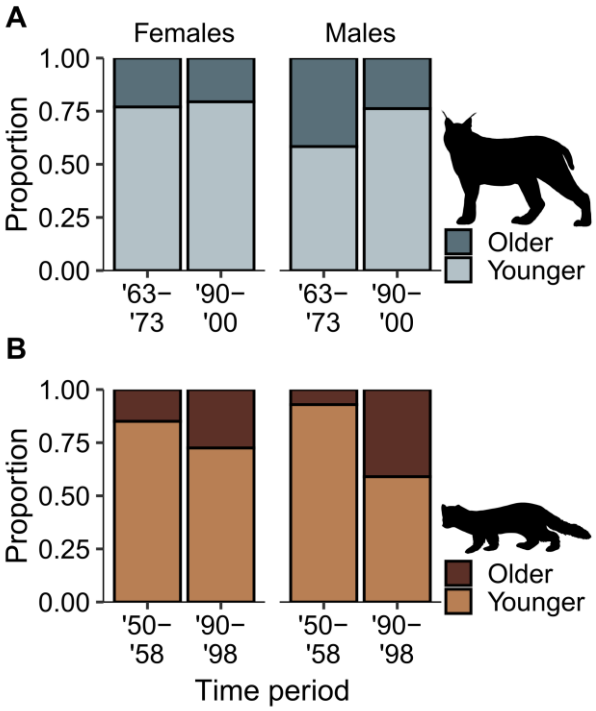


Figure 4. Temporal shifts in age structure in (A) Canadian Lynx (*Lynx canadensis*) and (B) American Marten (*Martes americana*). The proportion of the population comprising younger individuals is represented by lighter shading, and older individuals by darker shading. Significant differences (based on chi-square tests) are marked by *.

Discussion

Our results highlight the role of age structure in shaping temporal body-size variation in 2 species in which changes over time were previously proposed to be driven primarily by resource availability (Yom-Tov et al. 2007, 2008). In lynx and martens, there is a significant relationship between age and size throughout life in both species (prediction 1), and accounting for age (i.e., considering age alongside year, location, sex, and other conditions) produced better-fitting models of temporal size trends (prediction 3). Surprisingly, none of the skull measurements were invariant with adult age (prediction 2). While we did find temporal shifts in age structure (prediction

4), age did not explain all body-size trends (i.e., age-corrected mean size still changed over time in both species), suggesting that age effects act in concert with other factors. Together, these results support the age hypothesis, but indicate that this explanation complements, rather than replaces, many of the commonly investigated factors shaping body-size trends.

Shifts in age structure influence body-size changes

Our findings reveal that age is a significant contributor to body-size variation in lynx and martens and can influence our understanding of the importance of other predictive variables. In lynx, once age was accounted for there was a slight positive correlation between population density (i.e., predicted harvest) and mean size (Supplementary Data SD3), contrary to previous findings (Yom-Tov et al. 2007). Surprisingly, linear models including predicted harvest estimated for the year of collection fit the data better than those incorporating year of birth across all measurements (Table 1), which also runs counter to the original conclusions of Yom-Tov et al. (2007). The importance of population density (i.e., predicted harvest) during year of collection may reflect shifts in how individuals allocate energy for growth versus reproduction during population cycles; for instance, in small mammals that undergo cyclic population dynamics, suppression of reproduction (particularly in younger animals) during phases of high population density—and thus high competition—has been hypothesized to produce larger individuals because energy that would have been spent on reproduction is instead available for growth (Oli 1999). In lynx, pregnancy rates and litter sizes are generally lower among yearling females, particularly during periods of high competition for prey (Parker et al. 1983; Mowat et al. 1996), but more research is needed to determine if and how age-specific reproductive rates influence body-size trends. In martens, even after accounting for age, growing season conditions (i.e., climate PC1) were not a significant predictor of size in any model (Supplementary Data SD3). Similarly, Yom-Tov et al. (2008) did not find a significant relationship between estimated net primary productivity (NPP) and size, suggesting 2 possible explanations. First, variability (i.e., noise) in the estimates for spring and summer precipitation—or NPP, in the case of (Yom-Tov et al. 2008)—may obscure any signal. Alternatively, these environmental variables may not have strongly influenced marten body size, which may reflect other factors (e.g., prey abundance) more directly. Comparing our results to those of the previous authors demonstrates the importance of reevaluating existing studies, especially in light of new data, in order to improve our understanding of how multiple factors can contribute to body-size trends.

These results further highlight the complex nature of body-size responses to climate change. Notably, although evidence indicates that age is important to individual size, shifts in age structure alone do not explain the observed trends in size over time, i.e., including age does not eliminate the effects of year, which was negatively correlated with size PC1 in lynx and positively with size PC1 in martens (Supplementary Data SD3). This result suggests a role for other factors (e.g., more localized effects of temperature and/or precipitation, prey type and availability, habitat fragmentation, human activity, etc.) that may have changed over time but were not explicitly evaluated here. Ultimately, this is not surprising; the diversity of body-size literature (e.g., see reviews in Millien et al. 2006; Gardner et al. 2011; Yom-Tov and Geffen 2011) clearly indicates that body size is a complex trait shaped by a variety of context-dependent factors. Thus, a single explanation for changing size (be it age structure, temperature effects, food availability, etc.) is unlikely; however, understanding how age affects size, both on the individual and population level, can aid in identifying patterns and better understanding body-

size responses to global change.

Age structure shifts as a response to climate change

Demographic responses to climate change, including age structure shifts, are underexplored across many taxa (Paniw et al. 2021). Although our primary goal was to investigate whether age distribution in a sample influences the detection and interpretation of body-size trends, a corollary to our findings is the potential for size change to indicate underlying population-level demographic shifts. For example, a change in the proportion of younger and smaller individuals in a population may arise from changes in age- and/or sex-specific survivorship. Such changes may result in part from niche partitioning among sexes and ages—such as differences in prey type and variety between males and females (e.g., Pearson et al. 2002) or yearlings and breeding adults (e.g., Burstahler et al. 2016)—potentially leading to different responses to environmental change. Such effects may have ongoing consequences for population growth and persistence; for instance, high juvenile mortality and subsequent low recruitment may herald population decline (Middleton and Green 2015). Additionally, shifts towards younger age structure may hamper resilience to drought or other extreme weather events (Scheele et al. 2016). However, assessing the relationship between morphological and demographic trends will require additional data, as museum samples can be biased by trapping effort (Gotelli et al. 2023). In the case of lynx and martens in the present study, the vast majority of specimens were captured by trappers, meaning that sampling is temporally limited to the trapping season and spatially limited by state regulations and physical accessibility. While we must exercise caution in drawing population-level conclusions from the data presented here, we suggest that further evaluation of changes in age structure for taxa in which body-size shifts have been observed may reveal previously undocumented drivers of population change.

There are multiple non-mutually exclusive mechanisms that could produce the change in age structure found in both lynx and martens (prediction 4; Fig. 4) that warrant further study. First, these samples may be sex- and/or age-biased because trap vulnerability tends to be higher among younger individuals, particularly males as they disperse in search of territory (Slough and Mowat 1996). Changes in trapping effort or regulations over time may result in higher capture rates of younger individuals (which have been found to be overrepresented in trapped populations by as much as a 40% increase compared to non-trapped areas; Slough and Mowat 1996); however, that would not explain the apparent decrease in the proportion of younger males in martens. Second, the survival rate among younger individuals, particularly males, may have changed over time. For example, higher juvenile mortality has been shown to skew age structure towards older adults (e.g., Middleton and Green 2015; Branch et al. 2019). Conversely, shifts in age structure may result from changing mortality rate among later stages or age classes (e.g., Scheele et al. 2016). Finally, differences in the sex ratio at birth could also contribute to sex-specific trends in age structure (and shift toward a higher overall proportion of males in lynx). In some mammals and birds, a slight bias towards investment in male offspring has been linked to better maternal body condition (the Trivers-Willard hypothesis; Trivers and Willard 1973) and elevated stress (Cameron 2004), which may alter the proportion of young males recruited into the population. Identifying the underlying causes(s) of these trends in age structure, and particularly why they differ between species, warrants further study.

The feasibility of testing for age effects

While we encourage considering how age structure may influence detection and interpretation of body-size responses to climate change, determining age is challenging. Notably, we were unable to confirm a functionally constrained measurement of skull length (Fig. 2), contrary to predictions and conventional assumptions about mammal ontogeny, suggesting that some age classification of adults (versus conventional and simplistic subadult-adult categorization) is warranted.

The significant increase in lynx canine width with age runs contrary to the expectation that, once erupted, teeth should remain largely static throughout life (if not shrinking in some dimensions, due to wear). We ruled out 2 possible explanations; the trend is not explained by an effect of particularly young individuals having incomplete tooth eruption, nor by measurement method. Canine width has been used to approximate age class in live carnivorans, attributed to gum-line recession as individuals get older rather than a change in the tooth itself (Laundré et al. 2000; Santymire et al. 2012; Peers et al. 2021). However, if gum-line recession possibly alters the position of the tooth within the socket in museum specimens, this could affect the area exposed for measurement, producing an apparent age effect on tooth size. Additionally, individuals with larger teeth (or those that are larger in general) may be more likely to survive to older ages, emphasizing the need for further studies that integrate these morphological trends with population dynamics. Regardless of the mechanism, these results further highlight that age can influence size measurements—either by 'true' ontological changes or by influencing what and how we measure—which has yet to be widely investigated in mammal body-size research.

While relying on relative aging methods may obscure nuanced size trends, precise techniques—such as cementum-layer analysis (Morris 1972), eye lens weight (Augusteyn 2014), and skeletochronology (Halliday and Verrell 1988)—also present some limitations. For instance, they require a known-age series for reference, are not available for all species, tend to be costly and time consuming, and require permanently altering specimens. To mitigate these problems, known-age specimens (e.g., captive bred) are invaluable for developing and refining aging techniques and characterizing growth patterns. Data sharing and transparency is also critical so that destructive methods are not repeated unnecessarily. Despite these obstacles to age determination, it is still important to recognize age structure as a potential contributor to trends, and to consider the role of demographic effects in climate-change responses to the extent possible.

Implications for studying responses to global change

Body size provides a potential wealth of information about responses to climate change. The size of an individual reflects how a limited supply of energy is allocated to growth, maintenance, and reproduction at a given point in its development in a given environment (Brown et al. 1993). This balance can be influenced by a variety of factors, including type and abundance of resources, inter- or intraspecific competition, and climatic conditions (e.g., heat and moisture), all of which are potential consequences of rapid global change. Moreover, some dimensions of size (e.g., cranial measurements) can also be readily measured on museum specimens; thus, natural history collections spanning several decades are a powerful resource for understanding ongoing climate change (Sanders et al. 2023). Therefore, it is important to consider body size trends not just as a standalone outcome of global change, but as a sign of complex responses,

including demographic change.

Understanding links between size structure and age structure may aid in predicting future responses to environmental change and developing management strategies. For example, research on size declines in salmon implicated elevated competition and predation experienced by older ocean-dwelling age classes (Oke et al. 2020; Ohlberger et al. 2023); understanding such mechanisms, as well as the relationship between size and abundance, is vital to enacting management policies that mitigate economic and ecological consequences (Oke et al. 2020). Evaluating interactions between size structure and age structure can inform strategies for controlling population growth and reducing human-wildlife conflict (Vetter et al. 2020). Finally, in game species (including furbearers like lynx and martens), research on age structure can aid in identifying long-term population trends and inform harvest limits and other management policies (e.g., Mowat et al. 1996). To that end, continual collection of specimens and partnerships between state management agencies and museums are vital; hunted or trapped specimens can provide rich long-term datasets (including those used herein). These specimens enable the ongoing research needed to characterize the relationship between size structure and age structure in a population, as well as to track and predict responses to climate change.

Given the variability of body-size trends observed across taxa (Millien et al. 2006; Gardner et al. 2011), and the complexity of these trends and hypothesized drivers (e.g., Guralnick et al. 2020; Suzuki et al. 2020; Valenzuela-Toro et al. 2023), our results underscore the need for researchers to carefully consider a broad range of intrinsic and extrinsic factors in the effort to understand and model responses. Changes in body size are an informative signal of complex interrelated responses to climate change, including demographic shifts, which can have important consequences for population growth and persistence in a changing world. Therefore, characterizing links between morphological and demographic trends is vital to a holistic understanding of organismal responses to global change.

Acknowledgements

Our sincere thanks to Yoram and Shlomith Yom-Tov for inspiring this line of inquiry and sharing their data. Thanks also to the staff and volunteers of the University of Alaska Museum Mammalogy Department, especially Erica Moeller for marten skull measurements and collection manager Aren Gunderson. Thanks to Daniel Becker, Michael Kaspari, Jeffrey Kelly, and Jacqueline Lungmus for feedback on earlier versions of this manuscript, Lara Souza for guidance on assessing historical NPP, and 2 anonymous reviewers for their suggestions on improving the paper. Finally, we acknowledge the numerous hunters, trappers, collectors, and preparators without whom this and other specimen-based studies would not be possible.

Author Contributions

LEO and HCL developed the original concept for this study. MKT collected data, conducted analyses, and drafted the manuscript with input from LEO and HCL. All authors contributed to preparing and approving the final manuscript for publication.

Funding

This research was funded by Alaska Department of Fish and Game Division of Wildlife Conservation, a Grant-in-Aid of Research from the American Society of Mammalogists, the Calvin J. Lensink Graduate Fellowship from the University of Alaska Fairbanks, and the Adams Scholarship from the University of Oklahoma.

Data Availability

The raw data and R code associated with this study can be found at https://osf.io/6wkqf/?view_only=623802cccd494d5694c8defc7d236483.

References

Andersen T, Wiig Ø. 1984. Growth of the skull of Norwegian lynx. Acta theriologica 29(8):89–100. https://doi.org/10.4098/at.arch.84-8.

Augusteyn RC. 2014. Growth of the eye lens: I. Weight accumulation in multiple species. Molecular Vision 20:410–426. https://pubmed.ncbi.nlm.nih.gov/24715758

Bergmann C. 1847. Über die Verhältnisse der Wärmeökonomie der Thiere zu ihrer Grösse. Göttinger Studien 1:595–708.

Branch CL, Pitera AM, Kozlovsky DY, Sonnenberg BR, Benedict LM, Pravosudov VV. 2019. Elevation-related differences in the age structure of breeding birds suggest stronger selection at harsher elevations. Behavioral Ecology and Sociobiology 73(10):143. https://doi.org/10.1007/s00265-019-2750-4.

Brown JH, Marquet PA, Taper, ML. 1993. Evolution of body size: Consequences of an energetic definition of fitness. The American Naturalist 142(4):573–584. https://doi.org/10.1086/285558

Burnham KP, Anderson DR. 2002. Model selection and multimodel inference: a practical information-theoretic approach. 2nd ed. New York (NY, USA): Springer.

Burstahler CM, Roth JD, Gau RJ, Murray DL. 2016. Demographic differences in diet breadth of Canada Lynx during a fluctuation in prey availability. Ecology and Evolution 6(17):6366–6375. https://doi.org/10.1002/ece3.2115.

Cameron EZ. 2004. Facultative adjustment of mammalian sex ratios in support of the Trivers–Willard hypothesis: evidence for a mechanism. Proceedings of the Royal Society of London. Series B: Biological Sciences 271(1549):1723–1728. https://doi.org/10.1098/rspb.2004.2773.

Coltman DW, O'Donoghue P, Jorgenson JT, Hogg JT, Strobeck C, Festa-Bianchet M. 2003. Undesirable evolutionary consequences of trophy hunting. Nature 426(6967):655–658. https://doi.org/10.1038/nature02177.

Damuth JD, MacFadden BJ, editors. 2005. Body size in mammalian paleobiology: estimation and biological implications. Cambridge (UK): Cambridge University Press.

Daufresne M, Lengfellner K, Sommer U. 2009. Global warming benefits the small in aquatic ecosystems. Proceedings of the National Academy of Sciences of the United States of America 106:12788–12793. https://doi.org/10.1073/pnas.0902080106.

Del Grosso S, Parton W, Stohlgren T, Zheng D, Bachelet D, Prince S, Hibbard K, Olson R. 2008. Global potential net primary production predicted from vegetation class, precipitation, and temperature. Ecology 89(8):2117–2126. https://doi.org/10.1890/07-0850.1.

Elbroch M. 2006. Animal skulls: A guide to North American species. Mechanicsburg (PA, USA): Stackpole Books.

Elton C, Nicholson M. 1942. The ten-year cycle in numbers of the lynx in Canada. The Journal of Animal Ecology 11(2):215–244. https://doi.org/10.2307/1358.

Flynn RW, Schumacher TV. 2016. Determining sex and age of martens in the north Pacific coast: using skull length and temporal muscle coalescence. Alaska Department of Fish and Game, Division of Wildlife Conservation. https://doi.org/10.13140/RG.2.1.1546.2009.

Gardner JL, Peters A, Kearney MR, Joseph L, Heinsohn R. 2011. Declining body size: a third universal response to warming? Trends in Ecology & Evolution 26(6):285–291. https://doi.org/10.1016/j.tree.2011.03.005.

Gotelli NJ, Booher DB, Urban MC, Ulrich W, Suarez AV, Skelly DK, Russell DJ, Rowe RJ, Rothendler M, Rios N, et al. 2023. Estimating species relative abundances from museum records. Methods in Ecology and Evolution 14(2):431–443. https://doi.org/10.1111/2041-210X.13705.

Guralnick R, Hantak MM, Li D, McLean BS. 2020. Body size trends in response to climate and urbanization in the widespread North American Deer Mouse, *Peromyscus maniculatus*. Scientific Reports 10(1):8882. https://doi.org/10.1038/s41598-020-65755-x.

Halliday TR, Verrell PA. 1988. Body size and age in amphibians and reptiles. Journal of Herpetology 22(3):253–265. https://doi.org/10.2307/1564148.

Hiller TL, Nistler C, Reding D, White PA, Bled F. 2022. Sex identification and age estimation of bobcats and implications for management. Wildlife Society Bulletin 46(3):e1328. https://doi.org/10.1002/wsb.1328.

James FC. 1970. Geographic size variation in birds and its relationship to climate. Ecology 51(3):365–390. https://doi.org/10.2307/1935374.

Kim YJ, Gu C. 2004. Smoothing spline Gaussian regression: more scalable computation via efficient approximation. Journal of the Royal Statistical Society Series B: Statistical Methodology 66(2):337–356. https://doi.org/10.1046/j.1369-7412.2003.05316.x.

Laundré, JW, Hernández L, Streubel D, Altendorf K, González CL. 2000. Aging mountain lions using gum-line recession. Wildlife Society Bulletin 28(4):963–966. https://www.jstor.org/stable/3783855.

Law CJ. 2020. Sex-specific ontogenetic patterns of cranial morphology, theoretical bite force, and underlying jaw musculature in fishers and American martens. Journal of Anatomy 237(4):727–740. https://doi.org/10.1111/joa.13231.

Linderholm HW. 2006. Growing season changes in the last century. Agricultural and Forest Meteorology 137(1–2):1–14. https://doi.org/10.1016/j.agrformet.2006.03.006.

Little R, Gardner JL, Amano T, Delhey K, Peters A. 2017. Are long-term widespread avian body size changes related to food availability? A test using contemporaneous changes in carotenoid-based color. Ecology and Evolution 7(9):3157–3166. https://doi.org/10.1002/ece3.2739.

Martin AK, Sheridan JA. 2022. Body size responses to the combined effects of climate and land use changes within an urban framework. Global Change Biology 28(18):5385–5398. https://doi.org/10.1111/gcb.16292.

Mayr E. 1956. Geographical character gradients and climatic adaptation. Evolution 10(1):105–108. https://doi.org/10.2307/2406103.

McNab BK. 2010. Geographic and temporal correlations of mammalian size reconsidered: a resource rule. Oecologia 164(1):13–23. https://doi.org/10.1007/s00442-010-1621-5.

Meiri S, Guy D, Dayan T, Simberloff D. 2009. Global change and carnivore body size: data are stasis. Global Ecology and Biogeography 18(2):240–247. https://doi.org/10.1111/j.1466-8238.2008.00437.x.

Middleton J, Green DM. 2015. Adult age-structure variability in an amphibian in relation to population decline. Herpetologica 71(3):190–195. https://doi.org/10.1655/HERPETOLOGICA-D-14-00074.

Millien V, Lyons SK, Olson L, Smith FA, Wilson AB, Yom-Tov Y. 2006. Ecotypic variation in the context of global climate change: revisiting the rules. Ecology Letters 9(7):853–869. https://doi.org/10.1111/j.1461-0248.2006.00928.x.

Morris P. 1972. A review of mammalian age determination methods. Mammal Review 2(3):69–104. https://doi.org/10.1111/j.1365-2907.1972.tb00160.x.

Mowat G, Slough BG, Boutin S. 1996. Lynx recruitment during a snowshoe hare population peak and decline in southwest Yukon. The Journal of Wildlife Management 60(2):441–452. https://doi.org/10.2307/3802247.

Ohlberger, J, Cline TJ, Schindler DE, Lewis B. 2023. Declines in body size of sockeye salmon associated with increased competition in the ocean. Proceedings of the Royal Society B: Biological Sciences 290(1992):20222248. https://doi.org/10.1098/rspb.2022.2248.

Oke KB, Cunningham CJ, Westley PAH, Baskett ML, Carlson SM, Clark J, Hendry AP, Karatayev VA, Kendall NW, Kibele J, et al. 2020. Recent declines in salmon body size impact ecosystems and fisheries. Nature Communications 11(1):4155. https://doi.org/10.1038/s41467-020-17726-z.

Oli MK. 1999. The Chitty effect: A consequence of dynamic energy allocation in a fluctuating environment. Theoretical Population Biology 56(3):293–300. https://doi.org/10.1006/tpbi.1999.1427.

Pacifici M, Visconti P, Butchart SHM, Watson JEM, Cassola FM, Rondinini C. 2017. Species' traits influenced their response to recent climate change. Nature Climate Change 7(3):205–208. https://doi.org/10.1038/nclimate3223.

Paniw M, James TD, Ruth Archer C, Römer G, Levin S, Compagnoni A, Che-Castaldo J, Bennett JM, Mooney A, Childs DZ, et al. 2021. The myriad of complex demographic responses of terrestrial mammals to climate change and gaps of knowledge: A global analysis. Journal of Animal Ecology 90(6):1398–1407. https://doi.org/10.1111/1365-2656.13467.

Parker GR, Maxwell JW, Morton LD, Smith GEJ. 1983. The ecology of the lynx (*Lynx canadensis*) on Cape Breton Island. Canadian Journal of Zoology 61(4):770–786. https://doi.org/10.1139/z83-102.

Parmesan C. 2006. Ecological and evolutionary responses to recent climate change. Annual Review of Ecology, Evolution, and Systematics 37(1):637–669. https://doi.org/10.1146/annurev.ecolsys.37.091305.110100.

Pearson D, Shine R, How R. 2002. Sex-specific niche partitioning and sexual size dimorphism in Australian pythons (*Morelia spilota imbricata*). Biological Journal of the Linnean Society 77(1):113–125. https://doi.org/10.1046/j.1095-8312.1999.00075.x.

Pedersen EJ, Miller DL, Simpson GL, Ross N. 2019. Hierarchical generalized additive models in ecology: an introduction with mgcv. PeerJ 7:e6876. https://doi.org/10.7717/peerj.6876.

Peers MJL, Majchrzak YN, Studd EK, Menzies AK, Kukka PM, Konkolics SM, Boonstra R, Boutin S, Jung TS. 2021. Evaluation of gum-line recession for aging lynx (*Lynx canadensis*). Wildlife Society Bulletin 45(4):706–710. https://doi.org/10.1002/wsb.1239.

Peralta-Maraver I, Rezende EL. 2021. Heat tolerance in ectotherms scales predictably with body size. Nature Climate Change 11(1):58–63. https://doi.org/10.1038/s41558-020-00938-y.

Peters RH. 1983. The ecological implications of body size. Cambridge (UK): Cambridge University Press.

R Core Team. 2022. R: A language and environment for statistical computing. R Foundation for Statistical Computing, Vienna, Austria. https://www.R-project.org/.

Sanders NJ, Cooper N, Davis Rabosky AR, Gibson DJ. 2023. Leveraging natural history collections to understand the impacts of global change. Journal of Animal Ecology 92(2):232–236. https://doi.org/10.1111/1365-2656.13882.

Santymire RM, Wisely SM, Livieri TM, Howard J. 2012. Using canine width to determine age in the Black-footed Ferret *Mustela nigripes*. Small Carnivore Conservation 46:17–21.

Scheele BC, Hunter DA, Banks SC, Pierson JC, Skerratt LF, Webb R, Driscoll DA. 2016. High adult mortality in disease-challenged frog populations increases vulnerability to drought. Journal of Animal Ecology 85(6):1453–1460. https://doi.org/10.1111/1365-2656.12569.

Sheridan JA, Mendenhall CD, Yambun P. 2022. Frog body size responses to precipitation shift from resource-driven to desiccation-resistant as temperatures warm. Ecology and Evolution 12(12): e9589. https://doi.org/10.1002/ece3.9589.

Slough BG, Mowat G. 1996. Lynx population dynamics in an untrapped refugium. The Journal of Wildlife Management 60(4):946–961. https://doi.org/10.2307/3802397.

Suzuki TA, Martins FM, Phifer-Rixey M, Nachman MW. 2020. The gut microbiota and Bergmann's rule in wild house mice. Molecular Ecology 29(12):2300–2311. https://doi.org/10.1111/mec.15476.

Tang G, Beckage B, Smith B, Miller PA. 2010. Estimating potential forest NPP, biomass and their climatic sensitivity in New England using a dynamic ecosystem model. Ecosphere 1(6):1–20. https://doi.org/10.1890/ES10-00087.1.

Teplitsky C, Millien V. 2014. Climate warming and Bergmann's rule through time: is there any evidence? Evolutionary Applications 7(1):156–168. https://doi.org/10.1111/eva.12129.

Theriot MK, Lanier HC, Olson LE. 2023. Harnessing natural history collections to detect trends in body-size change as a response to warming: A critique and review of best practices. Methods in Ecology and Evolution 14(2):306–318. https://doi.org/10.1111/2041-210X.13861.

Trivers RL, Willard DE. 1973. Natural selection of parental ability to vary the sex ratio of offspring. Science 179(4068):90–92. https://doi.org/10.1126/science.179.4068.90.

Valenzuela-Toro AM, Costa DP, Mehta R, Pyenson ND, Koch PL. 2023. Unexpected decadal density-dependent shifts in California sea lion size, morphology, and foraging niche. Current Biology 33(10):2111–2119. https://doi.org/10.1016/j.cub.2023.04.026.

Van Valkenburgh B. 2005. Skeletal and dental predictors of body mass in carnivores. In: Damuth JD, MacFadden BJ, editors. Body size in mammalian paleobiology: estimation and biological implications. Cambridge (UK): Cambridge University Press; p. 181–205.

Vetter SG, Puskas Z, Bieber C, Ruf T. 2020. How climate change and wildlife management affect population structure in wild boars. Scientific Reports 10(1):7298. https://doi.org/10.1038/s41598-020-64216-9.

Wang T, Hamann A, Spittlehouse D, Carroll C. 2016. Locally downscaled and spatially customizable climate data for historical and future periods for North America. PLoS ONE 11(6):e0156720. https://doi.org/10.1371/journal.pone.0156720.

Watt C, Mitchell S, Salewski V. 2010. Bergmann's rule; a concept cluster? Oikos 119(1):89–100. https://doi.org/10.1111/j.1600-0706.2009.17959.x.

Weeks BC, Willard DE, Zimova M, Ellis AA, Witynski ML, Hennen M, Winger BM. 2020. Shared morphological consequences of global warming in North American migratory birds. Ecology Letters 23(2):316–325. https://doi.org/10.1111/ele.13434.

Williams CM, Henry HAL, Sinclair BJ. 2015. Cold truths: how winter drives responses of terrestrial organisms to climate change. Biological Reviews 90(1):214–235. https://doi.org/10.1111/brv.12105.

Wood SN. 2011. Fast stable restricted maximum likelihood and marginal likelihood estimation of semiparametric generalized linear models. Journal of the Royal Statistical Society Series B: Statistical Methodology 73(1):3–36. https://doi.org/10.1111/j.1467-9868.2010.00749.x.

Woodward G, Ebenman B, Emmerson M, Montoya J, Olesen J, Valido A, Warren P. 2005. Body size in ecological networks. Trends in Ecology & Evolution 20(7):402–409. https://doi.org/10.1016/j.tree.2005.04.005.

Yom-Tov Y, Geffen E. 2011. Recent spatial and temporal changes in body size of terrestrial vertebrates: probable causes and pitfalls. Biological Reviews 86(2):531–541. https://doi.org/10.1111/j.1469-185X.2010.00168.x.

Yom-Tov Y, Yom-Tov S, Jarrell G. 2008. Recent increase in body size of the American marten *Martes americana* in Alaska. Biological Journal of the Linnean Society 93(4):701–707. https://doi.org/10.1111/j.1095-8312.2007.00950.x.

Yom-Tov Y, Yom-Tov S, MacDonald D, Yom-Tov E. 2007. Population cycles and changes in body size of the lynx in Alaska. Oecologia 152(2):239–244. https://doi.org/10.1007/s00442-006-0653-3.

Zalewski A, Wereszczuk A, Brzeziński M. 2022. Polecat body size and sex ratio change over time: Impact of invasive competitor or climate warming? Global Ecology and Conservation 35:e02111. https://doi.org/10.1016/j.gecco.2022.e02111.

Supplementary Material

Supplementary Data SD3 for (Theriot et al. 2024): Raw data details, replication of previous studies and supplemental tables

Raw Data Details

Data available at https://osf.io/6wkqf/?view_only=623802cccd494d5694c8defc7d236483

Lynx Specimens

About:

CAT_NO: University of Alaska Museum Mammal Collection catalog number

Note that 9 of these specimens are listed under different identifiers than in (Yom-Tov et al. 2007); originally, they were identified with numbers that are used for internal UAM record-keeping, however, here we use the formal catalog numbers.

Catalog number	Cited by (Yom-Tov et al. 2007) as
UAM:Mamm:100355	33909
UAM:Mamm:100360	33830
UAM:Mamm:100636	33948
UAM:Mamm:100650	34020
UAM:Mamm:100652	34021
UAM:Mamm:100666	33914
UAM:Mamm:100677	33920
UAM:Mamm:100732	33937
UAM:Mamm:100738	34008

YEAR: year of collection

LAT: decimal latitude

LONG: decimal longitude (positive)

SEX: male or female, as determined by collector and/or preparator

AGE: estimated age in years based on cementum-layer analysis conducted at Matson's Laboratory in 2020 (unless otherwise noted)

AGING_CERTAINTY_CODE: degree of confidence in age estimate by Matson's Laboratory technicians. "A" = highest reliability, "B" = reliable within specified range, "C" = error likely, wider potential range

AGE_RANGE: for age estimates ranked B or C, the range of ages estimated to contain the true age

TOOTH_USED: either standard (lower canine) or otherwise specified

AGING_NOTES: other relevant details

GTL: greatest total length of the skull (mm), measured as the maximum distance from the anterior margin of the premaxilla to the posterior margin of the lambdoidal ridge with digital calipers to the nearest 0.01 mm

CPL: condylopremaxillary length (mm), measured as the maximum distance from the anterior margin of the premaxilla to the posterior margin of the occipital condyle with digital calipers to the nearest 0.01 mm

ZB: zygomatic breadth (mm), measured as the maximum skull width with digital calipers that read to the nearest 0.01 mm

IO: interorbital constriction (mm), measured as the minimum distance between the orbits with digital calipers to the nearest 0.01 mm

CAN: canine width (mm), measured as anteroposterior width of the canine tooth closest to the socket (or when the tooth is absent, the inner width of the socket itself) with digital calipers to the nearest 0.01 mm

Marten Specimens

CAT_NO: University of Alaska Museum Mammal Collection catalog number

YEAR: year of collection

LAT: decimal latitude

LONG: decimal longitude (positive)

SEX: male or female, as determined by collector and/or preparator

AGE: estimated age in years based on cementum-layer analysis conducted at Matson's Laboratory in 2020

AGING_CERTAINTY_CODE: degree of confidence in age estimate by Matson's Laboratory technicians. "A" = highest reliability, "B" = reliable within specified range, "C" = error likely, wider potential range

AGE_RANGE: for age estimates ranked B or C, the range of ages estimated to contain the true age

TOOTH_USED: either standard (lower fourth premolar) or otherwise specified

AGING_NOTES: other relevant details.

GTL_YT: greatest total length of the skull (mm), see (Yom-Tov et al. 2008, pg. 703)

ZB_YT: zygomatic breadth (mm), see (Yom-Tov et al. 2008, pg. 703)

PM4_YT: width of the fourth upper premolar (mm), see (Yom-Tov et al. 2008, pg. 703)

CAN_YT: canine width (mm), see (Yom-Tov et al. 2008, pg. 703)

CPL_EM: condylopremaxillary length (mm), measured as the maximum distance from the anterior margin of the premaxilla to the posterior margin of the occipital condyle with digital calipers to the nearest 0.01 mm

The climate data used to calculate climate PC1 are provided in separate sheets; Climate_data_YOC are the values estimated for the year of collection, while Climate_data_YOB includes those for the year of birth. These data were obtained from ClimateNA (Wang et al. 2016), specifically the web version of ClimateWNA, in October 2022. The estimates are based on year (PERIOD), decimal coordinates (LAT and LONG), and elevation (ELEV). Elevation was not reported in the specimen records, so we obtained estimates based on coordinates using the USGS National Map elevation tool (https://apps.nationalmap.gov/elevation/#). These data were not available for five specimens (UAM:Mamm 4195-4199).

REPLICATION ATTEMPT

The attempt at replicating Yom-Tov et al. (2007, 2008) is described below, followed by supplemental figures and tables detailing skull measurements, tests of measurement consistency, as well as the full results of linear and nonlinear models reported in the main text. We would like to note that Yom-Tov et al. (2007, 2008) are relatively unique in providing the metadata necessary to permit this sort of expansion on their research (see Theriot et al. 2023), and that it is only because they have provided catalog numbers and (for the martens) measurement data that our research became possible.

For the lynx, the original researchers georeferenced the majority of the specimens, however, the resulting coordinates were not linked with the specimens in the Arctos database. Therefore, we are using latitude and longitude values published online in Yom-Tov et al.'s (2008) supplementary material. We noticed some errors in these data (11 specimens mapping to locations in which lynx could not occur, such as in water). For these specimens, which are noted in the accompanying data, we used the verbatim locality reported on Arctos to obtain coordinates via GEOLocate (https://www.geo-locate.org/default.html). Specimen maps are provided below (Fig. S3.1).

All analyses were conducted using *R* version 4.2.2 (R Core Team 2022).

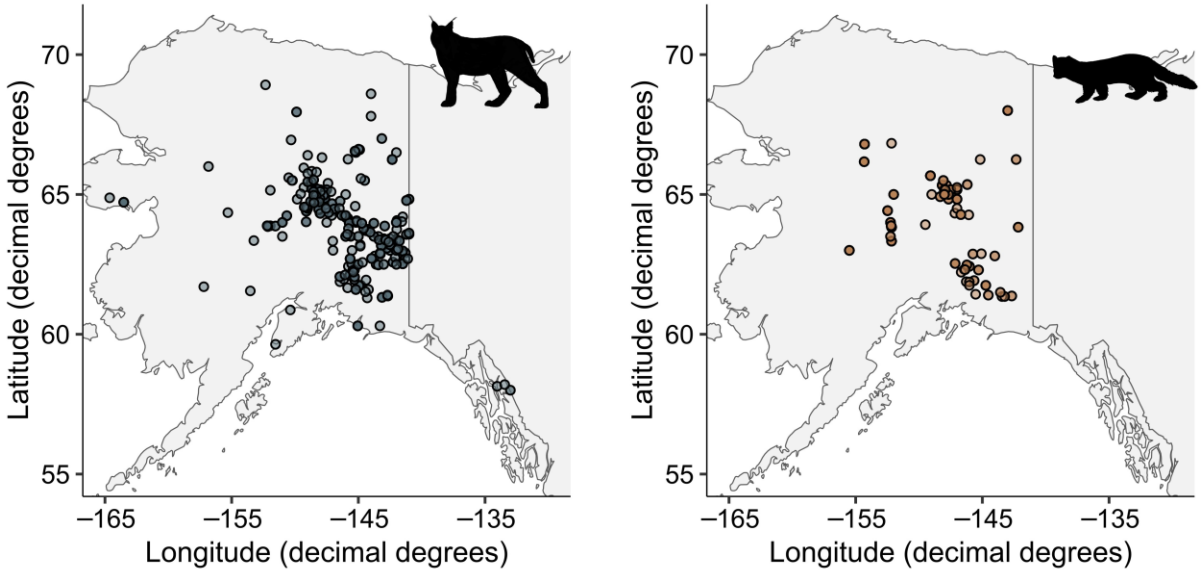


Fig. S3.1. Collection localities for lynx (left) and marten (right) specimens across Alaska. Darker/overlapping points indicate multiple specimens collected at the same locality.

Replication of Yom-Tov et al. (2007) analyses on lynx

The main findings from Yom-Tov et al. (2007) were that lynx skull size is negatively correlated with population size, and that there is some evidence for a decline in skull size over the study period (1953-2000). The authors did not publish their data, so we repeated the skull measurements: greatest total length of the skull (GTL), zygomatic breadth (ZB), width of the

interorbital constriction (IO), and canine width (CAN). Additionally, we measured condylopremaxillary length (CPL), to provide a (potentially) age-insensitive measure of skull size to contrast to other skull dimensions (GTL and ZB) that may change throughout life and thus affect the observed trends over time.

Size PCA.— Yom-Tov et al.'s PCA grouped GTL, ZB, and IO (not log-transformed, see main text for size PCA used in the present study) into a single factor (PC1). They reported an eigenvalue of 2.587 and proportion of variance explained of 86.2%.

To repeat the PCA, the data were edited to only include specimens for which all three of the above measurements were available (GTL, ZB, and IO). Two specimens were removed from this list due to error in the IO or GTL measurement (unrealistically large values). This resulted in 497 total specimens (of the 543 used in the present study, see main text). PCAs were run in *R* version *4.2.2* using the function *prcomp*, which grouped GTL, ZB, and IO into a PC1 that has an eigenvalue of 2.477 and explains 82.57% of the variance (Table S3.1).

Table S3.1.—Standard deviation, proportion of variation explained, and cumulative proportion of variance explained for the three principal components calculated for lynx cranial measurements (GTL, ZB, and IO).

	PC1	**PC2**	**PC3**
Standard deviation	1.574	0.536	0.486
Proportion of variance	0.826	0.096	0.079
Cumulative proportion	0.826	0.921	1.000

Table S3.2.—Loadings of each lynx cranial measurement on the first three principal components.

	PC1	**PC2**	**PC3**
GTL	0.577	-0.599	0.555
ZB	0.583	-0.174	-0.793
IO	0.572	0.782	0.249

Calculating predicted harvest.—For predicted harvest was calculated using the following function, which Yom-Tov et al. (2007) fit using harvest data from 1977-2003 (provided by the Alaska Department of Fish & Game):

sin((YEAR - 1974)*6*3.1415/27-2.89)*727.5+2176.8

Yom-Tov et al. stated (pg. 241): "Preliminary examination showed that year X-3 had the most significant effect on all skull parameters possibly indicating that the average age of our sample is 3 years), and in further tests we used the predicted harvest of this year as a proxy for population size (the percentage values for variation of residual PC1 explained by predicted harvest were 3.8, 9.1, 11.5, 22.2 and 9.9% for years X, X-1, X-2, X-3 and X-4, respectively, and only X-3 was significant at P = 0.0086)."

We calculated the predicted harvest at each time lag point by adjusting the above equation:

sin((YEAR –1–1974)*6*3.1415/27-2.89)*727.5+2176.8

sin((YEAR –2–1974)*6*3.1415/27-2.89)*727.5+2176.8

sin((YEAR –3–1974)*6*3.1415/27-2.89)*727.5+2176.8

sin((YEAR –4–1974)*6*3.1415/27-2.89)*727.5+2176.8

Here, "residual PC1" was considered to correspond with that depicted in Yom-Tov et al.'s Fig. 1 ("corrected for sex, longitude, and year of collection").

PC1~YEAR+ LONG+SEX

Output for lm(PC1~YEAR+ LONG+SEX):

```
Call:
lm(formula = PC1 ~ YEAR + LONG + SEX, data = Lynx_YT_HarvestTest)

Residuals:
    Min      1Q  Median      3Q     Max
-5.0131 -0.8051 -0.0274  0.8738  3.5901

Coefficients:
             Estimate Std. Error t value Pr(>|t|)
(Intercept)  6.709793   7.861252   0.854   0.3938
YEAR        -0.005963   0.003673  -1.623   0.1052
LONG         0.027890   0.014574   1.914   0.0562 .
SEXmale      1.968632   0.110987  17.738   <2e-16 ***
---
Signif. codes:  0 ‘***’ 0.001 ‘**’ 0.01 ‘*’ 0.05 ‘.’ 0.1 ‘ ’ 1

Residual standard error: 1.223 on 492 degrees of freedom
Multiple R-squared:  0.4012,  Adjusted R-squared:  0.3976
F-statistic: 109.9 on 3 and 492 DF,  p-value: < 2.2e-16
```

Next, we fit a series of linear models relating the resulting residuals to predicted harvest in the year of collection, and at each time lag (X-1, X-2, X-3, X-4). One additional specimen with a missing value in LONG was removed (bringing the dataset to 498 total specimens).

The results obtained using this method (Table S3.3) differ from those reported by (Yom-Tov et al. 2007, pg. 241).

Table S3.3.—Relationship between lynx residual size PC1 (corrected for sex, longitude, and year of collection) and predicted harvest estimated 0-4 years before the year of collection. Compare to (Yom-Tov et al. 2007, pg. 241).

Year of predicted harvest (X = year of collection)	**p-value**	**Multiple R^2**
X	0.001	0.022
X-1	0.612	0.0005
X-2	4.11×10^{-5}	0.034
X-3	1.19×10^{-9}	0.072
X-4	1.18×10^{-6}	0.047

It is possible that Yom-Tov et al.'s residual PC1 was corrected for year of collection, such that they averaged the values by year, as in their second multiple linear regression approach explored below. We fit PC1 ~ SEX+LONG, averaged the residuals by year, then fit linear models with predicted harvest at year X, X-1, X-2, X-3, and X-4 as predictors.

Table S3.4.—Relationship between lynx residual size PC1 (corrected for sex and longitude, then averaged by year of collection) and predicted harvest estimated 0-4 years before the year of collection. Compare to (Yom-Tov et al. 2007, pg. 241).

Year of predicted harvest (X = year of collection)	**p-value**	**Multiple R^2**
X	0.244	0.050
X-1	0.873	0.001
X-2	0.350	0.032
X-3	0.110	0.092
X-4	0.135	0.081

These results are still not aligned with those reported by (Yom-Tov et al. 2007), however, the authors may have used a different method to assess this relationship.

Linear models.— Yom-Tov et al. stated, "The data were analysed using two approaches. With the first, we used multiple regressions to test whether latitude, longitude, sex, year of collection and predicted harvest (at year X-3) affected the four skull parameters and PC1 of all individuals. Predicted harvest is the number of lynx estimated by the calculated cycle to be trapped at year X-3. With the second approach, we used multiple regressions to examine the effects of harvest data and year of collection on yearly means of the residual skull data corrected for sex and longitude

(parameters that were found to affect at least one skull parameter significantly)." (Yom-Tov et al. 2007, pg. 241)

We attempted Yom-Tov et al.'s approach 1 by fitting multiple linear regression models relating each of the original measurements (GTL, ZB, IO, Canine) and PC1 to year, sex, latitude, longitude, and predicted harvest at year X-3 (Table S3.5) Based on Yom-Tov et al.'s Table 1 (Yom-Tov et al. 2007, pg. 242) N varied by measurement, so the original data were used with NAs left in.

Table S3.5.—Replication of Yom-Tov et al.'s (2007) first linear model approach on lynx cranial measurements. Predicted harvest (Harvest) was estimated for three years prior to the year of collection (Year). Underlined p-values are statistically significant. Coefficients (b) that differ from Yom-Tov et al.'s by >5% are marked with * and p-values that lead to a different conclusion (i.e., statistically significant when Yom-Tov et al. found no relationship, or vice versa) are marked with †. Compare to Table 1 in (Yom-Tov et al. 2007).

	GTL	**ZB**	**IO**	**CAN**	**PC1**
Intercept	166.4	108.9	47.148	23.16*	13.597*
Sex, b	6.600	3.368	1.457	0.508*	1.748*
p	< 0.001	< 0.001	< 0.001	< 0.001	< 0.001
Year, b	-0.021*	-0.011*	-0.011	-0.007*	-0.008*
p	0.041†	0.272	0.009	< 0.001†	0.024
Latitude, b	0.028*	-0.047*	-0.034*	-0.053*	-0.007*
p	0.796	0.657	0.460	0.001†	0.866
Longitude, b	0.021*	0.057*	0.051	0.008*	0.026*
p	0.624	0.156	0.004	0.203	0.082†
Harvest, b	-0.002	-0.002	-0.0009*	-8.807×10^{-5}*	-0.0008*
p	< 0.001	< 0.001	< 0.001	0.072†	< 0.001
N	527	512	533	527	496
R^2	0.539	0.292	0.304	0.300	0.444
F-statistic	121.7	43.21	47.42	32.40	80.07
p	< 0.001	< 0.001	< 0.001	< 0.001	< 0.001

These results (Table S3.5) are fairly similar to Yom-Tov et al.'s findings. Notably, there is a significant decline in IO and PC1 over time which is similar in magnitude to the original reported results; however, there are also significant declines in canine and GTL.

Yom-Tov et al. (2007) employed a second approach to multiple linear regression models: "With the second approach, we used multiple regressions to examine the effects of harvest data and year of collection on yearly means of the residual skull data corrected for sex and longitude (parameters that were found to affect at least one skull parameter significantly). The second

approach was used in order to avoid the problem of varied sample sizes among years" (Yom-Tov et al. 2007, pg. 241). To replicate these methods, we first fit X ~ SEX + LONG (X = GTL, ZB, IO, or PC1) then averaged the residuals by year. Using the resulting values as the response, linear models were fit with year of collection and predicted harvest three years prior as predictors (Table S3.6).

Table S3.6.—Replication of Yom-Tov et al.'s (2007) second linear model approach of residual lynx cranial measurements (corrected for sex and longitude) averaged by year. Predicted harvest (Harvest) was estimated for three years prior to the year of collection (Year). Underlined p-values are statistically significant. Coefficients (b) that differ from Yom-Tov et al.'s by >5% are marked with * and p-values that lead to a different conclusion (i.e., statistically significant when Yom-Tov et al. found no relationship, or vice versa) are marked with †. Compare to Table 2 in (Yom-Tov et al. 2007).

	GTL	**ZB**	**IO**	**CAN**	**PC1**
Intercept	73.765*	59.133*	34.215*	15.419*	30.269*
Year, b	-0.036*	-0.029*	-0.017*	-0.008*	-0.015*
p	0.014	0.135†	0.012	0.022†	0.041
Harvest, b	-0.001	-0.001	-0.0006*	-0.0002*	-0.0004*
p	0.009	0.136†	0.007	0.129	0.071†
N	30	30	29	30	29
R^2	0.345	0.144	0.365	0.229	0.229
F statistic	7.128	2.271	7.464	4.014	3.867
p	0.003	0.123	0.003	0.030	0.034

Replication of Yom-Tov et al. (2008) analyses on martens

Climate PCA.—Yom-Tov et al. (2008) were interested in the role of resource availability as a driver of body-size trends. They reported using net primary productivity (NPP) as a proxy for resource availability; however, these data were not published, and we were unable to obtain them from the researcher Yom-Tov et al. credited, nor were we able to locate a different dataset covering the same temporal and spatial scope. Therefore, as a proxy for NPP (and by extension, resource availability), we calculated the first principal component of average spring temperature, average summer temperature, spring precipitation, and summer precipitation, using data from the ClimateNA model (Wang et al. 2016), specifically the online version of ClimateWNA. These climate variables—temperature and precipitation during the growing season—have been shown to be correlated with NPP in forest ecosystems (Del Grosso et al. 2008; Tang et al. 2010).

The ClimateNA model also requires elevation, which was not recorded for any of the specimens in this sample. Therefore, elevation was estimated using the USGS National Map Elevation Tool based on latitude and longitude. There were 5 specimens (UAM:Mamm 4195, 4196, 4197, 4198,

and 4199) for which elevation for their coordinates was not available (came back as “invalid”), so these were omitted.

ClimateNA seasonal variables:

Tave_sp = mean spring temperature (°C)

Tave_sm = mean summer temperature (°C)

PPT_sp = spring precipitation (mm)

PPT_sm = summer precipitation (mm)

Spring = March, April, May; Summer = June, July, August

For each specimen, we obtained these data for the collection locality in both the year of collection and estimated year of birth, to contrast the relative contributions of these two variables in a model of marten body size.

The first principal component of the four climate variables above (Table S3.7, SD3.8) was calculated such that two sets of data were included for each specimen, one for year of birth and one for year of collection. This ensures that climate PC1 is standardized between the models that include year of birth and those that include year of collection.

Table S3.7.—Standard deviation, proportion of variation explained, and cumulative proportion of variance explained for the four principal components calculated for climate variables (estimated mean temperature and precipitation for both spring and summer) in the year of collection and estimated year of birth.

	PC1	**PC2**	**PC3**	**PC4**
Standard deviation	1.428	1.073	0.660	0.611
Proportion of var.	0.510	0.288	0.109	0.093
Cumulative var.	0.510	0.798	0.907	1.000

Table S3.8.—Loadings of each climate variable on the four principal components.

	PC1	**PC2**	**PC3**	**PC4**
Ave. spring temp.	-0.187	0.852	-0.234	0.429
Ave. summer temp.	-0.572	0.270	0.641	-0.435
Spring precip.	0.590	0.144	0.709	0.359
Summer precip.	0.539	0.425	-0.178	-0.705

Climate PC1 is negatively correlated with average temperatures in spring and summer, positively correlated with spring and summer precipitation (i.e., high PC1 = cold and wet, low PC1 = hot and dry; Table S3.8) and explains 51.0% of the variance (Table S3.7).

Size PCA.—Yom-Tov et al. (2008) performed principal component analysis on four measurements–greatest total length of the skull (GTL), zygomatic breadth (ZB), width of fourth upper premolar (PM4), and width of upper canine (CAN). They reported that "PC1 clumped the two skull measurements (GTL and ZB) and PC2 the two teeth measurements (PM4 and canine) into two variables. Eigenvalues were 2.903 and 0.789, and the proportions of variance explained by these factors were 72.6% and 19.7%, respectively" (Yom-Tov et al. 2008, pg. 703).

Table S3.9.—Standard deviation, proportion of variation explained, and cumulative proportion of variance explained for the four principal components calculated for marten skull measurements: GTL, ZB, CAN, and PM4, all log-transformed as in (Yom-Tov et al. 2008).

	PC1	**PC2**	**PC3**	**PC4**
Standard deviation	1.705	0.887	0.420	0.364
Proportion of var.	0.726	0.197	0.044	0.033
Cumulative var.	0.726	0.923	0.967	1.000

Table S3.10.—Loadings of each log-transformed marten skull measurement on the four principal components.

	PC1	PC2	PC3	PC4
Log(GTL)	0.516	-0.412	0.617	-0.427
Log(ZB)	0.479	-0.572	-0.626	0.227
Log(PM4)	0.525	0.388	0.300	0.695
Log(CAN)	0.477	0.593	-0.370	-0.532

Our results indicate that although the proportion of variance explained by PC1 and PC2 (72.6% and 19.7%, respectively; Table S3.9) are similar to Yom-Tov et al.'s results, these findings do not agree with the authors' interpretation that PC1 represents the skull measurements while PC2 represent tooth measurements. Here, all four log-transformed measurements are approximately equally positively correlated with PC1. PC2 is negatively related to the skull measurements and positively related to the tooth measurements, but the magnitude of these loadings does not indicate that the tooth measurements have a greater influence (Table S3.10).

Linear models with year of collection climate data.—Yom-Tov et al. (2008) fit multiple linear regression models to the first two principal components that they calculated for the skull measurements. They tested for the effects of sex, year, latitude, longitude, and net primary productivity, and all possible two- and three-way interactions (except those with NPP, and the

lat-long interaction): sex*year, sex*latitude, year*latitude, sex*year*latitude, sex*longitude, year*longitude, sex*year*longitude.

We attempted to repeat these models, replacing NPP with our climate PC1 for year of collection, then compared to year of birth.

Table S3.11.—Results of linear model approach described by (Yom-Tov et al. 2008) on the first principal component of marten skull measurements (Size PC1). Instead of NPP, here we use the first principal component of estimated spring and summer temperature and precipitation during the year of collection. Compare to Table 1 in (Yom-Tov et al. 2008).

Size PC1			
Term	Estimate (b)	t-value	p-value
Intercept	-579.6	-0.447	0.655
Sex	261.0	0.170	0.865
Year	0.2886	0.441	0.659
Sex × Year	-0.1319	-0.170	0.865
Latitude	-6.205	-0.532	0.595
Sex × Latitude	-4.394	-0.306	0.759
Year × Latitude	3.154×10^{-3}	0.536	0.592
Sex × Year × Latitude	2.239×10^{-3}	0.310	0.757
Longitude	6.213	1.355	0.176
Sex × Longitude	0.102	0.018	0.986
Year × Longitude	-3.122×10^{-3}	-1.346	0.179
Sex × Year × Longitude	-5.003×10^{-5}	-0.017	0.986
Climate PC1 (Year of collection)	-9.842×10^{-3}	-0.230	0.818
R^2	0.6295		
$F_{12, 372}$	55.37		$< 2.2\times10^{-16}$

The model is significant over all ($F_{12, 372} = 55.37$, $p < 0.001$) and explains 62.95% of variance in size PC1 (comparable to the 64.2% reported by Yom-Tov et al.; Table S3.11). However, none of the predictors are statistically significant, which suggests that the model terms are each accounting for nearly the same variation (i.e., multicollinearity). In other words, these results suggest that the interaction terms are not contributing to the model beyond what their constituent predictors already explain. The rationale behind including the many two- and three-way interactions is unclear and there was not a model-selection process described in the original paper. Thus, we also fit a simplified model with no interactions:

SIZE_PC1 ~ SEX + YEAR + LAT + LONG + CLIM_PC1

Table S3.12.—Results of a simplified linear model based on the approach described by (Yom-Tov et al. 2008) on the first principal component of marten skull measurements (Size PC1). Instead of NPP, here we use the first principal component of estimated spring and summer temperature and precipitation during the year of collection. Compare to Table 1 in (Yom-Tov et al. 2008).

Size PC1			
Term	Estimate (b)	t-value	p-value
Intercept	-79.008	-7.914	2.76×10^{-14}
Sex	2.654	24.481	$< 2\times10^{-16}$
Year	0.032	8.533	3.47×10^{-16}
Latitude	0.0320	0.711	0.477
Longitude	0.081	3.975	8.44×10^{-5}
Climate PC1 (Year of collection)	-0.002	-0.049	0.961
R^2	0.623		
$F_{5,379}$	127.7		$< 2.2\times10\times10^{-16}$

This model is statistically significant ($F_{5,379} = 127.7$, $p < 0.001$), explains approximately the same amount of variation in size PC1 (62.26%), and indicates the same conclusions that Yom-Tov et al. reported: males are larger than females, size increased significantly over the study period and with longitude (east to west) (Table S3.12). Comparing the two models with AIC indicates that both fit the data equally well (more complex model AIC = 1135.724, simpler model AIC = 1135.953).

The results are similar for size PC2 (Table S3.13, SD3.14), which Yom-Tov et al. found primarily captures tooth measurements, width of canine and width of fourth upper premolar. In contrast, we found that size PC2 was negatively correlated with both log-GTL and log-ZB, and positively correlated with the tooth measurements, but less strongly (Table S3.10); this may represent individuals that have bigger teeth compared to the overall size of the skull, whereas PC1 is correlated with having a bigger skull overall including teeth.

Table S3.13.—Results of linear model approach described by (Yom-Tov et al. 2008) on the second principal component of marten skull measurements (Size PC2). Instead of NPP, here we use the first principal component of estimated spring and summer temperature and precipitation during the year of collection. Compare to Table 1 in (Yom-Tov et al. 2008).

Size PC2			
Term	Estimate (b)	t-value	p-value
Intercept	-215.5	-0.217	0.828
Sex	-1.672×10^{-3}	-1.421	0.156
Year	0.106	0.212	0.832
Sex × Year	0.839	1.415	0.158
Latitude	-6.139	-0.688	0.492
Sex × Latitude	17.22	1.570	0.117
Year × Latitude	3.127×10^{-3}	0.695	0.487
Sex × Year × Latitude	-8.665×10^{-3}	-1.568	0.118
Longitude	4.039	1.152	0.250
Sex × Longitude	3.793	0.878	0.380
Year × Longitude	-2.031×10^{-3}	-1.144	0.253
Sex × Year × Longitude	-1.897×10^{-3}	-0.867	0.386
Climate PC1	-7.283×10^{-4}	-0.022	0.982
(Year of collection)			
R^2	0.224		
$F_{12, 372}$	8.926		$\underline{4.484\times10^{-15}}$

Table S3.14.—Results of a simplified linear model based on the approach described by (Yom-Tov et al. 2008) on the second principal component of marten skull measurements (Size PC2). Instead of NPP, here we use the first principal component of estimated spring and summer temperature and precipitation during the year of collection. Compare to Table 1 in (Yom-Tov et al. 2008).

Size PC2			
Term	Estimate (b)	t-value	p-value
Intercept	-25.872	-3.380	$\underline{0.0008}$
Sex	-0.622	-7.487	$\underline{4.99\times10^{-13}}$
Year	0.006	2.174	$\underline{0.030}$
Latitude	0.052	1.496	0.1355
Longitude	0.070	4.477	$\underline{1.00\times10^{-5}}$
Climate PC1	0.015	0.473	0.636
(Year of collection)			

R^2	0.180	
$F_{5,379}$	17.87	6.474×10^{-16}

As with size PC1, the significant predictors in the simplified model are sex, year, and longitude (Table S3.14). Yom-Tov et al. also reported a significant year-longitude interaction for size PC2, so we also tested this response in a simpler model:

Table S3.15.—Results of a simplified linear model based on the approach described by (Yom-Tov et al. 2008) on the second principal component of marten skull measurements (Size PC2), including the interaction between year and longitude. Instead of NPP, here we use the first principal component of estimated spring and summer temperature and precipitation during the year of collection. Compare to Table 1 in (Yom-Tov et al. 2008).

Size PC2			
Term	Estimate (b)	t-value	p-value
Intercept	-909.1	-3.400	0.0007
Sex	-0.622	-7.578	2.72×10^{-13}
Year	0.454	3.350	0.0009
Latitude	0.083	2.340	0.0198
Longitude	6.016	3.343	0.0009
Climate PC1 (Year of collection)	-8.105×10^{-4}	-0.026	0.979
Year × Longitude	-3.020×10^{-3}	-3.304	0.001
R^2	0.201		
$F_{6,\ 378}$	17.1		6.474×10^{-16}

Our results also indicate a statistically significant year-longitude interaction (Table S3.15), the difference being that year on its own was not significant in Yom-Tov et al.'s size PC2 model, but is here, indicating that size PC2 has increased significantly over the study period. Additionally, Yom-Tov et al. found a negative correlation between size PC2 and longitude (which they propose may indicate that inland martens eat larger prey) but here we find a positive relationship that weakens over time (negative year-longitude interaction). Comparing these three models with AIC suggests that the simplified model including the year-longitude interaction fits the data better than either the complex model or the simple model without any interactions (AIC = 922.381, 929.422, 931.343 respectively).

Linear models with year of birth climate data.—Yom-Tov et al. (2008) conclude the paper by stating "we suggest that the lack of a significant relationship between NPP and body size was

due to the fact that we did not know the ages of our specimens, and thus could not fit NPP data of year of birth to any of them" (Yom-Tov et al. 2008, pg. 706). To test this prediction, we fit the same models described above with climate PC1 for year of birth (Table S3.16, SD3.17). The year of collection predictor was also replaced with year of birth (YEAR_ in code) in an attempt to capture any other environmental variation that may have occurred over time.

Table S3.16.—Results of linear model approach described by (Yom-Tov et al. 2008) on the first principal component of marten skull measurements (Size PC1). Instead of NPP, here we use the first principal component of estimated spring and summer temperature and precipitation during the estimated year of birth. Compare to Table 1 in (Yom-Tov et al. 2008).

Size PC1			
Term	Estimate (b)	t-value	p-value
Intercept	-1.025×10^{-3}	-0.828	0.4084
Sex	441.4	0.292	0.7703
Year of birth	0.514	0.823	0.4110
Sex × Year	-0.223	-0.292	0.7705
Latitude	-2.920	-0.256	0.7979
Sex × Latitude	-6.057	-0.425	0.6709
Year × Latitude	1.504×10^{-3}	0.262	0.7938
Sex × Year × Latitude	3.070×10^{-3}	0.427	0.6694
Longitude	7.786	1.736	0.0834
Sex × Longitude	-0.373	-0.066	0.948
Year × Longitude	-3.927×10^{-3}	-1.728	0.0847
Sex × Year × Longitude	1.899×10^{-4}	0.066	0.9474
Climate PC1	-0.059	-1.401	0.1620
(Year of birth)			
R^2	0.626		
$F_{12, 372}$	54.52		$< 2.2\times10^{-16}$

Table S3.17.—Results of a simplified linear model based on the approach described by (Yom-Tov et al. 2008) on the first principal component of marten skull measurements (Size PC1). Instead of NPP, here we use the first principal component of estimated spring and summer temperature and precipitation during the estimated year of birth. Compare to Table 1 in (Yom-Tov et al. 2008).

Size PC1			
Term	Estimate (b)	t-value	p-value
Intercept	-73.996	-7.310	1.60×10^{-12}
Sex	2.641	24.257	$< 2\times10^{-16}$
Year of birth	0.031	8.053	1.06×10^{-14}
Latitude	0.021	0.480	0.6311
Longitude	0.068	3.371	0.0008
Climate PC1 (Year of birth)	-0.064	-1.568	0.1178
R^2	0.619		
$F_{5,379}$	125.6		$< 2.2\times10^{-16}$

Although the p-value is lower for climate PC1 in the year of birth than it was for year of collection, it is still not statistically significant.

Replacing climate PC1 in year of collection with climate PC1 in the year of birth for models of size PC2 yields similar results (Table S3.18, SD3.19).

Table S3.18.—Results of linear model approach described by (Yom-Tov et al. 2008) on the second principal component of marten skull measurements (Size PC2). Instead of NPP, here we use the first principal component of estimated spring and summer temperature and precipitation during the year of birth. Compare to Table 1 in (Yom-Tov et al. 2008).

Size PC2			
Term	Estimate (b)	t-value	p-value
Intercept	-264.1	-0.280	0.779
Sex	-1.480×10^{-3}	-1.287	0.199
Year of birth	0.131	0.275	0.784
Sex × Year	0.742	1.279	0.202
Latitude	-5.492	-0.633	0.527
Sex × Latitude	16.400	1.513	0.131
Year × Latitude	2.804×10^{-3}	0.641	0.522
Sex × Year × Latitude	-8.266×10^{-3}	-1.512	0.131
Longitude	4.076	1.194	0.233
Sex × Longitude	2.827	0.655	0.513

Year × Longitude	-2.052×10^{-3}	-1.187	0.236
Sex × Year × Longitude	-1.405×10^{-3}	-0.642	0.521
Climate PC1	-0.023	-0.731	0.465
(Year of birth)			
R^2	0.199		
$F_{12, 372}$	8.935		4.304×10^{-15}

Table S3.19.—Results of a simplified linear model based on the approach described by (Yom-Tov et al. 2008) on the second principal component of marten skull measurements (Size PC2), including the interaction between year and longitude. Instead of NPP, here we use the first principal component of estimated spring and summer temperature and precipitation during the year of birth. Compare to Table 1 in (Yom-Tov et al. 2008).

Size PC2			
Term	Estimate (b)	t-value	p-value
Intercept	-838.3	-3.063	0.0024
Sex	-0.622	-7.584	2.62×10^{-13}
Year of birth	0.418	3.017	0.0027
Latitude	0.079	2.223	0.0268
Longitude	5.520	2.999	0.0029
Climate PC1	-0.021	-0.679	0.4976
(Year of birth)			
Year × Longitude	-2.770×10^{-3}	-2.962	0.0033
R^2	0.202		
$F_{6, 378}$	17.17		< 2.2e-16

Comparing the simplified models (including the year-longitude interaction term) by AIC shows that for both size PC1 and PC2, the year of birth models do not fit the data better than the year of collection models; for size PC1, AIC for year of birth and year of collection are 1140.077 and 1135.953 respectively, for size PC2, 922.0716 and 922.3806 respectively.

SUPPLEMENTAL TABLES

Skull measurements repeatability test.—For the present study, one of us (MKT) took all lynx skull measurements, repeating those used by (Yom-Tov et al. 2007). To assess consistency in measurement, a set of ten skulls were measured 15 times across several sessions. At the start of each measurement round (i.e., starting over at the first skull), all previous measurements were hidden to avoid bias. To quantify within- and among-specimen variation, intraclass correlation coefficient (ICC) was calculated for each measurement with catalog number as the grouping variable (Table S3.20). These values were obtained using the *R* package *ICC* (Wolak et al. 2012).

Table S3.20.—Intraclass correlation estimates for lynx skull measurements, calculated for 15 repeats on a set of 10 skulls. Estimates closer to 1, smaller confidence intervals, and minimized within-group variance relative to among-group variance indicate greater consistency in measurement.

Measurement	ICC estimate [95% Confidence interval]	Variance within groups	Variance among groups
GTL	0.999 [0.999, 1.000]	0.017	28.191
CPL	1.000 [0.999, 1.000]	0.009	20.727
ZB	0.998 [0.995, 1.000]	0.028	13.482
IO	0.995 [0.989, 0.999]	0.012	2.444
CAN	0.948 [0.893, 0.894]	0.007	0.124

Full Linear Model Results

Lynx.—

Conditions Models.–*Assess the role of conditions in the year of birth, including predicted harvest estimated for the year of birth.*

Model structure: Log(size measurement) ~ $Year_{birth}$ + Sex + Lat + Long + $PredictedHarvest_{birth}$

Table S3.21.—Results for the conditions linear model structure across lynx skull measurements. Coefficient estimates (b) are followed by the corresponding p-values (*p*), for which statistically significant results are underlined. These models include predicted harvest in the estimated year of birth ($Harvest_{yob}$) calculated using the equation reported by (Yom-Tov et al. 2007).

	GTL	ZB	IO	CAN	PC1	CPL
Intercept	5.090	4.839	4.163	4.301	24.901	5.101
Sex_{male}, b	0.056	0.043	0.059	0.072	2.180	0.056
p	<u>< 0.001</u>	<u>< 0.001</u>	<u>< 0.001</u>	<u>< 0.001</u>	<u>< 0.001</u>	<u>< 0.001</u>
$Year_{birth}$, b	-0.0002	-0.0002	-0.001	-0.001	-0.015	-0.0002
p	<u>0.034</u>	<u>0.035</u>	<u>< 0.001</u>	<u>< 0.001</u>	<u>< 0.001</u>	<u>0.016</u>
Latitude, b	0.0006	0.0001	-4.492×10^{-6}	-0.007	-0.015	-0.0001
p	0.500	0.924	0.998	<u>0.001</u>	0.728	0.900
Longitude, b	0.0001	0.001	0.002	0.001	0.024	2.104×10^{-5}
p	0.700	0.241	<u>0.014</u>	0.253	0.141	0.949
$Harvest_{yob}$, b	8.26×10^{-6}	2.927×10^{-6}	4.437×10^{-6}	3.162×10^{-6}	0.0002	7.322×10^{-6}
p	<u>0.007</u>	0.460	0.431	0.661	0.113	<u>0.016</u>

N	527	512	533	527	485	516
Adj. R^2	0.512	0.268	0.267	0.246	0.430	0.519
F statistic	111.3	38.47	39.68	35.37	73.97	112.0
p	< 0.001	< 0.001	< 0.001	< 0.001	< 0.001	< 0.001

Age-Growth Models.–Assess how including age affects models of size trends over time based on conditions in the year of collection, i.e., the data that are most readily available for the majority of body-size studies.

Model structure:

Log (size measurement) ~ $Year_{collection}$ + Sex + Age + Lat + Long + $PredictedHarvest_{collection}$

Table S3.22.—Results for the age-growth linear model structure across lynx skull measurements. Coefficient estimates (b) are followed by the corresponding p-values (*p*), for which statistically significant results are underlined. These models include predicted harvest in the year of collection ($Harvest_{yoc}$) calculated using the equation reported by (Yom-Tov et al. 2007).

	GTL	**ZB**	**IO**	**CAN**	**PC1**	**CPL**
Intercept	4.915	4.421	3.491	3.907	12.648	4.923
Sex_{male}, b	0.051	0.036	0.049	0.069	1.929	0.052
p	< 0.001	< 0.001	< 0.001	< 0.001	< 0.001	< 0.001
$Year_{col}$, b	-6.769×10^{-5}	-1.194×10^{-6}	-1.938×10^{-4}	-0.001	-0.008	-9.113×10^{-5}
p	0.379	0.990	0.133	< 0.001	0.017	0.233
Latitude, b	0.0002	-0.0003	4.514×10^{-5}	-0.004	-0.028	-2.979×10^{-4}
p	0.801	0.777	0.974	0.017	0.447	0.719
Longitude, b	-4.277×10^{-5}	0.0002	0.001	0.0005	0.013	-1.270×10^{-4}
p	0.893	0.546	0.059	0.523	0.322	0.686
Age, b	0.004	0.008	0.012	0.009	0.317	0.004
p	< 0.001	< 0.001	< 0.001	< 0.001	< 0.001	< 0.001
$Harvest_{yoc}$, b	1.312×10^{-5}	1.426×10^{-5}	1.801×10^{-5}	-9.977×10^{-6}	0.0005	9.912×10^{-6}
p	< 0.001	< 0.001	< 0.001	0.094	< 0.001	< 0.001
N	527	512	533	527	485	516
R^2	0.569	0.473	0.485	0.308	0.596	0.569
F statistic	116.9	77.44	84.51	39.96	119.9	114.5
p	< 0.001	< 0.001	< 0.001	< 0.001	< 0.001	< 0.001

Combination Models.–Assess the role of conditions in the year of birth, including predicted harvest estimated for the year of birth, while also correcting for age.

Model structure:

Log(size measurement) ~ $Year_{birth}$ + Sex + Age + Lat + Long + Age + $PredictedHarvest_{birth}$

Table S3.23.—Results for the combination linear model structure across lynx skull measurements. Coefficient estimates (b) are followed by the corresponding p-values (*p*), for which statistically significant results are underlined. These models include predicted harvest in the estimated year of birth ($Harvest_{yob}$) calculated using the equation reported by (Yom-Tov et al. 2007).

	GTL	**ZB**	**IO**	**CAN**	**PC1**	**CPL**
Intercept	4.887	4.395	3.469	3.880	10.932	4.902
Sex_{male}, b	0.053	0.039	0.052	0.067	2.001	0.053
p	< 0.001	< 0.001	< 0.001	< 0.001	< 0.001	< 0.001
$Year_{birth}$, b	-7.608×10^{-5}	-1.392×10^{-5}	-2.140×10^{-4}	-0.001	-0.008	-9.693×10^{-5}
p	0.332	0.882	0.102	< 0.001	0.018	0.208
Latitude, b	0.001	0.001	0.001	-0.006	0.002	1.949×10^{-4}
p	0.268	0.459	0.399	0.003	0.962	0.811
Longitude, b	-7.085×10^{-6}	0.0002	0.001	0.001	0.015	-1.084×10^{-4}
p	0.982	0.535	0.051	0.499	0.285	0.732
Age, b	0.004	0.008	0.012	0.008	0.299	0.004
p	< 0.001	< 0.001	< 0.001	< 0.001	< 0.001	< 0.001
$Harvest_{yob}$, b	9.703×10^{-6}	6.635×10^{-6}	9.580×10^{-6}	6.575×10^{-6}	0.0004	8.754×10^{-6}
p	0.001	0.054	0.047	0.344	0.005	0.002
N	527	512	533	527	485	516
R^2	0.555	0.452	0.470	0.305	0.585	0.563
F statistic	110.1	71.17	79.5	39.5	114.9	111.6
p	< 0.001	< 0.001	< 0.001	< 0.001	< 0.001	< 0.001

Model Comparison by AIC.–Model comparison by AIC indicates that age-growth models are consistently better for lynx, regardless of body-size measurement (Table S3.24).

Table S3.24.—Comparison of three linear models described above (Table S3.21-23) by Akaike Information Criterion (AIC). The number of estimated fixed effect parameters per model (K), the difference in AIC between a given model and the best-fitting model for a given measurement (ΔAIC), and corresponding Akaike weights are also included.

Measurement	**Model**	**K**	**AIC**	**ΔAIC**	**Akaike weight**
Greatest length	Age-growth	8	-2348.66	0.00	1.00

	Combination	8	-2330.68	17.98	0.00
	Conditions	7	-2283.89	64.77	0.00
Constrained length	Age-growth	8	-2312.46	0.00	0.98
	Combination	8	-2304.89	7.57	0.02
	Conditions	7	-2256.03	56.43	0.00
Skull width	Age-growth	8	-2111.79	0.00	1.00
	Combination	8	-2091.57	20.22	0.00
	Conditions	7	-1944.79	167.01	0.00
Interorbital width	Age-growth	8	-1823.08	0.00	1.00
	Combination	8	-1807.34	15.74	0.00
	Conditions	7	-1635.62	187.47	0.00
Canine width	Age-growth	8	-1404.32	0.00	0.72
	Combination	8	-1402.39	1.93	0.28
	Conditions	7	-1360.51	43.82	0.00
Size PC1	Age-growth	8	1457.50	0.00	1.00
	Combination	8	1469.81	12.32	0.00
	Conditions	7	1623.28	165.78	0.00

Martens.—

Conditions Models.–Assess the role of conditions in the year of birth, including climate PC1 estimated for the year of birth.

Model structure: Log(size measurement) ~ $Year_{birth}$ + Sex + Lat + Long + $Climate_{birth}$

Table S3.25.—Results for the conditions linear model structure across marten skull measurements. Coefficient estimates (b) are followed by the corresponding p-values (*p*), for which statistically significant results are underlined. These models include climate PC1 calculated for the estimated year of birth ($Climate_{yob}$). For details, refer to the main text and/or the "Replication of Yom-Tov et al. (2008) analyses on martens" section of this document.

	GTL	**ZB**	**PM4**	**CAN**	**PC1**	**CPL**
Intercept	3.842	1.611	-2.742	-7.939	-73.996	4.237
Sex_{male}, b	0.096	0.110	0.116	0.159	2.641	0.091
p	< 0.001	< 0.001	< 0.001	< 0.001	< 0.001	< 0.001

$Year_{birth}$, b	0.0003	0.001	0.002	0.003	0.031	0.0001
p	0.002	< 0.001	< 0.001	< 0.001	< 0.001	0.236
Latitude, b	-0.002	0.002	0.002	0.015	0.021	-0.002
p	0.071	0.269	0.501	0.024	0.631	0.023
Longitude, b	0.0003	-0.002	0.006	0.012	0.068	0.0003
p	0.524	0.025	< 0.001	< 0.001	< 0.001	0.479
$Climate_{yob}$, b	-0.002	-0.003	-0.004	-0.002	-0.064	-0.002
p	0.099	0.093	0.180	0.708	0.118	0.089
N	429	427	404	407	385	416
Adj. R^2	0.745	0.579	0.366	0.224	0.619	0.760
F statistic	251.6	118.2	47.57	24.5	125.6	264.4
p	< 0.001	< 0.001	< 0.001	< 0.001	< 0.001	< 0.001

Age-Growth Models.–Assessing how including age affects models of size trends over time based on conditions in the year of collection, i.e., the data that are most readily available for the majority of body-size studies.

Model structure:

Log (size measurement) ~ $Year_{collection}$ + Sex + Age + Sex:Age + Lat + Long + $Climate_{collection}$

Table S3.26.—Results for the age-growth linear model structure across marten skull measurements. Coefficient estimates (b) are followed by the corresponding p-values (*p*), for which statistically significant results are underlined. These models include climate PC1 calculated for the year of collection ($Climate_{yoc}$). For details, refer to the main text and/or the "Replication of Yom-Tov et al. (2008) analyses on martens" section of this document.

	GTL	**ZB**	**PM4**	**CAN**	**PC1**	**CPL**
Intercept	3.926	2.162	-2.892	-8.419	-72.162	4.293
Sex_{male}, b	0.089	0.093	0.121	0.166	2.533	0.087
p	< 0.001	< 0.001	< 0.001	< 0.001	< 0.001	< 0.001
$Year_{collect}$, b	0.0002	0.001	0.002	0.003	0.029	< 0.001
p	0.018	< 0.001	< 0.001	< 0.001	< 0.001	0.416
Latitude, b	-0.002	0.0005	0.003	0.017	0.013	-0.002
p	0.104	0.780	0.425	0.014	0.776	0.028
Longitude, b	0.001	-0.001	0.007	0.014	0.083	0.0004
p	0.235	0.064	< 0.001	< 0.001	< 0.001	0.408

Age, b	-0.0003	0.006	0.001	0.001	0.066	-0.0005
p	0.805	< 0.001	0.729	0.884	0.145	0.676
Age:Sex_m, b	0.008	0.020	-0.005	-0.007	0.133	0.004
p	< 0.001	< 0.001	0.379	0.494	0.061	0.016
$Climate_{yoc}$, b	< 0.001	-0.001	-0.0004	0.007	-0.002	-0.001
p	0.995	0.318	0.896	0.271	0.954	0.241
N	429	427	404	407	385	416
Adj. R^2	0.759	0.700	0.362	0.224	0.635	0.763
F statistic	194	143	33.63	17.71	96.37	192.1
p	< 0.001	< 0.001	< 0.001	< 0.001	< 0.001	< 0.001

Combination Models.–Assess the role of conditions in the year of birth, including climate PC1 estimated for the year of birth, while also correcting for age.

Model structure:

Log(size measurement) ~ $Year_{birth}$ + Sex + Age + Sex:Age + Lat + Long + Age + $Climate_{birth}$

Table S3.27.—Results for the age-growth linear model structure across marten skull measurements. Coefficient estimates (b) are followed by the corresponding p-values (*p*), for which statistically significant results are underlined. These models include climate PC1 calculated for estimated year of birth ($Climate_{yob}$). For details, refer to the main text and/or the "Replication of Yom-Tov et al. (2008) analyses on martens" section of this document.

	GTL	**ZB**	**PM4**	**CAN**	**PC1**	**CPL**
Intercept	3.986	2.192	-2.758	-7.972	-69.494	4.305
Sex_{male}, b	0.089	0.093	0.121	0.167	2.535	0.087
p	< 0.001	< 0.001	< 0.001	< 0.001	< 0.001	< 0.001
$Year_{birth}$, b	0.0002	0.001	0.002	0.003	0.029	< 0.001
p	0.021	< 0.001	< 0.001	< 0.001	< 0.001	0.435
Latitude, b	-0.002	0.0004	0.002	0.015	-0.004	-0.002
p	0.053	0.817	0.594	0.033	0.937	0.023
Longitude, b	0.0004	-0.002	0.006	0.012	0.074	0.0004
p	0.410	0.048	< 0.001	< 0.001	< 0.001	0.436
Age, b	< 0.001	0.007	0.003	0.004	0.100	-0.0003
p	0.997	< 0.001	0.333	0.538	0.028	0.790
Age:Sex_m, b	0.007	0.020	-0.005	-0.007	0.128	0.004

p	< 0.001	< 0.001	0.345	0.489	0.068	0.019
$Climate_{yob}$, b	-0.001	-0.002	-0.004	-0.002	-0.068	-0.002
p	0.141	0.119	0.164	0.687	0.090	0.108
N	429	427	404	407	385	416
Adj. R^2	0.761	0.701	0.365	0.222	0.638	0.764
F statistic	195.3	143.7	34.07	17.51	97.52	192.9
p	< 0.001	< 0.001	< 0.001	< 0.001	< 0.001	< 0.001

Model Comparison by AIC.–Model comparison by AIC indicates combination models are generally better for most cranial measurements, although similar to age-growth models for constrained length and skull width, but conditions in the year of birth are better for tooth measurements (Table S3.28).

Table S3.28.—Comparison of three linear models described above (Table S3.25-27) by Akaike Information Criterion (AIC). The number of estimated fixed effect parameters per model (K), the difference in AIC between a given model and the best-fitting model for a given measurement (ΔAIC), and corresponding Akaike weights are also included.

Measurement	**Model**	**K**	**AIC**	**ΔAIC**	**Akaike weight**
Greatest length	Combination	9	-1874.10	0.00	0.75
	Age-growth	9	-1871.89	2.21	0.25
	Conditions	7	-1849.46	24.64	0.00
Constrained length	Combination	9	-1877.03	0.00	0.60
	Age-growth	9	-1875.80	1.23	0.32
	Conditions	7	-1872.85	4.18	0.07
Skull width	Combination	9	-1501.32	0.00	0.68
	Age-growth	9	-1499.85	1.47	0.32
	Conditions	7	-1357.34	143.98	0.00
Premolar width	Conditions	7	-891.74	0.00	0.75
	Combination	9	-888.89	2.86	0.18
	Age-growth	9	-886.92	4.82	0.07
Canine width	Conditions	7	-328.48	0.00	0.68
	Age-growth	9	-326.10	2.39	0.20
	Combination	9	-325.02	3.46	0.12
Size PC1	Combination	9	1122.33	0.00	0.81

Age-growth	9	1125.27	2.94	0.19
Conditions	7	1140.08	17.75	0.00

Full generalized additive model results

In the tables below, edf = effective degrees of freedom. Values closer to 1 indicate a linear relationship, while values farther from 1 indicate greater nonlinearity. The reference degrees of (Ref.df) is used to calculate the test statistic and p-value.

Lynx.—

Table S3.29.—Generalized additive model results for lynx greatest total length of the skull (log-transformed). Predicted harvest is estimated for the year of collection, based on the equation provided by (Yom-Tov et al. 2007).

Parametric Coefficients				
Term	*Estimate*	*Std error*	*t-value*	*p-value*
Intercept	4.830	0.002	2978.95	< 0.001
Sex_{male}	0.051	0.002	22.25	< 0.001
Approximate significance of smooth terms				
Term	*edf*	*Ref. df*	*F*	*p-value*
$s(Year_{yoc})$	1.000	1.000	1.796	0.181
s(Age)	2.812	3.465	22.349	< 0.001
s(Lat, Long)	0.001	6.000	0.000	0.942
s(Predicted harvest)	1.000	1.001	44.951	< 0.001
N	526			
Adj. R^2	0.583			
Deviance explained	58.8%			

Table S3.30.—Generalized additive model results for lynx zygomatic breadth, or greatest width of the skull (log-transformed). Predicted harvest is estimated for the year of collection, based on the equation provided by (Yom-Tov et al. 2007).

Parametric Coefficients				
Term	*Estimate*	*Std error*	*t-value*	*p-value*
Intercept	4.490	0.002	2326.7	< 0.001
Sex_{male}	0.036	0.003	13.2	< 0.001

Approximate significance of smooth terms				
Term	*edf*	*Ref. df*	*F*	*p-value*
s($Year_{yoc}$)	1.000	1.000	0.25	0.618
s(Age)	3.030	3.705	59.98	< 0.001
s(Lat, Long)	0.001	6.000	0.000	0.676
s(Predicted harvest)	1.000	1.000	38.94	< 0.001
N	511			
Adj. R^2	0.494			
Deviance explained	50%			

Table S3.31.—Generalized additive model results for lynx interorbital width (interorbital constriction; log-transformed). Predicted harvest is estimated for the year of collection, based on the equation provided by (Yom-Tov et al. 2007).

Parametric Coefficients				
Term	*Estimate*	*Std error*	*t-value*	*p-value*
Intercept	3.331	0.003	1238.18	< 0.001
Sex_{male}	0.049	0.004	12.89	< 0.001
Approximate significance of smooth terms				
Term	*edf*	*Ref. df*	*F*	*p-value*
s($Year_{yoc}$)	1.752	2.130	3.412	0.028
s(Age)	3.067	3.751	69.165	< 0.001
s(Lat, Long)	0.177	6.000	0.045	0.186
s(Predicted harvest)	1.000	1.000	36.881	< 0.001
N	532			
Adj. R^2	0.505			
Deviance explained	51.2%			

Table S3.32.—Generalized additive model results for lynx canine width (log-transformed). Predicted harvest is estimated for the year of collection, based on the equation provided by (Yom-Tov et al. 2007).

Parametric Coefficients				
Term	*Estimate*	*Std error*	*t-value*	*p-value*
Intercept	1.966	0.004	501.95	< 0.001

Sex_{male}	0.072	0.006	12.84	< 0.001
Approximate significance of smooth terms				
Term	*edf*	*Ref. df*	*F*	*p-value*
s($Year_{yoc}$)	3.013	3.596	8.002	< 0.001
s(Age)	1.000	1.001	41.551	< 0.001
s(Lat, Long)	0.001	6.000	0.000	0.483
s(Predicted harvest)	3.331	3.931	4.907	0.002
N	526			
Adj. R^2	0.332			
Deviance explained	34.2%			

Table S3.33.—Generalized additive model results for lynx condylopremaxillary length (CPL). Predicted harvest is estimated for the year of collection, based on the equation provided by (Yom-Tov et al. 2007).

Parametric Coefficients				
Term	*Estimate*	*Std error*	*t-value*	*p-value*
Intercept	4.740	0.002	2916.24	< 0.001
Sex_{male}	0.052	0.002	22.37	< 0.001
Approximate significance of smooth terms				
Term	*edf*	*Ref. df*	*F*	*p-value*
s($Year_{yoc}$)	1.000	1.000	2.407	0.121
s(Age)	2.920	3.590	21.765	< 0.001
s(Lat, Long)	0.000	6.000	0.000	0.598
s(Predicted harvest)	1.000	1.001	26.384	< 0.001
N	515			
Adj. R^2	0.584			
Deviance explained	58.9%			

Table S3.34.—Generalized additive model results for lynx size PC1 (incorporates GTL, ZB, IO, and CAN, all log-transformed). Predicted harvest is estimated for the year of collection, based on the equation provided by (Yom-Tov et al. 2007).

Parametric Coefficients				
Term	*Estimate*	*Std error*	*t-value*	*p-value*
Intercept	-0.991	0.070	-14.24	< 0.001
Sex_{male}	1.946	0.100	19.49	< 0.001
Approximate significance of smooth terms				
Term	*edf*	*Ref. df*	*F*	*p-value*
$s(Year_{yoc})$	1.774	2.145	5.036	0.006
s(Age)	3.521	4.274	54.174	< 0.001
s(Lat, Long)	0.001	6.000	0.000	0.785
s(Predicted harvest)	2.199	2.679	13.608	< 0.001
N	485			
Adj. R^2	0.618			
Deviance explained	62.5%			

Martens.—

Table S3.35.—Generalized additive model results for marten greatest total length of the skull (log-transformed). Climate PC1 (incorporates estimated average temperature and precipitation for spring and summer) is calculated for the estimated year of birth.

Parametric Coefficients				
Term	*Estimate*	*Std error*	*t-value*	*p-value*
Intercept	4.351	0.002	2241.5	< 0.001
Sex_{male}	0.096	0.003	36.7	< 0.001
Approximate significance of smooth terms				
Term	*edf*	*Ref. df*	*F*	*p-value*
$s(Year_{yob})$	1.000	1.000	4.741	0.030
$s(Age):Sex_{female}$	1.621	1.998	0.577	0.561
$s(Age):Sex_{male}$	2.325	2.854	12.855	< 0.001
s(Lat, Long)	1.499	6.000	0.924	0.012
s(Climate PC1)	1.001	1.001	0.941	0.333
N	427			

R^2	0.766
Deviance explained	77.1%

Table S3.36.—Generalized additive model results for marten greatest zygomatic breadth (log-transformed). Climate PC1 (incorporates estimated average temperature and precipitation for spring and summer) is calculated for the estimated year of birth.

Parametric Coefficients				
Term	*Estimate*	*Std error*	*t-value*	*p-value*
Intercept	3.748	0.003	1369.17	< 0.001
Sex_{male}	0.111	0.004	30.14	< 0.001
Approximate significance of smooth terms				
Term	*edf*	*Ref. df*	*F*	*p-value*
$s(Year_{yob})$	1.000	1.000	42.907	< 0.001
$s(Age):Sex_{female}$	2.210	2.714	12.361	< 0.001
$s(Age):Sex_{male}$	3.500	4.133	63.550	< 0.001
s(Lat, Long)	0.006	6.000	0.001	0.249
s(Climate PC1)	2.004	2.509	1.286	0.431
N	425			
R^2	0.750			
Deviance explained	75.6%			

Table S3.37.—Generalized additive model results for marten canine width (log-transformed). Climate PC1 (incorporates estimated average temperature and precipitation for spring and summer) is calculated for the estimated year of birth.

Parametric Coefficients				
Term	*Estimate*	*Std error*	*t-value*	*p-value*
Intercept	1.332	0.012	115.814	< 0.001
Sex_{male}	0.150	0.016	9.609	< 0.001
Approximate significance of smooth terms				
Term	*edf*	*Ref. df*	*F*	*p-value*
$s(Year_{yob})$	3.911	4.642	13.121	< 0.001
$s(Age):Sex_{female}$	2.212	2.716	3.444	0.042

s(Age):Sex_{male}	1.000	1.000	0.549	0.459
s(Lat, Long)	1.884	6.000	1.109	0.011
s(Climate PC1)	1.000	1.000	0.363	0.547
N	405			
R^2	0.290			
Deviance explained	30.9%			

Table S3.38.—Generalized additive model results for marten fourth upper premolar width (log-transformed). Climate PC1 (incorporates estimated average temperature and precipitation for spring and summer) is calculated for the estimated year of birth.

Parametric Coefficients				
Term	*Estimate*	*Std error*	*t-value*	*p-value*
Intercept	2.045	0.006	352.62	< 0.001
Sex_{male}	0.114	0.008	14.49	< 0.001
Approximate significance of smooth terms				
Term	*edf*	*Ref. df*	*F*	*p-value*
s($Year_{yob}$)	2.205	2.739	10.380	< 0.001
s(Age):Sex_{female}	1.928	2.380	1.718	0.256
s(Age):Sex_{male}	1.000	1.000	0.840	0.360
s(Lat, Long)	3.121	6.000	3.356	< 0.001
s(Climate PC1)	1.000	1.000	1.575	0.210
N	402			
R^2	0.398			
Deviance explained	41.3%			

Table S3.39.—Generalized additive model results for marten condylopremaxillary length (log-transformed). Climate PC1 (incorporates estimated average temperature and precipitation for spring and summer) is calculated for the estimated year of birth.

Parametric Coefficients				
Term	*Estimate*	*Std error*	*t-value*	*p-value*
Intercept	4.343	0.002	2367.53	< 0.001
Sex_{male}	0.091	0.002	36.45	< 0.001
Approximate significance of smooth terms				

Term	*edf*	*Ref. df*	*F*	*p-value*
$s(Year_{yob})$	1.000	1.000	0.634	0.426
$s(Age):Sex_{female}$	1.411	1.707	0.338	0.577
$s(Age):Sex_{male}$	1.627	2.014	4.275	0.015
s(Lat, Long)	1.900	6.000	1.391	0.004
s(Climate PC1)	1.001	1.001	1.451	0.229
N	414			
R^2	0.766			
Deviance explained	77.1%			

Table S3.40.—Generalized additive model results for marten size PC1 (incorporates GTL, ZB, PM4, and CAN, all log-transformed). Climate PC1 (incorporates estimated average temperature and precipitation for spring and summer) is calculated for the estimated year of birth.

Parametric Coefficients				
Term	*Estimate*	*Std error*	*t-value*	*p-value*
Intercept	-1.432	0.076	-18.72	< 0.001
Sex_{male}	2.623	0.104	25.11	< 0.001
Approximate significance of smooth terms				
Term	*edf*	*Ref. df*	*F*	*p-value*
$s(Year_{yob})$	3.184	3.866	15.273	< 0.001
$s(Age):Sex_{female}$	1.748	2.161	4.400	0.014
$s(Age):Sex_{male}$	1.714	2.128	9.824	< 0.001
s(Lat, Long)	2.070	6.000	1.389	0.005
s(Climate PC1)	1.000	1.001	2.470	0.117
N	383			
R^2	0.653			
Deviance explained	66.3%			

LITERATURE CITED

Del Grosso S, Parton W, Stohlgren T, Zheng D, Bachelet D, Prince S, Hibbard K, Olson R. 2008. Global potential net primary production predicted from vegetation class, precipitation, and temperature. Ecology 89(8):2117–2126. https://doi.org/10.1890/07-0850.1.

R Core Team. 2022. R: A language and environment for statistical computing. R Foundation for Statistical Computing, Vienna, Austria. <https://www.R-project.org/>.

Tang G, Beckage B, Smith B, Miller PA. 2010. Estimating potential forest NPP, biomass and their climatic sensitivity in New England using a dynamic ecosystem model. Ecosphere 1(6):1–20. https://doi.org/10.1890/ES10-00087.1.

Theriot MK, Lanier HC, Olson LE. 2023. Harnessing natural history collections to detect trends in body-size change as a response to warming: A critique and review of best practices. Methods in Ecology and Evolution 14(2):306–318. https://doi.org/10.1111/2041-210X.13861.

Wang T, Hamann A, Spittlehouse D, Carroll C. 2016. Locally downscaled and spatially customizable climate data for historical and future periods for North America. PloS ONE 11(6):e0156720. https://doi.org/10.1371/journal.pone.0156720.

Wolak ME, Fairbairn DJ, Paulsen YR. 2012. Guidelines for estimating repeatability. Methods in Ecology and Evolution 3(1):129–137. https://doi.org/10.1111/j.2041-210X.2011.00125.x.

Yom-Tov Y, Yom-Tov S, Jarrell G. 2008. Recent increase in body size of the American Marten *Martes americana* in Alaska. Biological Journal of the Linnean Society 93(4):701–707. https://doi.org/10.1111/j.1095-8312.2007.00950.x.

Yom-Tov Y, Yom-Tov S, MacDonald D, Yom-Tov E. 2007. Population cycles and changes in body size of the lynx in Alaska. Oecologia 152(2):239–244. https://doi.org/10.1007/s00442-006-0653-3.

CHAPTER 2

DIETARY DOWNGRADE? USING MUSEUM SPECIMENS TO TEST NUTRIENT DILUTION AS A DRIVER OF BODY SIZE DECLINES IN THE EASTERN COTTONTAIL (*SYLVILAGUS FLORIDANUS*)

Miranda K. Theriot and Hayley C. Lanier

[1]*Sam Noble Oklahoma Museum of Natural History, School of Biological Sciences, University of Oklahoma, Norman, OK 73072, United States*

Abstract

Shifts in body size represent a major category of organismal responses to global change. While resource availability has frequently been cited as a key driver, gaps still remain in our knowledge of the effects of resource quality. For herbivores, higher forage abundance may come at the expense of nutrient dilution, or greater plant biomass but lower concentrations of micronutrients resulting from changing environmental conditions, particularly elevated CO_2 in the atmosphere. Here, I evaluated the potential effects of nutrient dilution in a small, obligately herbivorous mammal, the Eastern Cottontail (*Sylvilagus floridanus*). Using museum specimens, I tested for connections among body size (approximated using cranial measurements), signs of nitrogen limitation ($\delta^{15}N$ and nitrogen content in hair samples), diet composition (hair $\delta^{13}C$), and physiological stress (hair cortisol concentration). The best-fitting linear models suggested a significant positive correlation between body size and $\delta^{13}C$ values, with $\delta^{15}N$ and/or cortisol having weaker or non-significant associations with size. To evaluate broader-scale size trends, I analyzed total length derived from digital museum records of Eastern Cottontails and two congeners, Desert Cottontails (*S. audubonii*), and Mountain Cottontails (*S. nuttallii*). Size has significantly declined in the latter two species over seven decades, whereas there was a slight, but not statistically significant, decrease in mean total length of Eastern Cottontails. Altogether, these results suggest that, on a local scale, cottontails may be able to compensate for nutrient dilution through diet and/or habitat selection, allowing some individuals to grow and maintain larger bodies. However, the range-wide declines in size suggest detrimental impacts of nutrient dilution and other climate-change effects, as decreasing population trends have been reported for the majority of *Sylvilagus* species. This work highlights how the extended specimen can be leveraged to track the effects of nutrient dilution, an understudied yet widespread phenomenon with global consequences for wildlife and humans.

Introduction

Over the last century of global change, researchers have documented a diverse array of organismal responses. With the continual advent of new technologies and targeted techniques for detecting and predicting biological and ecological changes over time, our focal questions now extend beyond simply documenting trends to evaluating the nuanced drivers and mechanisms underlying major patterns (Chuang and Peterson 2016; Pacifici *et al.* 2017; Paniw *et al.* 2021). Changes in body size are of particular interest, signaling shifts in how animals grow and develop,

interact with the environment, and function within ecological communities (Peters 1983; Woodward *et al.* 2005). Additionally, size trends can be readily evaluated over decades (or longer) of environmental change due to historical samples provided by natural history collections. Traditionally, observed changes in size over time have been attributed to two major effects: 1) reductions in mean size coinciding with climate warming as predicted by Bergmann's rule, an ecogeographical pattern describing a tendency towards smaller mean size at lower latitudes (Bergmann 1847; Daufresne *et al.* 2009); 2) increases in size linked with an extended growing season, provisioning individuals with more resources to allocate to growth (McNab 2010; Huston and Wolverton 2011). For the latter, many studies have focused on addressing the role of resource availability (Yom-Tov and Geffen 2011; Eastman *et al.* 2012; Correll *et al.* 2016; Henry *et al.* 2023); however, the quality of those resources may be equally, if not more, important to body-size trends. Yet, diet quality can be challenging to quantify—especially among past populations—presenting a gap in our knowledge of responses to global change.

For herbivores, although climate change has generally increased the length of the growing season (Linderholm 2006), greater food availability may come at the expense of reduced nutrient content per unit of vegetation consumed. This nutrient dilution occurs as elevated atmospheric CO_2 along with changes in temperature and precipitation regimes drive increases in plant biomass, thus decreasing the concentrations of essential nutrients such as zinc, iron, calcium, and, critically, nitrogen (Kaspari and Welti 2024; Ter Haar *et al.* 2025). Despite anthropogenic deposition of nitrogen associated with agriculture and other human activity, declining nitrogen content in plant tissues has been documented across terrestrial ecosystems (McLauchlan *et al.* 2010; Mason *et al.* 2022). Even in crop plants, for which nitrogen is artificially added via fertilizer, there is evidence for nutrient dilution, indicating severe consequences for environmental and human health (Loladze 2002; Ter Haar *et al.* 2025). Among wildlife, nutrient dilution has been linked to declines in insect abundance (Welti *et al.* 2020) and shifts in diet composition in large grazing mammals (Craine *et al.* 2015, 2016). The consequences of nutrient dilution are global in scale, yet this phenomenon remains understudied in the context of organismal responses to global change.

Here, I evaluated the potential relationship between nutrient dilution and body-size trends in an obligately herbivorous small mammal, the Eastern Cottontail (*Sylvilagus floridanus*). These rabbits are an apt study species, as they are widely distributed and can be used to better understand drivers of decline in climate-threatened and endangered congeners. They are also generally well represented in museum collections, providing a means to evaluate global-change responses over time.

Although body size is sensitive to environmental conditions, there is a significant genetic component, which means naturally larger individuals have more body tissues to grow and maintain, and thus a net higher nutrient demand. If and how larger individuals survive and attain their growth potential can be informative about how nutrient dilution, and other environmental change, may impact population-level size distributions. Therefore, when faced with a reduction in diet quality, we expect animals to respond in a few ways: 1. shift what they eat to compensate for deficits; 2. survive by having reduced nutritional needs (i.e., growing to a smaller stable size and/or having fewer offspring); 3. lacking any other means to cope, incur physiological stress. Leveraging collections and extended specimen concept (Webster 2017) offers a means to evaluate these possibilities.

While it is rarely (if ever) possible to preserve the full breadth of a wild-caught individual's diet upon collection, stable isotope ratios of nitrogen and carbon in body tissues can serve as an indicator of food sources. For instance, plants vary in $\delta^{13}C$ based on differences in photosynthetic pathways, which in turn is incorporated into consumers (Ben-David and Flaherty 2012). Additionally, laboratory experiments have linked very poor nutrition with $\delta^{15}N$ enrichment in animal tissues (Hobson *et al.* 1993). Nitrogen isotope ratios can also be indicative of trophic level, but as we do not expect cottontails to consume large quantities of animal tissues, $\delta^{15}N$ may serve as an indicator of widespread, decreased nutrient content in food among wild animals. Stable isotope analysis also provides estimates of the weight of total nitrogen (and carbon) in a sample. Therefore, we can also evaluate whether the declines in overall nitrogen concentration in plant tissues (McLauchlan *et al.* 2010) is passed to these consumers. On the other hand, physiological stress may also be correlated with diet in several ways. If individuals are unable to offset a change in diet quality, through eating something else and/or reducing their total nutritional needs, we would expect them to incur signs of stress. Elevation of glucocorticoids throughout life may also influence growth and development directly (Names *et al.* 2024). One indicator of stress is elevated levels of the hormone cortisol, which is thought to be relatively stable in hair samples (Russell *et al.* 2012; although see Stewart *et al.* 2018), and thus can be measured in museum specimens.

Combining body-size measurements, stable isotope ratios, and stress hormone concentrations can provide insights into the effects of changing resource quality due to nutrient dilution in this small mammalian herbivore. Specifically, I have four non-mutually exclusive predictions under the nutrient dilution hypothesis for body-size trends:

1) If reduction of nitrogen availability due to nutrient dilution directly influences growth, body size will be correlated with nitrogen concentration and composition ($\delta^{15}N$) in animal tissues (hair).
2) If nutrient dilution causes extreme nutritional stress, then body size will be correlated with elevated $\delta^{15}N$ and elevated cortisol.
3) If cottontails cope with nutrient dilution via reduced nutritional demand, then body size will be positively correlated with elevated cortisol, but not with stable isotope ratios.
4) If cottontails cope with nutrient dilution solely by shifting what they eat, then size will be correlated with signatures of forage type ($\delta^{13}C$).

Materials and Methods

Specimens and skull measurements

To minimize region-specific variation in both cottontail size and surrounding plant communities, I searched for series of specimens collected within neighboring counties on VertNet (now incorporated into GBIF). I identified 27 specimens collected in central Oklahoma (housed at the Sam Noble Oklahoma Museum of Natural History) and 31 specimens from Ellis County, Kansas (Fort Hays Sternberg Museum of Natural History). These locations are climatically similar, and I expect the differences in latitude to be negligible, as latitude is not a strong predictor of body size in Eastern Cottontails (Olcott and Barry 2000). Oklahoma specimens were collected from 1930-2006 and Kansas specimens from 1968-2018, though collecting effort was uneven through time (Supplementary Material).

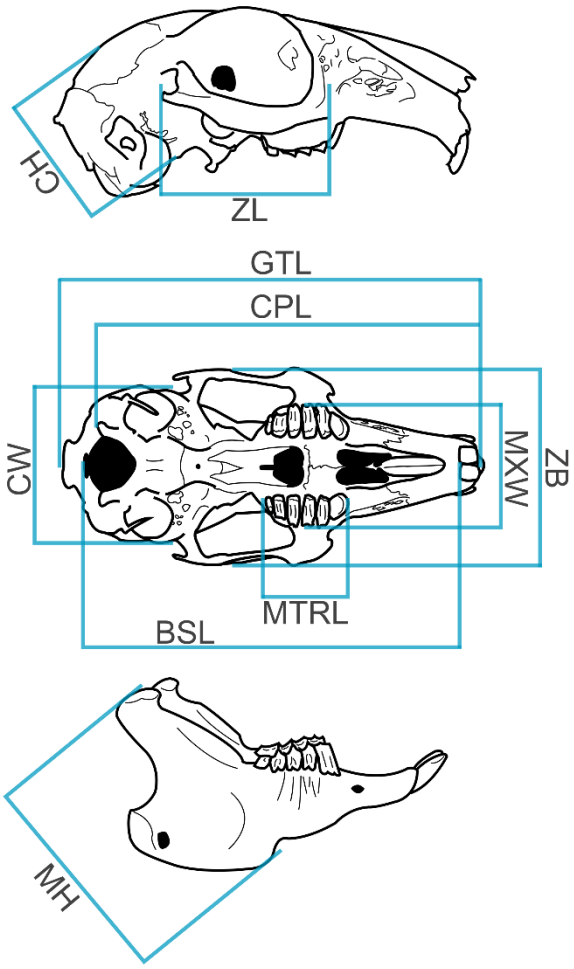


Figure 1. Cranial measurements used to estimate size, adapted from (Olcott and Barry 2000): Cranial height (CH), zygomatic length (ZL), greatest total length (GTL), condylopremaxillary length (CPL), maxillary width (MXW), zygomatic breadth (ZB), maxillary toothrow length (MTRL), basilar length (BSL), Cranial Width (CW), and mandible height (MH). For full descriptions, see Supplementary Material.

On inspection, 6 specimens (4 from Oklahoma, 2 from Kansas) were identified as subadults based on overall skull size and partially open exoccipital-supraoccipital skull sutures (Hoffmeister and Zimmerman 1967). There were also 2 Kansas specimens without a collection year in the specimen record. Omitting these specimens resulted in a total sample size of 49 specimens. I approximated body size through a set of skull measurements—modeled after (Olcott and Barry 2000)—encompassing the length, width, and height of the skull as well as the size (height) of the mandible (Figure 1). Measurements were preferentially taken on the right side (unless broken) and were conducted by one researcher (MKT). Repeatability was assessed by measuring a subset of specimens multiple times and calculating intraclass correlation coefficient, or the ratio of among-specimen variation to total variation based on one-way ANOVA ('ICCest' in package *ICC*; Wolak *et al.* 2012). A large ratio suggests relatively small variation among replicates of the same specimen, indicating high measurement consistency.

Hair sampling

Hair samples were obtained by cutting approximately 1 g of hair from a standard location (the outer thigh, which is typically thickly furred) of each specimen using scissors and forceps. Hair samples were washed in accordance with standard procedures conducive for measuring both cortisol and stable isotope ratios (Sergiel *et al.* 2017). In brief, each sample was gently rocked in 40 µl HPLC-grade methanol (Fisher Chemical) three times for three minutes per wash. Between washes, samples were gently blotted with paper towels, and hair clumps were manually pulled apart, cleaned of debris, and mixed. Samples were air dried on clean paper towels in petri dishes lined in a light layer of unscented Static Guard at room temperature for 24 hours. Dried samples were split into two portions, one for the measurement of stable isotope ratios, the other for cortisol.

Stable isotope analysis

For stable isotope analysis, a small portion of each sample (approximately 1 mg) was cut into small fragments (1-3 mm) using scissors and forceps, encapsulated in tin (EA Consumables Tin Capsules Pressed Standard Weight 8×5 mm), and weighed to the nearest 0.001 mg on a microbalance. Carbon ($\delta^{13}C$) and nitrogen ($\delta^{15}N$) isotope ratios, as well as total carbon and nitrogen content per sample, were analyzed at the University of California Davis Stable Isotope Facility on a Carlo Erba NC2500 elemental analyzer (Thermo Fisher Scientific, formerly CE Instruments/Carlo Erba) interfaced to a Sercon 20-22 IRMS (Sercon Ltd., Cheshire, United Kingdom). I included duplicates of four specimens to assess variation.

Over the last century, the burning of fossil fuels has altered the carbon isotope makeup of the atmosphere and consequently the tissues of living organisms. To account for this artificial difference through time (the Suess effect) I corrected the $\delta^{13}C$ data using the model and protocol developed by (Dombrosky 2020). In brief, I calculated the difference in atmospheric $\delta^{13}C$ between each year represented in our sample and the most recent (2018), producing Suess correction scores which were then subtracted from the corresponding $\delta^{13}C$ measurements to obtain Suess-corrected values.

Hair cortisol concentration

To prepare samples for cortisol analysis, approximately 25 mg of washed hair was transferred into 2 ml tubes containing six 3.175 mm stainless steel beads (MP Biomedicals Lysing Matrix S), and ground to powder using a FastPrep-24 Classic Instrument (MP Biomedicals, Irvine, California) for two, one-minute intervals at a speed of 6.0 m/s. Hair cortisol concentrations were obtained via methanol extraction and an enzyme immunoassay procedure (Oxford Biomedical cortisol kit) at the University of Saskatchewan Toxicology Centre.

While cortisol is much more stable in hair samples than other materials (e.g., blood), some degree of degradation has been reported over long periods of storage. In a study on deer mouse (*Peromyscus maniculatus*) museum specimens, Stewart et al. (2018) calculated a rate of decline in hair cortisol concentrations of approximately 3% per year (i.e., for a linear model fit to natural-log-transformed cortisol concentration, their estimated coefficient for year was 0.0325). Using this as a benchmark, I applied a correction to the cortisol data, increasing values for older specimens relative to the most recent specimen in the sample: $\ln(cort)_{corrected} = \ln(cort)_{original} +$

(2018-year)*0.03. Due to the difference in study species and sampling circumstances, I do not claim that this correction derived from Stewart et al. (2018) will improve the absolute accuracy of cortisol measurements; rather, this provides a means to test whether the assumption that cortisol is stable in museum specimens long term influences model selection and interpretation. As such, I analyzed the cortisol data both with and without the correction.

Broadscale body-side trends in cottontails

There are many ways to quantify body size, each with their own benefits, drawbacks, and information they can impart about climate-change responses (Bailey *et al.* 2020; Theriot *et al.* 2023). Standard external measurements (total length, weight, etc.) available through museum databases, although generally less precise than cranial measurements, can provide large sample sizes across a broad spatial and temporal scope. Here, I obtained digital museum specimen data from GBIF, targeting three common, sympatric cottontails: The Eastern Cottontail (*Sylvilagus floridanus*), Desert Cottontail (*S. audubonii*), and Mountain Cottontail (*S. nuttallii*). External measurements were extracted and cleaned to standardize units (mm for lengths, g for weight) and omit biologically unrealistic values, i.e., far exceeding length and weight ranges indicated in species accounts (Chapman 1975; Chapman and Willner 1978; Chapman *et al.* 1980). Similarly, latitude and longitude coordinates were mapped and visually assessed to exclude errors and potential outliers (e.g., small numbers of specimens collected at the very southern edge of the expected species range; see Supplementary Material). To model size trends, I sought to only include "adults," so I performed a simple k-means clustering procedure ('kmeans' function in the *stats* package in base *R*) on the matrix of total length and weight values, and validated the resulting clusters—which I designated as either "adult" or "juvenile/subadult"—using the subset of specimens for which the collectors or preparators identified age class upon specimen collection.

Statistical analyses

All analyses were conducted in *R version 4.5.1* (R Core Team 2025). The nutrient dilution test dataset was evaluated using a series of linear models. The number of predictors per model was limited to prevent overfitting, therefore each model targeted a specific aspect of the predicted effects of nutrient dilution (Table 1). Based on initial analyses, skull size did not differ between females and males—consistent with (Olcott and Barry 2000)—so not all models need be sex-corrected; however, sex-specific reproductive demands may influence stress physiology, so models incorporating cortisol were corrected for sex. These candidate models were compared using Akaike Information Criterion with a correction for small sample size, or 'AICc' in the *MuMIn* package (Bartoń 2025). I fit these models to five different response variables, four univariate—representing skull length (greatest total length, GTL), skull width (zygomatic breadth, ZB), toothrow length (maxillary toothrow length, MTRL), and size of the mandible (mandible height, MH)—and the first principal component of the cranial measurements (excluding the mandible, as this structure is commonly broken or lost, particularly in some older specimens), hereafter cranial PC1.

Model	Structure	Description
Time/location	~ sex + year + state	Size is primarily influenced by time- and/or space-dependent factors not explicitly tested in the other models
Nitrogen availability	~ δ^{15}N + N Content	Nutrient dilution influences body size through poorer nitrogen content in food
Forage content	~ State + δ^{13}C	Coping with nutrient dilution requires individuals of different sizes forage on different vegetation (corrected for location)
Stress	~ Sex + log(Cort)	Size-dependent consequences of nutrient dilution means individuals of different size experience different levels of stress (corrected for sex)
Nitrogen availability and stress	~ Sex + log(Cort) + δ^{15}N	Individuals of different sizes differ in their ability to escape poorer nitrogen content due to nutrient dilution, thus incurring different levels of stress (corrected for sex)

Table 1. Candidate models compared to evaluate the effects of nutrient dilution in a sample of Eastern Cottontail (*Sylvilagus floridanus*) specimens. Cortisol concentrations were natural-log-transformed.

Total length for the large museum datasets were also analyzed using linear models, including sex—as female leporids are generally larger in length and weight (Chapman 1975; Chapman and Willner 1978; Chapman *et al.* 1980)—year, latitude, and longitude as predictors.

Results

Repeatability and PCA of cranial measurements

Estimated intraclass correlation coefficient (ICC) was generally > 0.90 across measurements, indicating that variation among replicates was small compared to variation among different specimens, suggesting a high degree of measurement consistency and repeatability (Supplementary Material).

The first principal component of the cranial measurements (cranial PC1) accounts for 75% of variance. PC2 accounts for 10% of variance, and the remaining PCs explain 5% or less. PC1 is positively associated with all cranial measurements with similar magnitude of the loadings, i.e., cranial PC1 represents larger size in all dimensions, with no one measurement contributing much more strongly than the others.

Size, stable isotopes, and stress

Four duplicates (i.e., samples derived from the same specimen) were included in the stable isotope analysis. The average absolute difference between replicates was 1.12 ‰ δ^{13}C and 0.08 ‰ for δ^{15}N. One (non-duplicated) specimen had overall nitrogen and carbon concentration values that fell far outside the range reported for the rest of the sample (see Supplementary

Material) and was omitted from further analyses.

The forage content model—$\delta^{13}C$ corrected for location (state)—fit the data best for cranial PC1 and all univariate responses (Table 2). In all measurements except skull length (GTL), mean size was significantly smaller in Oklahoma than in Kansas. Across all responses, there was a significant positive association between size and $\delta^{13}C$ (Table 3). This translates to a slight clustering of smaller individuals in the left (more negative) portion of isotopic space along the carbon axis (Figure 2). Associations between size and $\delta^{15}N$ were generally weak and not statistically significant; however, mean skull length (GTL) was positively correlated with $\delta^{15}N$ (estimated coefficient = 0.395, SE = 0.191, *p*-value = 0.046, in the nitrogen availability model). Overall nitrogen concentration was not a significant contributor to size variation in any model.

Models were also fit with a correction to the log-transformed cortisol measurements—increasing the values from older specimens to account for potential degradation—but this did not influence selection or interpretation of the best-fitting model; however, it did improve normality of the residuals in the models including cortisol. Cortisol-corrected models indicated a slight negative relationship between stress hormone concentration and size, but this was not statistically significant (see Supplementary Material).

Model	Overall cranial size (PC1)	Skull length (GTL)	Skull width (ZB)	Tooth row length (MTRL)	Mandible size (MH)
Time/location	11.25	4.24	9.78	9.06	5.36
Nitrogen availability	11.57	4.74	12.50	9.13	7.39
Forage content	**0.00**	**0.00**	**0.00**	**0.00**	**0.00**
Stress	10.83	7.92	10.25	11.15	8.87
Nitrogen content and stress	9.92	6.27	10.69	10.79	6.22
Cortisol-corrected models					
Stress	10.833	7.919	10.246	11.148	8.866
Nitrogen content and stress	9.918	6.266	10.685	10.787	6.218

Table 2. ΔAICc for five candidate models. The best-fitting model (bolded) was forage content across overall cranial size and the univariate measurements. Alternate models were fit in which a correction was applied to natural-log-transformed cortisol concentrations to account for degradation over years of storage, which did not affect the best-fitting model.

Body-size trends in three widespread, cottontail species

For the museum datasets, age classes were estimated through a k-means clustering approach on total lengths and weights. For specimens with age classes reported by the collectors or preparators, the clustering approach resulted in accurate classification—i.e., placement in either an "adult" or "subadult/juvenile" category corresponding with the original age class determination—of 189/203 (93.1%), 425/441 (96.4%), and 61/72 (84.7%) for Eastern, Desert, and Mountain Cottontails respectively. After cleaning the GBIF data and filtering for adult-sized animals, analyses included 282, 441, and 76 specimens for Eastern, Desert, and Mountain Cottontails respectively.

Mean total length has declined significantly over time in two of the three focal species: Desert Cottontails and Mountain Cottontails (Table 4, Figure 3). Longitude was a strong

		Overall cranial size (PC1)	Skull length (GTL)	Skull width (ZB)	Tooth row length (MTRL)	Mandible size (MH)
	n	34	39	40	43	36
State	β_{OK}	-2.612	-1.720	-1.379	-0.574	-1.421
	SE	0.833	0.888	0.408	0.231	0.474
	p-value	**0.004**	0.061	**0.002**	**0.017**	**0.005**
$\delta^{13}C$	β	0.432	0.378	0.180	0.112	0.182
	SE	0.123	0.132	0.060	0.035	0.071
	p-value	**0.001**	**0.007**	**0.005**	**0.003**	**0.016**
	Adj. R^2	0.298	0.165	0.248	0.200	0.221

Table 3. Outputs for best-fitting linear model (forage content) by response.

predictor of total length in Eastern Cottontails, with mean size increasing from west to east. There was also a significant geographic trend in the size of Mountain Cottontails, with total length increasing from north to south. However, there was a correlation between latitude and longitude in this species (specimen records were clustered in the northwest and southeast portions of the range; see Supplementary Material), introducing collinearity into the model, so only latitude was included. In other words, the observed trend could also represent an increase in mean total length from west to east.

Discussion

Nutrient dilution is a widespread consequence of climate change, altering ecosystems across the globe. To advance our understanding of how this phenomenon continues to impact food webs and shape ecosystem-level responses to global change, a key aspect is to identify the impacts of nutrient dilution at the organismal level. To that end, here, I demonstrated a method to leverage the long-term data sets of museum collections, focusing on body size, diet composition, and stress. My results indicate that the types of forage cottontails consume—measured by carbon stable isotope ratios—is the strongest predictor of body

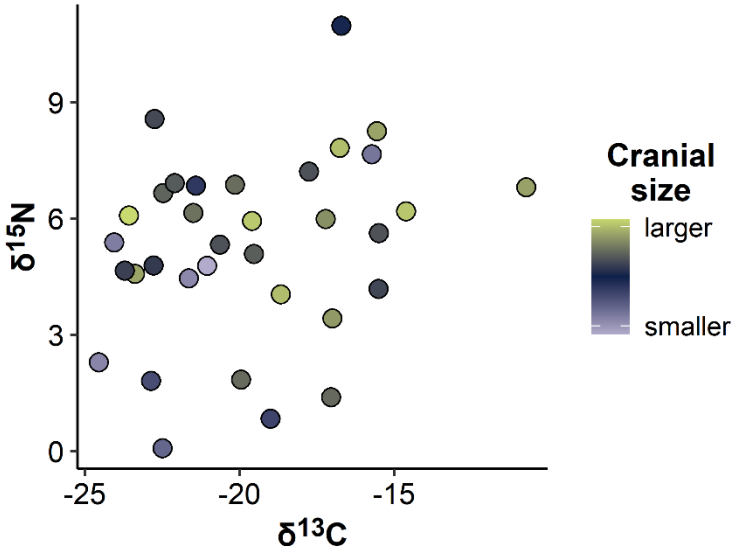


Figure 2. Cranial size (first principal component of cranial measurements) plotted in carbon-nitrogen isotopic space. Smaller individuals (blue–purple color) are slightly clustered on the lower (more negative) segment of the carbon axis, reflecting the positive correlation between size and $\delta^{13}C$.

size, suggesting that small herbivores may cope with nutrient dilution through dietary shifts. However, I also found evidence that cottontails are declining in mean size across their range, which points to long-term limitations in this strategy.

		Eastern Cottontail (*S. floridanus*)	**Desert Cottontail (*S. audubonii*)**	**Mountain Cottontail (*S. nuttallii*)**
	n	282	441	76
Sex	β_{male}	-6.207	-5.743	-1.303
	SE	5.106	3.49	7.783
	p-value	0.225	0.101	0.867
Year	β	-0.196	-0.254	-0.611
	SE	0.11	0.087	0.23
	p-value	0.076	**0.004**	**0.010**
Latitude	β	-0.364	0.491	-1.984
	SE	0.316	0.607	0.968
	p-value	0.25	0.418	**0.044**
Longitude	β	1.01	0.526	
	SE	0.233	0.858	
	p-value	**< 0.001**	0.541	
	Adj. R^2	0.075	0.019	0.085

Table 4. Linear model results for trends in total length over time (year) and space (latitude and longitude), in three widespread cottontail species: Eastern Cottontail (*Sylvilagus floridanus*), Desert Cottontail (*S. audubonii*), and Mountain Cottontail (*S. nuttallii*). For the latter, latitude and longitude were colinear, so longitude was dropped from the model.

Small mammals may compensate for nutrient dilution through forage selection

Models centered on diet composition, rather than limitation in nitrogen availability or physiological stress, provided the best-fitting explanation for overall body-size variation in Eastern Cottontails. Carbon isotope ratios in consumer tissues generally reflect the photosynthetic pathways used by plants forming the foundation of their food web. Specifically, the carbon-fixation processes in C_4 plants (as well as those that use crassulacean acid metabolism, or CAM) can more readily uptake the heavier carbon isotope, ^{13}C, compared to C_3 plants, which are more selective for the lighter isotope, ^{12}C; this results in comparatively more depleted $\delta^{13}C$ in C_3 plants, a signature which is detectable in consumers, providing information about diet (Ben-David and Flaherty 2012). Here, larger skulls were associated with elevated $\delta^{13}C$, which may reflect size-specific differences in diet composition, specifically an increase in the relative proportion of C_4 to C_3 plants consumed. This interpretation is consistent with observations in large grazing mammals, in which bison were found to consume lower amounts of C_3 grasses and select for higher-protein forage under climate warming and widespread decline in diet quality (Craine *et al.* 2015). This trend coincided with reduced body size in warmer

grasslands where the combined effects of temperature and nutrient dilution are more severe (Craine 2013).

An alternative explanation for these results in cottontails is that the relationship between size and $\delta^{13}C$ may relate less to diet selection, but rather habitat selection. Rabbits differ from large-bodied herbivores in their lower space and resource needs, allowing them to take advantage of more varied or even fragmented habitats. Cottontails are commonly found in areas of high human disturbance, like agricultural fields and suburbs, which may influence their carbon isotope ratios in several ways. First, consumption of certain crops, particularly corn (a C_4 plant) and its derivatives, is associated with elevated $\delta^{13}C$ in animal tissues (Walsh and Tucker 2023; Fletcher *et al.* 2025). Second, greater water input via irrigation can increase $\delta^{13}C$, particularly in water-limited C_3 plants (Wallace *et al.* 2013). Third, urban plant communities in temperate regions favor greater diversity and abundance of C_4 plants, as the urban heat island effect likely improves growth and persistence of these relatively cold-intolerant species (Duffy and Chown 2016). These effects may in part explain the relationship between size and $\delta^{13}C$ in cottontails if anthropogenic habitats offer a potential buffer against the effects of widespread nutrient dilution, with the types and relative concentration of resources (e.g., fields, gardens, and other greenspaces) allowing individuals to grow and maintain larger bodies. Indeed, the specimens in my sample with lower $\delta^{13}C$ tend to be those whose verbatim localities are described relative to smaller towns or wildlife management areas, providing some support for this possibility.

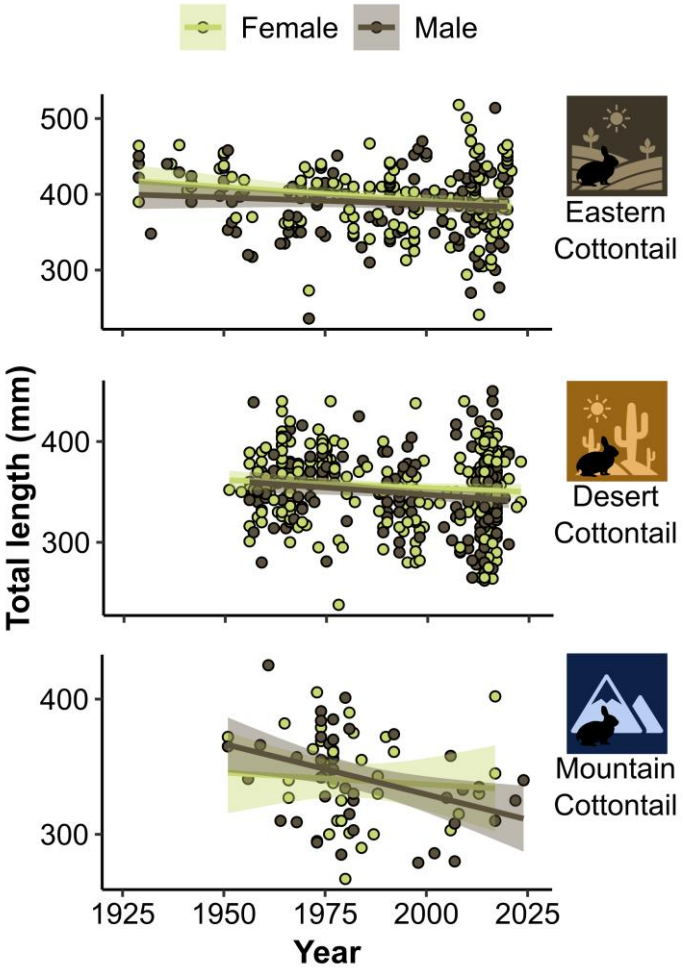


Figure 3. Mean total length over time in three widespread cottontail species. Eastern Cottontails (top) show a slight, but not statistically significant, decrease in total length over a century. Total length has significantly declined in Desert Cottontails (middle) and Mountain Cottontails (bottom) over approximately 7 decades.

Finally, elevated $\delta^{13}C$ with size may be an effect of seasonal timing and individual age. Stable isotope ratios are only informative about the time period in which a given tissue was grown (Ben-David and Flaherty 2012). Like many mammals, cottontails molt twice annually, in spring and fall; for young of the year, their fall molt is their first coat turnover since replacing

their subadult pelage (Negus 1958). In leporids, molt cycles are triggered by photoperiod, so these timeframes are not expected to change rapidly under climate change on decadal timescales (Zimova *et al.* 2018). Therefore, in fall-caught individuals, the stable isotope ratios in hair likely relate to the conditions and nutritional status experienced coming off of their first summer. Alternatively, the hair of a spring/summer-caught individual may represent conditions at the end of winter. Younger and older individuals can differ in size, physiology, and nutritional status, whereas the type and abundance of available forage also varies by season, which together could produce the apparent association between skull size and $\delta^{13}C$. Although I cannot entirely rule out such an effect with the available data, cranial sizes and $\delta^{13}C$ values do not appear strongly clustered by month (Figure 4), indicating that diet or habitat selection may be the predominant driver of the observed changes in isotopic values.

*Despite potential buffer*s *against nutrient dilution, declines in mean body size are range-wide*

Although diet or habitat selection may buffer against some of the effects of nutrient dilution, this may not remain a successful strategy long term. Crops (and other human-cultivated plants) are still suffering nutrient losses under climate change (Loladze 2002; Ter Haar *et al.* 2025) indicating that this is a challenge that will continue to affect all members of biological communities, including humans. Here, I found evidence that mean body size in cottontails is already declining on a range-wide scale (Table 4, Figure 3). While these trends are consistent with Bergmann's rule, the relationship between size and latitude—a commonly used proxy for temperature in studying biogeographical "rules" and patterns (Watt et al. 2010)—is weak in Eastern Cottontails (Olcott and Barry 2000). This is consistent with my models, latitude being a poor predictor of total length in both Eastern and Desert Cottontails (and possibly conflated with a longitudinal trend in Mountain Cottontails), suggesting that other environmental factors have a stronger effect on body-size trends than temperature. Thus, while forage selection—particularly in human-associated habitats—may provide a means to partially compensate for nutrient dilution, allowing individuals to grow and maintain larger sizes in the short term, the general trend is towards shrinking body size. This may be an effect of nutritional constraints limiting growth and/or reflect an advantage of smaller size under such conditions. Fundamentally, an animal's potential body size

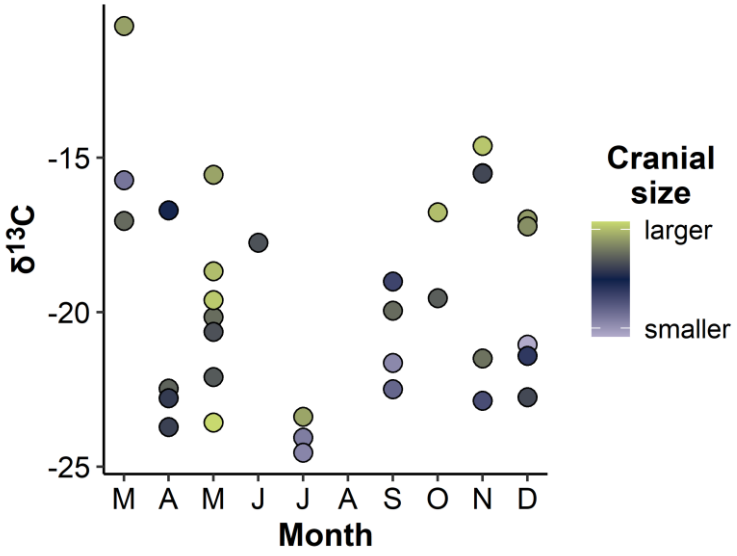


Figure 4. Carbon isotopic ratio by month of collection and cranial size (first principal component of cranial measurements). There are no specimens represented from January or February, so the Month axis begins with March (M) and continues through December (D).

has a significant genetic component. Although mass-specific metabolic rate decreases with size, larger animals have greater net requirements for energy and matter in order to maintain a larger volume of living tissue (Peters 1983). Meeting these needs may prove a greater challenge during periods of food/nutrient scarcity, such that there is an advantage to being smaller. However, varying nutritional requirements is only one axis of the functional differences between smaller and larger individuals; while there may be a slight disadvantage to sustaining a larger body under nutrient dilution, this may be relatively minor compared to other ways in which size potentially influence fitness, e.g., litter size (Tablado et al. 2009) and mobility (Davis and Roth 2008). Here, results suggest that larger size is not a severe detriment under nutrient dilution, revealing no strong evidence that larger animals are significantly and consistently more stressed. Furthermore, the apparent reductions in mean body size coincide with declining population trends; as of March 2026, the IUCN lists 21/22 *Sylvilagus* species as decreasing (including *S. audubonii* and *S. nuttallii*) or trend unknown (*S. floridanus*), suggesting that these rabbits and may be generally vulnerable to nutrient dilution and other effects of climate change, which may be potentially constraining both growth and fecundity. This is particularly pertinent to the future of all cottontail species (and lagomorphs at large), as many are limited in range and habitat, and thus have less capacity to behaviorally compensate for environmental change.

Future Directions

This work presents a framework for using museum-specimen-derived data to track nutrient dilution over time, which can be extended in several ways. First, one limitation to the present study is sample size; although Eastern Cottontails are comparatively well represented in museum collections, collecting effort is uneven over space and time, presenting challenges to obtaining comparable series of specimens that minimize variation, particularly in size and stable isotope ratios, due to habitat or geography. Targeted collecting, particularly in locations that are already well sampled, can provide a more robust basis of comparison and potentially a clearer picture of nutrient dilution. Moreover, modern preparation and storage practices can improve the preservation and stability of physiological indicators, like cortisol, reducing noise introduced by degradation via chemicals, light and temperature, etc. (Stewart *et al.* 2018). For rabbits, age can be more accurately estimated from fresh specimens (Lord 1959), so active collecting can also provide an opportunity to simultaneously understand how stable isotope values vary by age, season, and habitat. In addition to expanding sample sizes by collecting, applying other metrics of nutritional status to existing specimens may unlock more information about nutrient dilution; for example, compound-specific stable isotope analysis can more precisely target how an animal's diet is processed into its own body tissues (Whiteman *et al.* 2019). Finally, museum studies may be augmented by working in tandem with laboratory experiments. Feeding captive animals controlled diets that simulate nutrient dilution—e.g., vegetation grown with varying exposure to CO_2—can provide targets for detecting the effects of nutrient dilution in wild counterparts, such as specific isotopic signatures, stress, and/or changes in metabolites.

Combining multiple forms and sources of data to pinpoint the intersections of morphology, physiology, and ecology provides a pathway to understanding the impacts of environmental change from organisms to ecosystems. Here, I highlight how the study of body size can advance this work, particularly highlighting how overemphasis of the effects of lengthening growing seasons and improved resource availability leaves out the critical role of resource quality. Nutrient dilution threatens ecosystems worldwide, and understanding how the consequences of

micronutrient deficits resonate throughout food webs begins with the species that occupy vital nodes of those networks, those like rabbits, which are both a common primary consumer and essential prey source. Although diet or habitat selection may provide some capacity to buffer against nutrient dilution, expanded investigations will further uncover the correlates and drivers of intra- and interspecific variation in responses to shifting resources. Thorough evaluation of the effects of nutrient dilution across habitats and levels of organization is key to mitigation, and to making conservation decisions for the health of humans and wildlife alike.

Acknowledgements

I would like to thank the museum personnel, particularly Rebecca Hawkins at the Sam Noble Oklahoma Museum of Natural History as well as Lorelei Patrick and Jackson Roberts at the Sternberg Museum of Natural History, for facilitating access and sampling of the specimens used for this study. Additionally, the research would not have been possible without the work and expertise of Lucy Kapronczai in the Janz lab at the University of Saskatchewan and the technicians at the University of California Davis Stable Isotope Facility. I am also grateful to Laura Stein, Michelle St. John, and Eric Arredondo for their generous advice and guidance. Finally, I would like to thank my dissertation committee for their ideas and feedback that greatly improved this project.

Author Contributions

MKT conceptualized the project, took samples and measurements, analyzed the data, and wrote this manuscript, with input and editorial feedback from HCL.

Funding

This work was supported by a Grant-in-Aid of Research from the American Society of Mammalogists as well as a Dissertation Completion Fellowship from the Dodge Family College of Arts and Sciences and the Eddie Carol Smith Scholarship from the Graduate College at the University of Oklahoma.

Data Availability

Raw data can be viewed at:
https://osf.io/64b83/overview?view_only=7a2f4643c8b346419f57836639916f48

GBIF data used in this study are available at the following:

S. floridanus: GBIF.org (20 November 2025) GBIF Occurrence Download:
https://doi.org/10.15468/dl.6gdnjp

S. audubonii: GBIF.org (7 January 2026) GBIF Occurrence Download:
https://doi.org/10.15468/dl.5nvjxc

S. nuttallii: GBIF.org (7 January 2026) GBIF Occurrence Download: https://doi.org/10.15468/dl.q9c3g9

References

Bailey LD, Kruuk LEB, Allen R, Clayton M, Stein J, Gardner JL. 2020. Using different body size measures can lead to different conclusions about the effects of climate change. Journal of Biogeography 47(8):1687–1697. https://doi.org/10.1111/jbi.13850

Bartoń K. 2025. MuMIn: Multi-Model Inference.

Ben-David M, Flaherty EA. 2012. Stable isotopes in mammalian research: a beginner's guide. Journal of Mammalogy 93(2):312–328. https://doi.org/10.1644/11-MAMM-S-166.1

Bergmann C. 1847. Über die Verhältnisse der Wärmeökonomie der Thiere zu ihrer Grösse. Göttinger Studien 1:595–708.

Chapman JA. 1975. *Sylvilagus nuttallii*. Mammalian Species 56:1–3. https://doi.org/10.2307/3503902

Chapman JA, Hockman JG, Ojeda MM. 1980. *Sylvilagus floridanus*. Mammalian Species 136:1–8.

Chapman JA, Willner GR. 1978. *Sylvilagus audubonii*. Mammalian Species 106:1–4.

Chuang A, Peterson CR. 2016. Expanding population edges: theories, traits, and trade-offs. Global Change Biology 22(2):494–512. https://doi.org/10.1111/gcb.13107

Correll RA, Prowse TAA, Prideaux GJ. 2016. Lean-season primary productivity and heat dissipation as key drivers of geographic body-size variation in a widespread marsupial. Ecography 39(1):77–86. https://doi.org/10.1111/ecog.01243

Craine JM. 2013. Long-term climate sensitivity of grazer performance: a cross-site study. PLoS ONE 8(6):e67065. https://doi.org/10.1371/journal.pone.0067065

Craine JM, Angerer JP, Elmore A, Fierer N. 2016. Continental-scale patterns reveal potential for warming-induced shifts in cattle diet. PLOS ONE 11(8):e0161511. https://doi.org/10.1371/journal.pone.0161511

Craine JM, Towne EG, Miller M, Fierer N. 2015. Climatic warming and the future of bison as grazers. Scientific Reports 5(1):16738. https://doi.org/10.1038/srep16738

Daufresne M, Lengfellner K, Sommer U. 2009. Global warming benefits the small in aquatic ecosystems. Proceedings of the National Academy of Sciences of the United States of America 106(31):12788–12793. https://doi.org/10.1073/pnas.0902080106

Davis CM, Roth VL. 2008. The evolution of sexual size dimorphism in cottontail rabbits (*Sylvilagus*, Leporidae). Biological Journal of the Linnean Society 95(1):141–156. https://doi.org/10.1111/j.1095-8312.2008.01035.x

Dombrosky J. 2020. A ~1000-year^{13} C Suess correction model for the study of past ecosystems. The Holocene 30(3):474–478. https://doi.org/10.1177/0959683619887416

Duffy GA, Chown SL. 2016. Urban warming favours C_4 plants in temperate European cities. Journal of Ecology 104(6):1618–1626. https://doi.org/10.1111/1365-2745.12652

Eastman LM, Morelli TL, Rowe KC, Conroy CJ, Moritz C. 2012. Size increase in high elevation ground squirrels over the last century. Global Change Biology 18(5):1499–1508. https://doi.org/10.1111/j.1365-2486.2012.02644.x

Fletcher JWJ, Tollington S, Cox R, Tolhurst BA, Newton J, McGill RAR, Cropper P, Berry N, Illa K, Scott DM. 2025. Utilisation of anthropogenic food by red foxes (*Vulpes vulpes*) in Britain as determined by stable isotope analysis. Ecology and Evolution 15(3):e70844. https://doi.org/10.1002/ece3.70844

Henry E, Santini L, Huijbregts MAJ, Benítez-López A. 2023. Unveiling the environmental drivers of intraspecific body size variation in terrestrial vertebrates. Global Ecology and Biogeography 32(2):267–280. https://doi.org/10.1111/geb.13621

Hobson KA, Alisauskas RT, Clark RG. 1993. Stable-nitrogen isotope enrichment in avian tissues due to fasting and nutritional stress: implications for isotopic analyses of diet. The Condor 95(2):388–394. https://doi.org/10.2307/1369361

Hoffmeister DF, Zimmerman EG. 1967. Growth of the skull in the cottontail (Sylvilagus floridanus) and its application to age-determination. American Midland Naturalist 78(1):198. https://doi.org/10.2307/2423380

Huston MA, Wolverton S. 2011. Regulation of animal size by eNPP, Bergmann's rule, and related phenomena. Ecological Monographs 81(3):349–405. https://doi.org/10.1890/10-1523.1

Kaspari M, Welti EAR. 2024. Nutrient dilution and the future of herbivore populations. Trends in Ecology & Evolution 39(9):809–820. https://doi.org/10.1016/j.tree.2024.05.001

Linderholm HW. 2006. Growing season changes in the last century. Agricultural and Forest Meteorology 137(1–2):1–14. https://doi.org/10.1016/j.agrformet.2006.03.006

Loladze I. 2002. Rising atmospheric CO_2 and human nutrition: toward globally imbalanced plant stoichiometry? Trends in Ecology & Evolution 17(10):457–461. https://doi.org/10.1016/S0169-5347(02)02587-9

Lord RD. 1959. The lens as an indicator of age in cottontail rabbits. The Journal of Wildlife Management 23(3):358–360. https://doi.org/10.2307/3796900

Mason RE, Craine JM, Lany NK, Jonard M, Ollinger SV, Groffman PM, Fulweiler RW, Angerer J, Read QD, Reich PB *et al.* 2022. Evidence, causes, and consequences of declining nitrogen availability in terrestrial ecosystems. Science 376(6590):eabh3767. https://doi.org/10.1126/science.abh3767

McLauchlan KK, Ferguson CJ, Wilson IE, Ocheltree TW, Craine JM. 2010. Thirteen decades of foliar isotopes indicate declining nitrogen availability in central North American grasslands. New Phytologist 187(4):1135–1145. https://doi.org/10.1111/j.1469-8137.2010.03322.x

McNab BK. 2010. Geographic and temporal correlations of mammalian size reconsidered: a resource rule. Oecologia 164(1):13–23. https://doi.org/10.1007/s00442-010-1621-5

Names GR, Grindstaff JL, Westneat DF, Heidinger BJ. 2024. Climate change and its effects on body size and shape: the role of endocrine mechanisms. Philosophical Transactions of the Royal Society B: Biological Sciences 379(1898):20220509. https://doi.org/10.1098/rstb.2022.0509

Negus NC. 1958. Pelage stages in the cottontail rabbit. Journal of Mammalogy 39(2):246. https://doi.org/10.2307/1376198

Olcott SP, Barry RE. 2000. Environmental correlates of geographic variation in body size of the eastern cottontail (Sylvilagus floridanus). Journal of Mammalogy 81(4):986–998. https://doi.org/10.1644/1545-1542(2000)081%253C0986:ECOGVI%253E2.0.CO;2

Pacifici M, Visconti P, Butchart SHM, Watson JEM, Cassola FM, Rondinini C. 2017. Species' traits influenced their response to recent climate change. Nature Climate Change 7(3):205–208. https://doi.org/10.1038/nclimate3223

Paniw M, James TD, Ruth Archer C, Römer G, Levin S, Compagnoni A, Che-Castaldo J, Bennett JM, Mooney A, Childs DZ *et al.* 2021. The myriad of complex demographic responses of terrestrial mammals to climate change and gaps of knowledge: A global analysis. Journal of Animal Ecology 90(6):1398–1407. https://doi.org/10.1111/1365-2656.13467

Peters RH. 1983. The ecological implications of body size. Cambridge, UK: Cambridge University Press.

R Core Team. 2025. R: A Language and Environment for Statistical Computing.

Russell E, Koren G, Rieder M, Van Uum S. 2012. Hair cortisol as a biological marker of chronic stress: Current status, future directions and unanswered questions. Psychoneuroendocrinology 37(5):589–601. https://doi.org/10.1016/j.psyneuen.2011.09.009

Sergiel A, Hobson KA, Janz DM, Cattet M, Selva N, Kapronczai L, Gryba C, Zedrosser A. 2017. Compatibility of preparatory procedures for the analysis of cortisol concentrations and stable isotope (δ13C, δ15N) ratios: a test on brown bear hair. Conservation Physiology 5(1). https://doi.org/10.1093/conphys/cox021

Stewart ND, Reilly A, Gilman C, Mastromonaco GF, Burness G. 2018. Evidence of degradation of hair corticosterone in museum specimens. General and Comparative Endocrinology 268:128–133. https://doi.org/10.1016/j.ygcen.2018.08.011

Tablado Z, Revilla E, Palomares F. 2009. Breeding like rabbits: global patterns of variability and determinants of European wild rabbit reproduction. Ecography 32(2):310–320. https://doi.org/10.1111/j.1600-0587.2008.05532.x

Ter Haar SF, Van Bodegom PM, Scherer L. 2025. CO_2 Rise Directly Impairs Crop Nutritional Quality. Global Change Biology 31(11):e70568. https://doi.org/10.1111/gcb.70568

Theriot MK, Lanier HC, Olson LE. 2023. Harnessing natural history collections to detect trends in body-size change as a response to warming: A critique and review of best practices. Methods in Ecology and Evolution 14(2):306–318. https://doi.org/10.1111/2041-210X.13861

Wallace M, Jones G, Charles M, Fraser R, Halstead P, Heaton THE, Bogaard A. 2013. Stable carbon isotope analysis as a direct means of inferring crop water status and water management practices. World Archaeology 45(3):388–409. https://doi.org/10.1080/00438243.2013.821671

Walsh LL, Tucker PK. 2023. Evaluating anthropogenic influence on a mesopredator: opossum (*Didelphis virginiana*) isotope values influenced by corn agriculture more than urbanization. Canadian Journal of Zoology 101(5):307–316. https://doi.org/10.1139/cjz-2021-0172

Watt C, Mitchell S, Salewski V. 2010. Bergmann's rule; a concept cluster? Oikos 119(1):89–100. https://doi.org/10.1111/j.1600-0706.2009.17959.x

Webster MS. 2017. The extended specimen. In: Webster MS, editor. *The extended specimen: emerging frontiers in collections-based ornithological research*. Studies in Avian Biology. Boca Raton, FL: CRC Press; p. 1–9.

Welti EAR, Roeder KA, de Beurs KM, Joern A, Kaspari M. 2020. Nutrient dilution and climate cycles underlie declines in a dominant insect herbivore. Proceedings of the National Academy of Sciences 117(13):7271–7275. https://doi.org/10.1073/pnas.1920012117

Whiteman JP, Elliott Smith EA, Besser AC, Newsome SD. 2019. A guide to using compound-specific stable isotope analysis to study the fates of molecules in organisms and ecosystems. Diversity 11(1):8. https://doi.org/10.3390/d11010008

Wolak ME, Fairbairn DJ, Paulsen YR. 2012. Guidelines for estimating repeatability. Methods in Ecology and Evolution 3(1):129–137. https://doi.org/10.1111/j.2041-210X.2011.00125.x

Woodward G, Ebenman B, Emmerson M, Montoya J, Olesen J, Valido A, Warren P. 2005. Body size in ecological networks. Trends in Ecology & Evolution 20(7):402–409. https://doi.org/10.1016/j.tree.2005.04.005

Yom-Tov Y, Geffen E. 2011. Recent spatial and temporal changes in body size of terrestrial vertebrates: probable causes and pitfalls. Biological Reviews 86(2):531–541. https://doi.org/10.1111/j.1469-185X.2010.00168.x

Zimova M, Hackländer K, Good JM, Melo-Ferreira J, Alves PC, Mills LS. 2018. Function and underlying mechanisms of seasonal colour moulting in mammals and birds: what keeps them changing in a warming world? Biological Reviews 93(3):1478–1498. https://doi.org/10.1111/brv.12405

Supplementary Material

Range-wide trends in cottontail body size

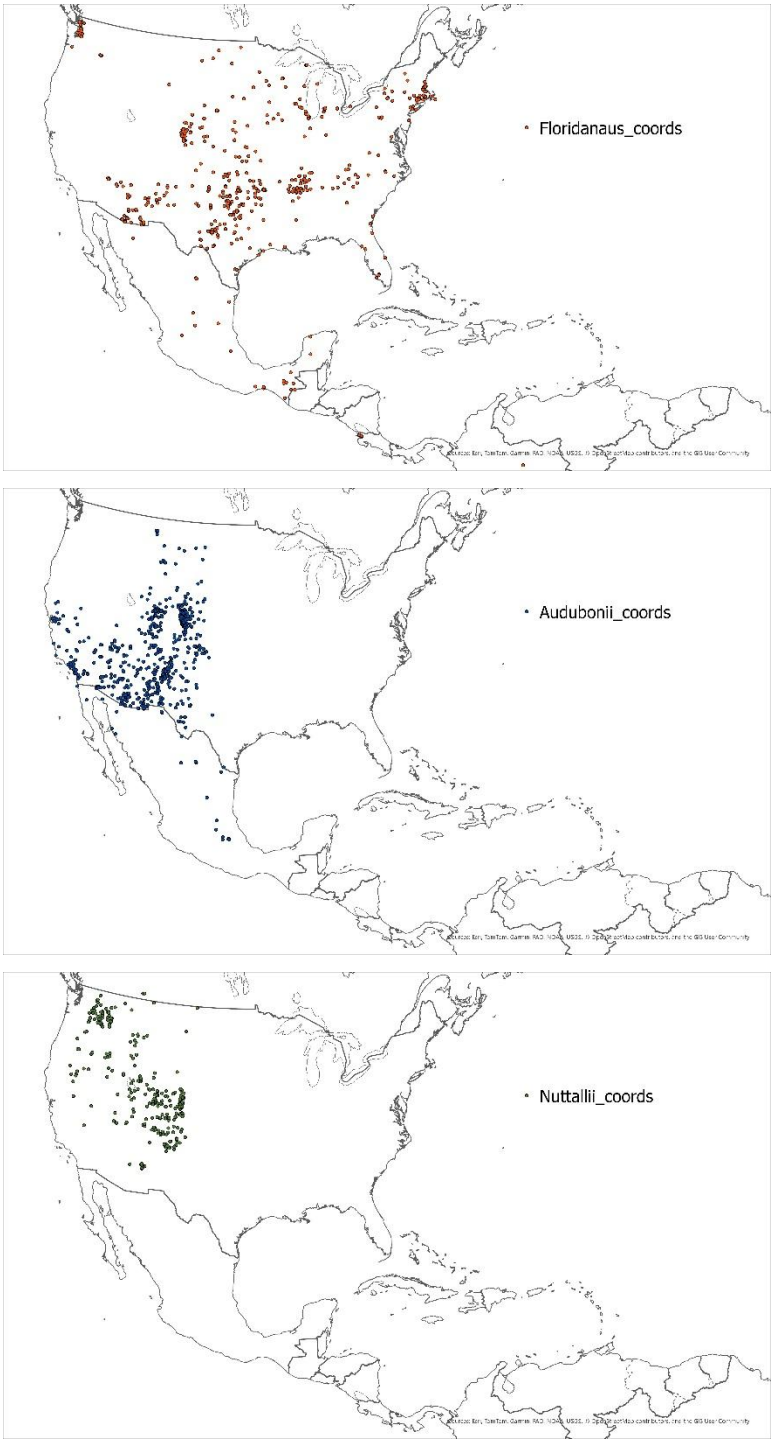


Figure S1. Map of cottontail specimens obtained from GBIF: *Sylvilagus floridanus* (top), *S. audubonii* (middle), and *S. Nuttallii* (bottom).

Nutrient dilution test—Description of skull measurements

Cranial measurements used to estimate size, adapted from (Olcott and Barry 2000):

Cranial height (CH): distance from the crown of the skull (anteriomost point of the interparietal) to the base of the braincase (foramen cavernosum of the basisphenoid)

Zygomatic length (ZL): distance from the anteriormost to posteriormost points of the zygomatic arch

Greatest total length (GTL): distance from the anteriormost point of skull (the premaxilla superior to the first incisor) to the posteriormost point (posterior margin of the supraoccipital)

Condylopremaxillary length (CPL): distance from anteriormost point of the skull (the premaxilla superior to the incisors) to the posterior margin of the occipital condyle

Cranial width (CW): maximum width of the cranium perpendicular to the midline

maxillary width (MXW): maximum width of the maxillae centered at the third cheek teeth (P3) and perpendicular to the midline

zygomatic breadth (ZB): maximum width between zygomatic arches perpendicular to the midline

Maxillary toothrow length (MTRL): distance from the anterior margin of the bony socket of the first cheek tooth (alveolus of P1) to the posterior margin of that of the last cheek tooth (alveolus of M3)

Basilar length (BSL): distance from the posterior margin of the socket of the second incisor (alveolus of I2) to inner surface of the posterior lip of the foramen magnum

Mandible height (MH), distance from the anterior point formed by the lateral edge of the mandible to the crest of the mandibular condyle

Nutrient dilution test—Repeatability of skull measurements

Measurement	**Round 1**	**Round 2**	**Combined**
Greatest total length (GTL)	0.999 [0.996,1]	0.999 [0.998,1]	0.999 [0.996,1]
Condylo-premaxillary length (CPL)	0.998 [0.994,1]	0.999 [0.996,1]	0.998 [0.995,1]
Basilar length (BSL)	0.997 [0.992,1]	0.999 [0.996,1]	0.998 [0.994,1]
Zygomatic breadth (ZB)	0.999 [0.997,1]	0.999 [0.995,1]	0.999 [0.997,1]
Zygomatic length (ZL)	0.94 [0.831,0.992]	0.998 [0.992,1]	0.957 [0.882,0.995]
Cranial width (CW)	0.997 [0.989,1]	0.987 [0.956,0.999]	0.993 [0.981,0.999]
Cranial height (CH)	0.967 [0.904,0.996]	0.989 [0.962,0.999]	0.974 [0.926,0.997]

Measurement	Round 1	Round 2	Combined
Maxillary width (MXW)	0.994 [0.982,0.999]	0.995 [0.981,0.999]	0.994 [0.983,0.999]
Maxillary tooth row length (MTRL)	0.912 [0.764,0.989]	0.938 [0.805,0.992]	0.909 [0.767,0.988]
Mandible height (MH)	0.789 [0.528,0.97]	0.994 [0.978,0.999]	0.767 [0.513,0.966]

Table S1. Repeatability of cottontail skull measurements, including estimated intraclass correlation coefficients with 95% confidence interval. The first round was completed before measuring the Oklahoma specimens (OMNH). The second round, conducted on the same specimens, was completed before measuring the Kansas specimens (FHSM). Measurements from both rounds are combined in the third column.

Nutrient dilution test—Spread of specimens through time by state

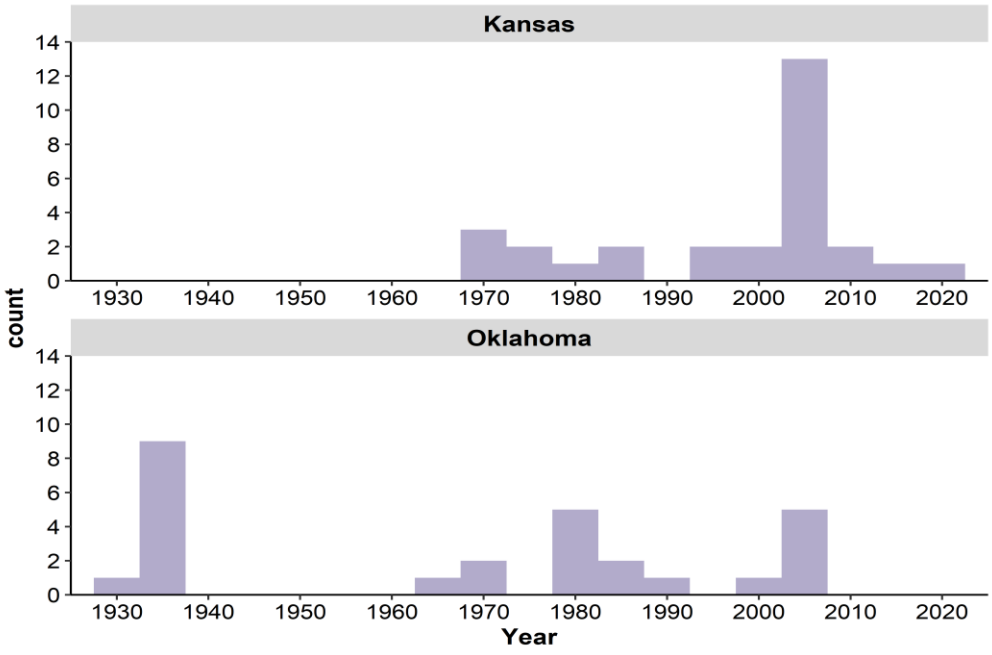


Figure S2. Number of specimens collected over time by state.

Nutrient dilution test—Nitrogen versus carbon concentrations (µg/mg sample) in hair

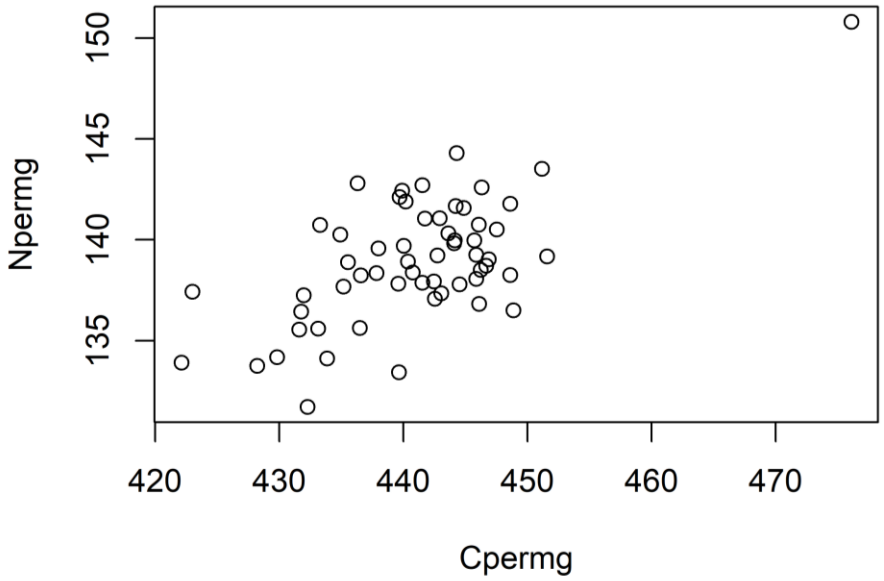


Figure S3. Nitrogen versus carbon concentrations (µg/mg sample) in cottontail hair samples. One specimen had higher than expected values based on the rest of the sample—removed from analyses.

Nutrient dilution test—Full linear model results

	Estimate	Std. Error	t value	Pr(>|t|)
(Intercept)	56.3304511	43.8367753	1.2850044	0.2086237
Sexmale	0.8744062	1.0200557	0.8572142	0.3981228
Year	-0.0280262	0.0219334	-1.2777871	0.2111240
StateOklahoma	-2.2006998	1.0515943	-2.0927270	0.0449340
Adjusted r^2	0.0695483			
F statistic	1.822215			
df	3,30			

Table S2. Full results for linear model 1 (time location) for cranial measurement PC1.

	Estimate	Std. Error	t value	Pr(>|t|)
(Intercept)	-3.7466810	26.3914354	-0.1419658	0.8880257
X15N	0.2967697	0.1889978	1.5702289	0.1265141
Npermg	0.0157373	0.1904306	0.0826406	0.9346687
Adjusted r^2	0.0140827			
F statistic	1.235684			
df	2,31			

Table S3. Full results for linear model 2 (nitrogen availability) for cranial measurement PC1.

	Estimate	Std. Error	t value	Pr(>|t|)
(Intercept)	9.4805171	2.5836718	3.669397	0.0009070
StateOklahoma	-2.6121074	0.8326465	-3.137115	0.0037245
X13C_corrected	0.4316796	0.1229855	3.510003	0.0013951
Adjusted r^2	0.2984798			
F statistic	8.020348			
df	2,31			

Table S4. Full results for linear model 3 (forage content) for cranial measurement PC1.

	Estimate	Std. Error	t value	Pr(>|t|)
(Intercept)	2.2251285	1.3454006	1.6538781	0.1082448
Sexmale	0.5640418	1.0348677	0.5450376	0.5896278
log(Cort)	-1.6440093	0.8344246	-1.9702312	0.0578004
Adjusted r^2	0.0821536			
F statistic	2.476864			
df	2,31			

Table S5. Full results for linear model 4 (stress) for cranial measurement PC1.

Model 4 (Stress, with cort correction)

	Estimate	Std. Error	t value	Pr(>|t|)
(Intercept)	2.397278	1.8560479	1.2916037	0.2060419
Sexmale	0.893227	1.0363421	0.8619036	0.3953591
Cort_correction	-1.106190	0.7482439	-1.4783811	0.1493955
Adjusted r^2	0.0352401			
F statistic	1.602701			
df	2,31			

Table S6. Full results for linear model 4 (stress) with cortisol correction for cranial measurement PC1.

	Estimate	Std. Error	t value	Pr(>|t|)
(Intercept)	0.9061831	1.5878045	0.5707145	0.5724437
Sexmale	0.1692993	1.0487877	0.1614238	0.8728419
log(Cort)	-1.6768252	0.8186426	-2.0482995	0.0493695
X15N	0.2761359	0.1849145	1.4933165	0.1457981
Adjusted r^2	0.1171814			
F statistic	2.460091			
df	3,30			

Table S7. Full results for linear model 5 (Nitrogen availability and stress) for cranial measurement PC1.

Model 5 (Nitrogen availability and stress, with cort correction)

	Estimate	Std. Error	t value	Pr(>|t|)
(Intercept)	1.4260497	1.8627537	0.7655600	0.4499196
Sexmale	0.3539284	1.0396318	0.3404363	0.7359004
Cort_correction	-1.4357783	0.7422196	-1.9344386	0.0625395
X15N	0.3548982	0.1916803	1.8515107	0.0739622
Adjusted r^2	0.1053167			
F statistic	2.294853			
df	3,30			

Table S8. Full results for linear model 5 (Nitrogen availability and stress) with cortisol correction for cranial measurement PC1.

Greatest total length of the skull (GTL)

	Estimate	Std. Error	t value	Pr(>|t|)
(Intercept)	165.4584307	43.2718454	3.823697	0.0005182
Sexmale	1.0859768	0.9633551	1.127286	0.2672908
Year	-0.0478357	0.0216627	-2.208202	0.0338744
StateOklahoma	-2.1607452	1.0236846	-2.110753	0.0420097
Adjusted r^2	0.1048388			
F statistic	2.483486			
df	3,35			

Table S9. Full linear model results for model 1 (time and location) for greatest total length of the skull (GTL).

	Estimate	Std. Error	t value	Pr(>|t|)
(Intercept)	68.9623939	24.5385393	2.8103708	0.0079536
X15N	0.3952422	0.1911400	2.0678155	0.0459015
Npermg	-0.0084109	0.1774219	-0.0474063	0.9624514
Adjusted r^2	0.0565799			
F statistic	2.13949			
df	2,36			

Table S10. Full linear model results for model 2 (nitrogen availability) for greatest total length of the skull (GTL).

	Estimate	Std. Error	t value	Pr(>|t|)
(Intercept)	77.9108301	2.7356090	28.480251	0.0000000
StateOklahoma	-1.7197406	0.8881366	-1.936347	0.0607063
X13C_corrected	0.3784096	0.1317427	2.872338	0.0067900
Adjusted r^2	0.1646041			
F statistic	4.743709			
df	2,36			

Table S11. Full linear model results for model 3 (forage content) for greatest total length of the skull (GTL).

	Estimate	Std. Error	t value	Pr(>|t|)
(Intercept)	71.7071474	1.3428977	53.397325	0.0000000
Sexmale	0.6045038	1.0289900	0.587473	0.5605531
log(Cort)	-1.4701523	0.8577264	-1.714011	0.0951260
Adjusted r^2	0.0537579			
F statistic	2.079429			
df	2,36			

Table S12. Full linear model results for model 4 (stress) for greatest total length of the skull (GTL).

	Estimate	Std. Error	t value	Pr(>|t|)
(Intercept)	69.5722496	1.7699252	39.3080170	0.0000000
Sexmale	1.0925259	1.0447108	1.0457688	0.3026390
Cort_correction	-0.0003744	0.7276216	-0.0005145	0.9995923
Adjusted r^2	-0.0234615			
F statistic	0.5644493			
df	2,36			

Table S13. Full linear model results for model 4 (stress) with cortisol correction for greatest total length of the skull (GTL).

	Estimate	Std. Error	t value	Pr(>|t|)
(Intercept)	69.8846775	1.5332616	45.5790954	0.0000000
Sexmale	0.2930032	0.9910129	0.2956603	0.7692366
log(Cort)	-1.5888723	0.8191052	-1.9397658	0.0605007
X15N	0.3978631	0.1844281	2.1572803	0.0379316
Adjusted r^2	0.1409483			
F statistic	3.078274			
df	3,35			

Table S14. Full linear model results for model 5 (nitrogen availability and stress) for greatest total length of the skull (GTL).

	Estimate	Std. Error	t value	Pr(>|t|)
(Intercept)	68.4878993	1.7817849	38.4378039	0.0000000
Sexmale	0.7124831	1.0202936	0.6983119	0.4895962
Cort_correction	-0.4075426	0.7269587	-0.5606132	0.5786327
X15N	0.4050435	0.2006665	2.0184904	0.0512544
Adjusted r^2	0.0570628			
F statistic	1.766536			
df	3,35			

Table S15. Full linear model results for model 5 (nitrogen availability and stress) with cortisol correction for greatest total length of the skull (GTL).

Zygomatic breadth (ZB)

	Estimate	Std. Error	t value	Pr(>|t|)
(Intercept)	59.4351018	20.9725795	2.8339433	0.0074906
Sexmale	-0.1492243	0.4823768	-0.3093522	0.7588371
Year	-0.0121086	0.0104904	-1.1542585	0.2559994
StateOklahoma	-1.2386588	0.4997833	-2.4783917	0.0180209
Adjusted r^2	0.076176			
F statistic	2.071944			
df	3,36			

Table S16. Full linear model results for model 1 (time and location) for zygomatic breadth (ZB).

	Estimate	Std. Error	t value	Pr(>|t|)
(Intercept)	33.3769654	11.8894680	2.8072716	0.0079263
X15N	0.0923393	0.0949455	0.9725509	0.3370921
Npermg	0.0073233	0.0859306	0.0852232	0.9325434
Adjusted r^2	-0.0272239			
F statistic	0.4832041			
df	2,37			

Table S17. Full linear model results for model 2 (nitrogen availability) for zygomatic breadth (ZB).

	Estimate	Std. Error	t value	Pr(>|t|)
(Intercept)	38.8877775	1.2515425	31.071880	0.0000000
StateOklahoma	-1.3792232	0.4083316	-3.377704	0.0017320
X13C_corrected	0.1798922	0.0601890	2.988789	0.0049537
Adjusted r^2	0.2483846			
F statistic	7.44412			
df	2,37			

Table S18. Full linear model results for model 3 (forage content) for zygomatic breadth (ZB).

	Estimate	Std. Error	t value	Pr(>|t|)
(Intercept)	36.0424796	0.6323811	56.9948700	0.0000000
Sexmale	-0.2811672	0.4997707	-0.5625925	0.5771055
log(Cort)	-0.7953620	0.4098933	-1.9404123	0.0599788
Adjusted r^2	0.0438402			
F statistic	1.89408			
df	2,37			

Table S19. Full linear model results for model 4 (stress) for zygomatic breadth (ZB).

	Estimate	Std. Error	t value	Pr(>|t|)
(Intercept)	36.2298609	0.7856048	46.117155	0.0000000
Sexmale	-0.1556886	0.4941758	-0.315047	0.7544960
Cort_correction	-0.5833682	0.3292215	-1.771963	0.0846363
Adjusted r^2	0.028944			
F statistic	1.58123			
df	2,37			

Table S20. Full linear model results for model 4 (stress) with cortisol correction for zygomatic breadth (ZB).

	Estimate	Std. Error	t value	Pr(>|t|)
(Intercept)	35.5434430	0.7973818	44.5751887	0.0000000
Sexmale	-0.3746049	0.5076450	-0.7379269	0.4653422
log(Cort)	-0.7873374	0.4096742	-1.9218622	0.0625661
X15N	0.0954767	0.0930393	1.0261974	0.3116448
Adjusted r^2	0.0452099			
F statistic	1.615558			
df	3,36			

Table S21. Full linear model results for model 5 (nitrogen availability and stress) for zygomatic breadth (ZB).

	Estimate	Std. Error	t value	Pr(>|t|)
(Intercept)	35.7424570	0.8475106	42.1734606	0.0000000
Sexmale	-0.3015505	0.4981953	-0.6052856	0.5487862
Cort_correction	-0.6692209	0.3303499	-2.0257945	0.0502468
X15N	0.1337649	0.0941329	1.4210216	0.1639152
Adjusted r^2	0.054978			
F statistic	1.756295			
df	3,36			

Table S22. Full linear model results for model 5 (nitrogen availability and stress) with cortisol correction for zygomatic breadth (ZB).

Maxillary toothrow length (MTRL)

	Estimate	Std. Error	t value	Pr(>|t|)
(Intercept)	34.9198042	11.9737964	2.916352	0.0058453
Sexmale	-0.0148335	0.2735950	-0.054217	0.9570390
Year	-0.0103761	0.0059945	-1.730943	0.0913679
StateOklahoma	-0.5775011	0.2753628	-2.097238	0.0425052
Adjusted r^2	0.046073			
F statistic	1.676178			
df	3,39			

Table S23. Full linear model results for model 1 (time and location) for Maxillary toothrow length (MTRL).

	Estimate	Std. Error	t value	Pr(>|t|)
(Intercept)	9.7369000	6.4297014	1.5143627	0.1377965
X15N	0.0750179	0.0532545	1.4086670	0.1666599
Npermg	0.0284388	0.0465031	0.6115465	0.5442981
Adjusted r^2	0.011008			
F statistic	1.233745			
df	2,40			

Table S24. Full linear model results for model 2 (nitrogen availability) for Maxillary toothrow length (MTRL).

	Estimate	Std. Error	t value	Pr(>|t|)
(Intercept)	16.4841045	0.7322199	22.512506	0.0000000
StateOklahoma	-0.5742153	0.2307023	-2.488989	0.0170710
X13C_corrected	0.1122280	0.0353237	3.177129	0.0028653
Adjusted r^2	0.200275			
F statistic	6.259035			
df	2,40			

Table S25. Full linear model results for model 3 (forage content) for Maxillary toothrow length (MTRL).

	Estimate	Std. Error	t value	Pr(>|t|)
(Intercept)	14.7485487	0.3600671	40.9605581	0.0000000
Sexmale	-0.1523130	0.2822914	-0.5395594	0.5924920
log(Cort)	-0.4748988	0.2351735	-2.0193549	0.0501862
Adjusted r^2	0.047157			
F statistic	2.039307			
df	2,40			

Table S26. Full linear model results for model 4 (stress) for Maxillary toothrow length (MTRL).

	Estimate	Std. Error	t value	Pr(>|t|)
(Intercept)	14.3981500	0.4714018	30.5432639	0.0000000
Sexmale	-0.0395647	0.2881543	-0.1373039	0.8914794
Cort_correction	-0.1421925	0.1964931	-0.7236517	0.4734906
Adjusted r^2	-0.03641			
F statistic	0.262213			
df	2,40			

Table S27. Full linear model results for model 4 (stress) with cortisol correction for Maxillary toothrow length (MTRL).

	Estimate	Std. Error	t value	Pr(>|t|)
(Intercept)	14.3469941	0.4389516	32.6846844	0.0000000
Sexmale	-0.1986264	0.2791125	-0.7116357	0.4809257
log(Cort)	-0.4810600	0.2312178	-2.0805496	0.0440915
X15N	0.0798128	0.0515980	1.5468200	0.1299838
Adjusted r^2	0.079215			
F statistic	2.204423			
df	3,39			

Table S28. Full linear model results for model 5 (nitrogen availability and stress) for Maxillary toothrow length (MTRL).

	Estimate	Std. Error	t value	Pr(>|t|)
(Intercept)	14.0948382	0.4963508	28.3969299	0.0000000
Sexmale	-0.1063072	0.2849089	-0.3731271	0.7110743
Cort_correction	-0.2140310	0.1971504	-1.0856231	0.2843108
X15N	0.0910643	0.0549169	1.6582217	0.1052958
Adjusted r^2	0.007023			
F statistic	1.099021			
df	3,39			

Table S29. Full linear model results for model 5 (nitrogen availability and stress) with cortisol correction for Maxillary toothrow length (MTRL).

Mandible height (MH)

	Estimate	Std. Error	t value	Pr(>|t|)
(Intercept)	73.6118178	24.4309350	3.0130577	0.0050242
Sexmale	0.4158515	0.5556839	0.7483598	0.4597084
Year	-0.0196362	0.0122241	-1.6063516	0.1180211
StateOklahoma	-1.4877974	0.5454761	-2.7275210	0.0102723
Adjusted r^2	0.135353			
F statistic	2.82632			
df	3,32			

Table S30. Full linear model results for model 1 (time and location) for mandible height (MH).

	Estimate	Std. Error	t value	Pr(>|t|)
(Intercept)	36.4995590	13.2653513	2.7514958	0.0095600
X15N	0.2068295	0.1108255	1.8662626	0.0709130
Npermg	-0.0253149	0.0954394	-0.2652462	0.7924697
Adjusted r^2	0.043576			
F statistic	1.797321			
df	2,33			

Table S31. Full linear model results for model 2 (nitrogen availability) for mandible height (MH).

	Estimate	Std. Error	t value	Pr(>|t|)
(Intercept)	38.1800165	1.4710488	25.954283	0.0000000
StateOklahoma	-1.4210563	0.4738565	-2.998917	0.0051213
X13C_corrected	0.1823439	0.0714564	2.551821	0.0155327
Adjusted r^2	0.221104			
F statistic	5.967705			
df	2,33			

Table S32. Full linear model results for model 3 (forage content) for mandible height (MH).

	Estimate	Std. Error	t value	Pr(>|t|)
(Intercept)	35.342053	0.7663073	46.1199515	0.0000000
Sexmale	0.329024	0.5813973	0.5659194	0.5752769
log(Cort)	-0.944533	0.5021371	-1.8810262	0.0688165
Adjusted r^2	0.064463			
F statistic	2.205839			
df	2,33			

Table S33. Full linear model results for model 4 (stress) for mandible height (MH).

	Estimate	Std. Error	t value	Pr(>|t|)
(Intercept)	35.0553017	0.9706137	36.1166352	0.0000000
Sexmale	0.5356228	0.5894098	0.9087443	0.3700744
Cort_correction	-0.4722324	0.4132226	-1.1428037	0.2613437
Adjusted r^2	0.003589			
F statistic	1.063029			
df	2,33			

Table S34. Full linear model results for model 4 (stress) with cortisol correction for mandible height (MH).

	Estimate	Std. Error	t value	Pr(>|t|)
(Intercept)	34.3361043	0.9443018	36.3613662	0.0000000
Sexmale	0.1065122	0.5790452	0.1839446	0.8552176
log(Cort)	-0.9223062	0.4877876	-1.8907946	0.0677356
X15N	0.1892159	0.1093466	1.7304238	0.0931892
Adjusted r^2	0.117781			
F statistic	2.557555			
df	3,32			

Table S35. Full linear model results for model 5 (nitrogen availability and stress) for mandible height (MH).

	Estimate	Std. Error	t value	Pr(>|t|)
(Intercept)	34.3601918	0.9650348	35.6051330	0.0000000
Sexmale	0.2231289	0.5724857	0.3897546	0.6993001
Cort_correction	-0.7605762	0.4097954	-1.8559900	0.0726845
X15N	0.2610538	0.1152042	2.2660084	0.0303511
Adjusted r^2	0.114535			
F statistic	2.50908			
df	3,32			

Table S36. Full linear model results for model 5 (nitrogen availability and stress) with cortisol correction for mandible height (MH).

CHAPTER 3

NO SHAPE FITS ALL: TRENDS IN CRANIAL MORPHOLOGY ARE NOT CONSISTENT WITH DOMESTICATION SYNDROME ACROSS FOUR URBAN-DWELLING MAMMALS

Miranda K. Theriot, Emilyn J. Gilmore, and Hayley C. Lanier

Sam Noble Oklahoma Museum of Natural History, School of Biological Sciences, University of Oklahoma, Norman, OK 73072, United States

Abstract

Conserving biodiversity in anthropogenic habitats necessitates unraveling patterns of wildlife responses to urbanization across spatial, temporal, and taxonomic scales. A central question in this endeavor concerns identifying the characteristics which enable some species to thrive in urban environments while others are excluded or displaced. Comparing cranial morphology between rural and urban habitats serves as a method to investigate common effects of urbanization among populations and species. For example, a link has been proposed between behavioral adaptations and skull features similar to those observed in some domesticated species (i.e., domestication syndrome), though the extent of this phenomenon remains unknown. In this study, we used museum specimens to quantify differences in skull shape between rural and urban environments, aiming to identify shared trends across species and whether these align with the expectations of domestication syndrome. We focused on four widespread, urban-dwelling mammals: Northern Raccoon (*Procyon lotor*), Virginia Opossum (*Didelphis virginiana*), Eastern Fox Squirrel (*Sciurus niger*), and Eastern Cottontail (*Sylvilagus floridanus*), assessing shape variation via a series of two-dimensional landmarks on skull photographs. The results indicated no universal trends across species at a broad geographic scale. In all but the squirrels, there were some significant shape differences between rural and urban habitat categories, although none of these differences followed predictions derived from domestication syndrome. Notably, the shape trends associated with advancing age classes in raccoons mirrored those found in more rural habitats, suggesting that age structure may significantly influence population-level morphological trends. These findings contribute to an expanding body of work revealing the complexity and diversity of urban ecosystems. While there is no "one size fits all" form or adaptive strategy that applies universally, understanding the context-dependent regularities among varied responses and their underlying factors is key to characterizing how wildlife will continue to be shaped by rapidly changing anthropogenic habitats.

Introduction

Human activity has profound and widespread effects on ecosystems worldwide. Urbanization drives some of the most significant impacts, dramatically transforming landscapes for human use. Although urban habitats have historically received little attention in ecology (McDonnell 2011), a growing body of research has revealed the myriad altered characteristics and processes

shaping these ecosystems and producing unique patterns of biodiversity (Shochat et al. 2006, Grimm et al. 2008, Zhang et al. 2022). As with most aspects of global change, urbanization will continue to intensify in coming decades; today, cities are home to over half the world's human population and rising (United Nations 2019). Understanding the ecological effects of urbanization is pivotal to fostering resilient ecosystems that can sustain human life into the future (Tanner et al. 2014, Apfelbeck et al. 2020).

Urban habitats are ecologically complex, presenting unique risks and benefits to wildlife. In and around cities, animals can incur greater rates of injury related to roadways (Kent et al. 2021, Moncrief et al. 2022) as well as illnesses from parasites and toxins (Murray et al. 2019, Green et al. 2022). Simultaneously, urban environments offer supplemental resources, either through intentional feeding or refuse, influencing population-and community-level structure and dynamics (Fischer et al. 2012, Hansen et al. 2024). Balancing risk avoidance while taking advantage of potential rewards produces a spectrum of interactions with urban habitats, from exploiters to avoiders (Blair 1996); Identifying the long-term effects of these opposing pressures is key to predicting ongoing responses to rapid habitat alteration as cities expand.

Morphology, particularly shifts in skull shape, can reflect responses to the local environment, including behavioral adaptations. In mammals, close association with humans has been linked to a suite of morphological characteristics—reduced brain size, shorter snout length, smaller teeth—common among some domesticated species (Wilkins et al. 2014, Lord et al. 2020). This phenomenon, often referred to as "domestication syndrome," has been hypothesized to stem from shared developmental pathways linking physical traits and behavior, namely tameness and reduced fear (Wilkins et al. 2014; although see Lord et al. 2020, 2025). Similar pressures may affect wild animals living alongside humans. Fear can be a strong driver of behavioral patterns (Laundré et al. 2001, Hof et al. 2012), particularly in human-dominated habitats, which favor a mixture of cautious and bold strategies (Ritzel and Gallo 2020, Padovani et al. 2021). Thus, domestication syndrome provides a basis for relating habitat use, fear response, and behavior in urban mammal communities. Although domestication-syndrome-like trends have been reported in wild mammals, including red foxes (Parsons et al. 2020) and raccoons (Apostolov et al. 2025, Sluka et al. 2025), the taxonomic and geographic extent of this effect remains unknown.

Beyond behavior and environmental interactions, cranial morphology depends on individual factors, chiefly age. On the population level, morphological variation can be influenced by subtle differences in skeletal structures between younger and older animals, even in mammals, despite often being assumed to attain a stable adult size (Elbroch 2006, Theriot et al. 2024). Morphological patterns can thereby be informative about demographic responses to global change—including urbanization—which are not yet well understood (Paniw et al. 2021). In urban environments, this means considering age- or life-stage-specific mortality and behaviors (e.g., Prange et al. 2003, Padovani et al. 2020) that can alter population age structure and/or produce morphological trends that can mask those we may expect under domestication syndrome.

Here, we evaluated the prevalence of domestication syndrome in multiple urban mammal species by leveraging natural history collections to detect the effects of habitat change over space (i.e., different localities) and time (i.e., collection years) simultaneously. If domestication syndrome is a common process affecting urban mammals through shared pressures on behavior and developmental mechanisms, we predicted: 1) trends in cranial shape will be similar across

urban mammal species; and 2) these trends will generally be consistent with expectations under domestication syndrome, namely reduced braincase size and a shortened rostrum relative to the rest of the skull. We also assessed an alternative hypothesis—that skull shape is primarily influenced by age—in raccoons (for which we had sufficient sample size and age determination methods). Associating morphology with responses to urbanization can help us better predict future ecological effects of such emerging landscape shifts, as common skull shape trends may indicate broader processes in urban environments that influence mammal communities at large. Alternatively, if morphological patterns are taxon- or context-specific, this may reflect variation in successful urban-dweller strategies (Santini et al. 2019) and aid in pinpointing species and populations that are responding rapidly versus those that may be of conservation concern. Overall, this work contributes to the growing body of knowledge on urban mammals and how they are shaped by a complex, rapidly changing environment.

Materials and Methods

Focal species

We selected four species that are prevalent in urbanized environments and well represented in museum collections: Northern Raccoon (*Procyon lotor*), Virginia Opossum (*Didelphis virginiana*), Eastern Fox Squirrel (*Sciurus niger*), and Eastern Cottontail (*Sylvilagus floridanus*). These species exhibit moderate to high tolerance to human disturbances, often characterized as "urbanophilic" (e.g., Haverland and Veech 2017) or "urban adapters" (McKinney 2002). Both raccoons and opossums are generalist mesopredators known for their success in exploiting anthropogenic food sources, though the latter may do so to a lesser extent (Haverland and Veech 2017, Walsh and Tucker 2023). Fox squirrels occupy diverse urban habitats throughout their native and introduced ranges, particularly on college campuses (Peplinski and Brown 2020). In contrast, cottontails, while common in suburban areas (McKinney 2002), are arguably the least adapted to urban environments, avoidant to neutral towards human activities (Haverland and Veech 2017). These focal species, although commonplace in anthropogenic habitats, differ in size, diet, life, history, and behavior, thereby providing an opportunity to test whether patterns in skull morphology are consistent across urban-dwelling species—e.g., a domestication-syndrome-like effect—or whether observed trends are influenced by specific lifestyle and behavioral strategies for coping with human disturbance.

Specimen photography

To maximize consistency and repeatability, all specimen photography, landmarking, and (when applicable) age assessments described below were conducted by a single researcher.

Specimens were collected in Oklahoma, Tennessee, California, and Mississippi (one series of fox squirrels) and are housed at the Sam Noble Oklahoma Museum of Natural History and the Natural History Museum of Los Angeles County. Sample sizes were determined by availability of known-sex specimens in these collections, resulting in a total of 398 raccoons, 100 opossums, 119 fox squirrels, and 113 cottontails, collected between 1917-2023, with the majority (~60%) from the 1970s and 1980s. Each skull was photographed in the dorsal, ventral, and lateral aspects using a Nikon D750 camera (mounted on a tripod and positioned parallel to the table using a level) and a ten-centimeter scale bar positioned in the same plane as the maxillary

toothrow. Some skulls were partially broken, so sample sizes vary slightly across skull aspects. For a complete list of specimens and associated details, see Supplementary Material.

Landmarking

Drawing from previously published work (Marcus et al. 2000, Drake and Klingenberg 2010, Parsons et al. 2020), A series of two-dimensional, fixed landmarks were developed as along with sets of semilandmarks in the dorsal and lateral aspects, placed along the curve of the braincase and zygomatic arch then resampled to be evenly spaced (Figure 1). Landmark sets differed slightly among species—selected to capture the shape of the braincase, rostrum, and overall skull while maximizing consistency in placement—so different species and aspects were aligned and analyzed separately. Landmarks were only placed on the right side of the skull (unless broken, in which case the left side was mirrored) ensuring that bilateral points are not weighted more heavily than those along the midline in analyses, as asymmetry was not a focus of this study (Zelditch et al. 2012). Replicates were performed across multiple sessions on subsets of specimens for each species in the dorsal aspect to assess repeatability of the landmarking procedure. Files were prepared using *tpsUtil version 1.82* (Rohlf 2022) and landmarks were digitized in *tpsDig2 version 2.32* (Rohlf 2021).

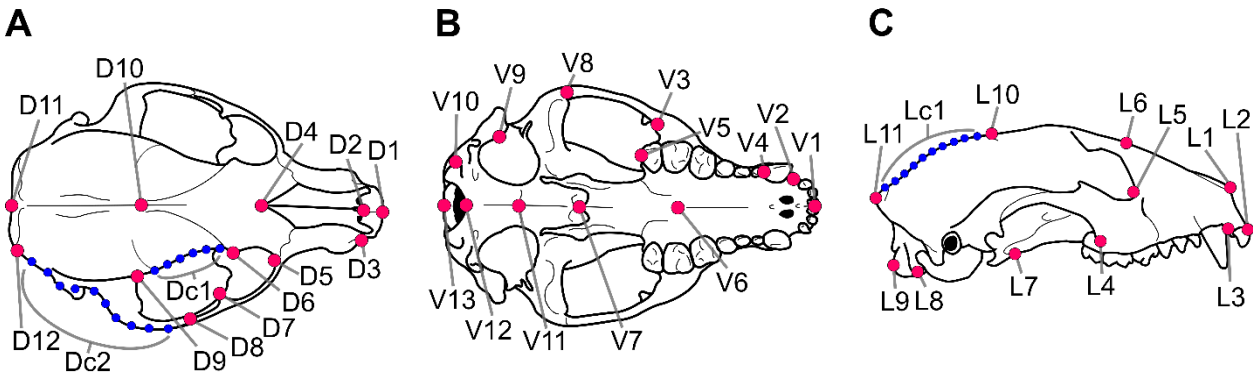


Figure 1. Landmarks for geometric morphometric analysis in the dorsal (A), ventral (B), and lateral (C) skull aspects. Landmarks are represented by large pink circles, semilandmarks (curves, denoted by "c" in the labels) small blue circles. Here, Northern Raccoon (*Procyon lotor*) is used as an example; for landmark placement on all four species, as well as full landmark descriptions, see Supplementary Material.

Age determination in raccoons

Age can be an important contributor to variation in skull morphology, even into adulthood; however, methods for determining exact age from museum specimens are often destructive and require specialized techniques (Morris 1972). In some species, relative age may be estimated based on the development of certain skull features; we delineated raccoon specimens into four age classes based on suture closure (Junge and Hoffmeister 1980) with tooth wear as a secondary criterion (Grau et al. 1970): Juvenile (likely < 1 year old), young adult (approximately 1-2 years old), adult (approximately 3-5 years old), and old adult (approximately 5+ years old). A subset of specimens were assessed twice to ensure consistency (see Supplementary Material). We focused

on raccoons because: 1) they have a relatively long potential lifespan in the wild (Lotze and Anderson 1979); 2) aging criteria have been detailed in known-age specimens (Grau et al. 1970, Junge and Hoffmeister 1980); and 3) we had a large sample size, thus improving the chances that the representation of older age classes—which are generally rarer in collections due to high early mortality—is sufficient to make meaningful comparisons.

Assigning habitat category

We defined habitat category using two similar methods: by verbatim locality in the specimen record (e.g., within a town including specific street names, or in a more general fashion as distance to town), or by human population density for the county of collection derived from decadal US Census Records (Schroeder et al. 2025). For the latter method, we categorized counties with >200 people/ km^2 as urban and further split the remainder into rural (10-200 people/ km^2) and highly rural (<10 people/ km^2) (see Ratcliffe et al. 2016; Supplementary Material). Categorizations based on verbatim locality and county-level human population density per decade coincided for ~80% of specimens (Table 1).

	Verbatim locality based			Human population density based				
Species	Rural	Urban	Unk.	Highly Rural	Rural	Urban	Unk.	% Agree
Raccoons	214	51	133	49	268	77	4	81.2%
Opossums	71	24	5	21	57	22	0	83.2%
Squirrels	66	53	0	34	53	26	6	77.9%
Cottontails	86	24	3	38	57	17	1	80.7%

Table 1. Number of specimens in urban and rural categories across four focal species, Northern Raccoon (*Procyon lotor*), Virginia Opossum (*Didelphis virginiana*), Eastern Fox Squirrel (*Sciurus niger*), and Eastern Cottontails (*Sylvilagus floridanus*). Agreement between the two methods for assigning habitat type—based on the verbatim locality and surrounding features or based on the county average human population density during the decade of collection calculated from US Census records (Schroeder et al. 2025)—was calculated as the percent of specimens with the same determination, excluding unknowns. Rural in the verbatim locality method was considered to correspond to both highly rural and rural in the human population density method.

Statistical analyses

For each aspect and species, specimens were aligned through Generalized Procrustes Analysis—using the 'gpagen' function in the *geomorph* package *version 4.0.5* (Baken et al. 2021, Adams et al. 2022)—which removes variation due to skull position, size, and rotation (Zelditch et al. 2012). Semilandmarks (curves) were superimposed by sliding along their tangent directions to minimize bending energy. Using the resulting Procrustes coordinates, we visualized differences among specimens using principal component analysis (PCA), and performed statistical tests to assess: 1) differences in skull shape among urban and rural categories, state, sex, and age class (raccoons only), controlled for skull size via centroid size; 2) differences in the intraspecific variation of skull shape among groupings of these variables (morphological disparity); and 3) To

what degree these variables can be used to accurately distinguish among specimens. All analyses were conducted in *R version 4.5.1* (R Core Team 2025).

A Procrustes ANOVA was performed using the 'ProcD.lm' function in the *geomorph* package. For each species and aspect, we fit two models, each controlling for centroid size, sex, age class (raccoons only), and the state in which specimens were collected, differing only by the method used to categorize urban versus rural habitat, either the verbatim locality or human population density approach as described above. Statistical significance was evaluated through permutation using a residual randomization procedure (999 iterations) (Collyer and Adams 2018, 2021). Full regression and fit details can be viewed in Supplementary Material.

Geography (i.e., state) is hypothesized to be a major determinant of cranial variation, which can be attributed to both environmental and genetic factors. While we cannot directly evaluate the role of each of these components, we extended the Procrustes ANOVA models with measures of climate variability. If the state variable primarily captures genetic differences in skull shape, the addition of climate variables should have minimal influence in the models. Conversely, if climate variables account for overlapping variation with geography (i.e., changing the significance or effect of the state variable in the models), this would suggest that climate is an important factor. We obtained decadal averages in seasonal climate variables (temperature, precipitation, and solar radiation) estimated by ClimateNA *version 7.60* (Wang et al. 2016, 2025) for each specimen based on reported latitude and longitude, or when absent, the latitude and longitude of the centroid of the county of collection (calculated using ArcGIS software). We performed PCA on the resulting dataset and included the first two principal component scores as continuous variables in additional Procrustes ANOVA models, both alongside and without state.

To test whether some groupings (i.e., habitat categories, sexes, states, or ages classes) exhibit greater variance in skull shape than others, morphological disparity was calculated using the 'morphol.disparity' function in the *geomorph* package. This method estimates Procrustes variance using the residuals of a model fit using the 'ProcD.lm' function as above and is therefore able to account for possible covariates. We subsequently performed pairwise comparisons between groups, using 1000 randomized permutations to test for statistically significant differences.

Finally, to assess differentiation among grouping variables, we applied a canonical variate analysis (CVA)—conducted using the 'cva' function in the *morpho* package (Schlager 2017)—an ordination method which maximizes the differences in the group means (contrast to PCA, which maximizes variation among individual points). Each specimen was categorized in the closest group—based on the smallest Mahalanobis distance to group means—to evaluate how accurately a given grouping variable can discriminate among specimens. Notably, this is not an indicator of statistical significance—this method will optimize differences among predefined groups even if such differences are negligible—so these results should only be interpreted in tandem with those from other methods presented here.

Results

Across all four focal species, the strongest and most consistent contributors to overall skull shape variation were skull size (meeting expectations for these methods), geography (state), and for raccoons, age class. Generally, there were little to no differences in skull shape or morphological

disparity between sexes once all other variables had been accounted for, the exceptions being in opossums (significant mean shape differences in all skull aspects, with greater shape variation among males in the dorsal aspect), raccoons (shape differences in the ventral aspect only), and cottontails (no differences in mean shape, with greater shape variation among males in the lateral aspect) (Table 2).

Statistically significant, albeit subtle, differences exist in mean skull shape and morphological disparity between rural and urban habitat categories, though the observed patterns were not constant across species. There were stronger differences by degree of urbanization as categorized by human population density, therefore here we will primarily report on those models (hereafter "urban-density models") unless otherwise noted. For full statistical results see Supplementary Material.

Geography and climate

The state in which specimens were collected was a major contributor to skull shape variation across all four species: raccoons (dorsal, lateral, and ventral P=0.001), opossums (dorsal P=0.001, ventral P=0.044, lateral P=0.023), fox squirrels (dorsal P=0.012, ventral P=0.040, lateral P=0.041), and cottontails (dorsal, ventral, and lateral P=0.001). Furthermore, state generally had a greater estimated effect size (based on Z scores) than either sex or habitat category in all models (Table 2).

Geographic shape variation was strongly linked to climate. The first principal component of the climate variables explained 53.25% of total variation and was most strongly associated with colder winter and autumn temperatures, as well as higher solar radiation across all seasons. Climate PC2 explained 27.28% of variation and was most strongly associated with cooler spring and summer temperatures. Inclusion of climate PC1 and PC2 in the urban-density models influenced the statistical significance and effect size attributed to state (and vice versa) across species and skull aspects, suggesting overlap in the portion of variance explained by these variables. See Supplementary Material for detailed results.

Morphological disparity varied significantly among state categories in the dorsal aspect for all four species, but there were no consistent trends (e.g., Oklahoma specimens had the greatest morphological disparity in raccoons and cottontails, California specimens in opossum and squirrels; see Supplementary Material).

Applying CVA, using state of collection as the discriminator consistently outperformed habitat category (urban or rural). The proportion of specimens correctly classified to state varied from 78% (fox squirrels in the ventral aspect) to 100% (opossums in the lateral aspect), with an average of 92.8% accuracy across all species and aspects.

Centroid size	Raccoons			Opossums			Squirrels			Cottontails		
	F	*Z*	*p-value*	*F*	*Z*	*p-value*	*F*	*Z*	*p-value*	*F*	*Z*	*p-value*
Dorsal	34.619	7.543	**0.001**	17.888	5.316	**0.001**	4.272	3.739	**0.001**	15.057	6.511	**0.001**
Ventral	20.006	7.313	**0.001**	32.861	5.422	**0.001**	10.105	5.187	**0.001**	17.890	6.777	**0.001**
Lateral	21.348	6.770	**0.001**	12.654	4.456	**0.001**	4.665	3.295	**0.002**	15.830	5.613	**0.001**
Sex												
Dorsal	1.963	1.641	0.052	3.205	2.479	**0.008**	1.145	0.517	0.287	1.109	0.377	0.350
Ventral	5.076	4.402	**0.001**	3.998	3.315	**0.001**	1.044	0.296	0.379	0.654	-0.743	0.777
Lateral	1.920	1.612	0.052	3.564	2.610	**0.005**	0.924	0.079	0.472	0.800	-0.293	0.620
State												
Dorsal	4.746	4.813	**0.001**	3.834	3.623	**0.001**	2.392	2.530	**0.012**	4.068	3.722	**0.001**
Ventral	3.335	4.883	**0.001**	1.558	1.571	**0.044**	1.826	1.602	**0.040**	6.047	4.483	**0.001**
Lateral	11.923	6.473	**0.001**	2.020	2.010	**0.023**	1.827	1.816	**0.041**	4.257	3.307	**0.001**
Urban/Rural												
Dorsal	2.441	2.778	**0.003**	0.803	-0.381	0.646	1.001	0.259	0.399	0.810	-0.587	0.715
Ventral	1.945	2.416	**0.012**	1.007	0.148	0.432	1.728	1.418	0.072	1.296	0.987	0.167
Lateral	3.278	3.532	**0.001**	1.910	1.760	**0.041**	1.246	0.776	0.226	2.190	2.527	**0.006**
Age class												
Dorsal	23.625	9.973	**0.001**									
Ventral	12.180	11.213	**0.001**									
Lateral	4.682	5.394	**0.001**									

Table 2. Procrustes ANOVA results by species—Northern Raccoon (*Procyon lotor*), Virginia Opossum (*Didelphis virginiana*), Eastern Fox Squirrel (*Sciurus niger*), and Eastern Cottontails (*Sylvilagus floridanus*)—and skull aspect. Urban/rural categories were determined based on human population density. *P*-values were generated through 1000 permutations using a residual randomization procedure. Effect sizes (*Z* scores) relate to the difference between the observed *F*-value and the expected value under the null hypothesis, computed as the mean of the distribution of *F*-values generated by the permutation process. For full results see Supplementary Material.

Urban versus rural habitat

Habitat categorization based on verbatim locality was a significant contributor to skull shape variation only for raccoons (dorsal P=0.010, ventral P=0.001, lateral P=0.006). In contrast, the urban-density models revealed stronger shape trends; however, raccoons were the only species to show significant differences in the dorsal and ventral aspects (dorsal P=0.003, ventral P=0.012). Relative to the rural category—presumably the intermediate habitat and thus used as the reference for shape trends throughout—highly rural specimens were characterized by a much broader zygomatic arch, shorter and more steeply angled frontal, whereas urban specimens had a slightly broader zygomatic arch (Figure 2).

There were more significant shape trends across species in the lateral aspect (Table 2, Figure 3). In raccoons (P=0.001), highly rural specimens had a slightly taller braincase, whereas urban specimens differed from rural counterparts primarily in a shorter rostrum profile. In opossums, (P=0.041), there was a longer and deeper braincase among highly rural specimens and a taller and shorter braincase in urban specimens. Finally, cottontails were characterized by a shorter rostrum and deeper braincase in the highly rural group, and a longer and deeper braincase with a taller rostrum in the urban group (P=0.006).

In the models based on verbatim-locality, urban and rural groups had comparable morphological disparity in all species and aspects. However, there were some slight but significant differences among habitat groups in the urban-density models, almost exclusively in the dorsal aspect: significantly higher among urban specimens in fox squirrels (P=0.048 compared to rural), but lower in raccoons (P=0.001 compared to highly rural) and (P=0.004 compared to highly rural, P=0.003 to rural). Additionally, in the latter, the rural group had significantly lower disparity in the ventral aspect (P=0.010 compared to highly rural).

In raccoons, grouping by verbatim locality in the CVA resulted in accurate classification of approximately 83-89% of specimens, depending on aspect. In the urban-density model, classification accuracy was slightly lower, around 69-79%. For the other cases in which urban-density habitat category was a significant contributor to skull shape variation based on Procrustes ANOVA, the lateral aspect for opossums and cottontails, CVA resulted in 93.3% and 86.5% classification accuracy, respectively.

Notably, classification accuracy was relatively high even in cases when habitat category was not found to be a significant contributor to skull shape variation. For example, in opossums, highly rural, rural, and urban specimens were correctly discriminated 83.5% of the time in the dorsal aspect despite not being a statistically significant variable in Procrustes ANOVA (P=0.646). This is likely due to other variables in the model that are not accounted for in the CVA (e.g., geography), which here only assesses variation for one categorical variable at a time.

Age

In raccoons, we assessed age-based shape variation using 216 specimens identified as juvenile, 103 young adults, 54 adults, and 25 old adults. In the urban-density models, age class was a significant contributor to skull variation (P=0.001 across all aspects) with the highest effect size (Z-score) of any variable in the dorsal and ventral aspects, and second only to state in the lateral aspect model (Table 2). On average, aging is associated with a progressive widening of the zygomatic breadth, relative shortening of the frontal, and subtle deepening of the braincase (Figure 4).

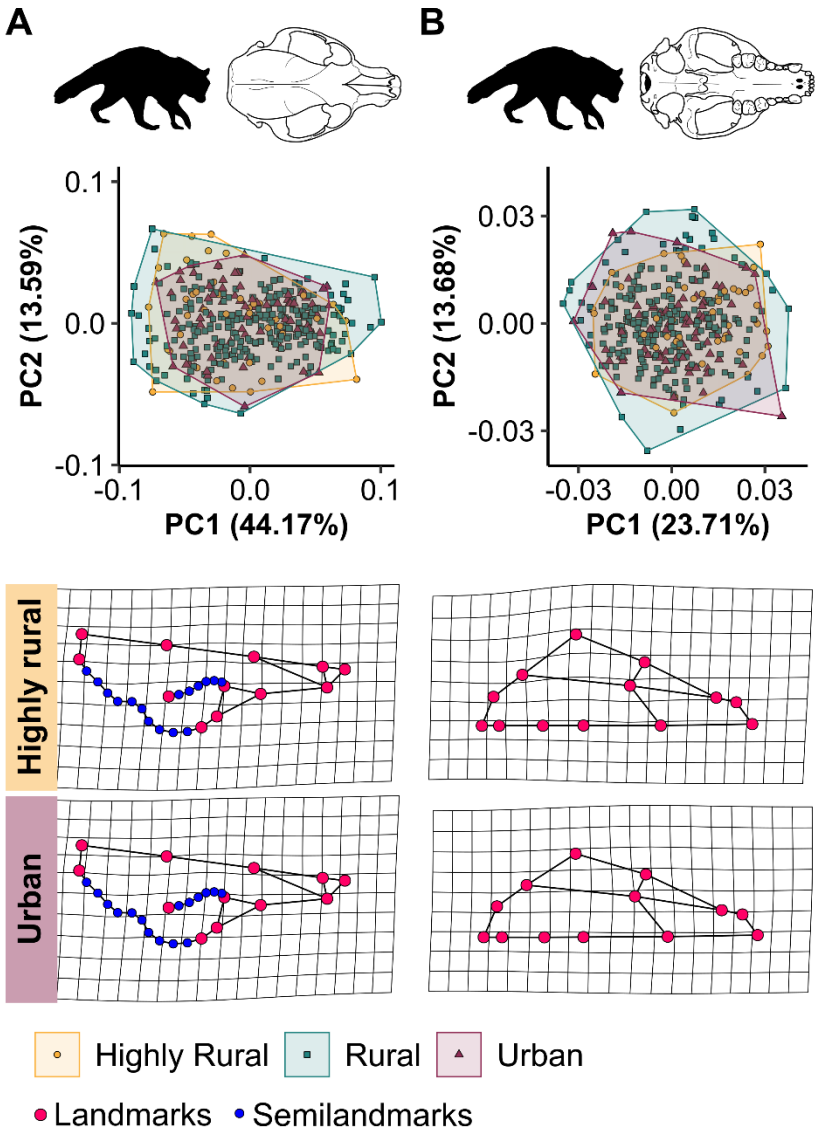


Figure 2. Skull shape differences across highly rural, rural, and urban habitat types categorized based on the county average human population density in the dorsal (A), and ventral (B) skull aspects in raccoons (*Procyon lotor*). Differences among individual specimens in morphospace are depicted in scatterplots of the first two principal component axes of Procrustes shape coordinates (top). Grid diagrams depict the relative displacement of landmarks (large pink points) and curves of semilandmarks (small blue points) in the mean shapes of the highly rural (yellow, middle) and urban (purple, bottom) groups compared to rural group, which was used as the reference. Displacement is magnified 3x for clearer visualization.

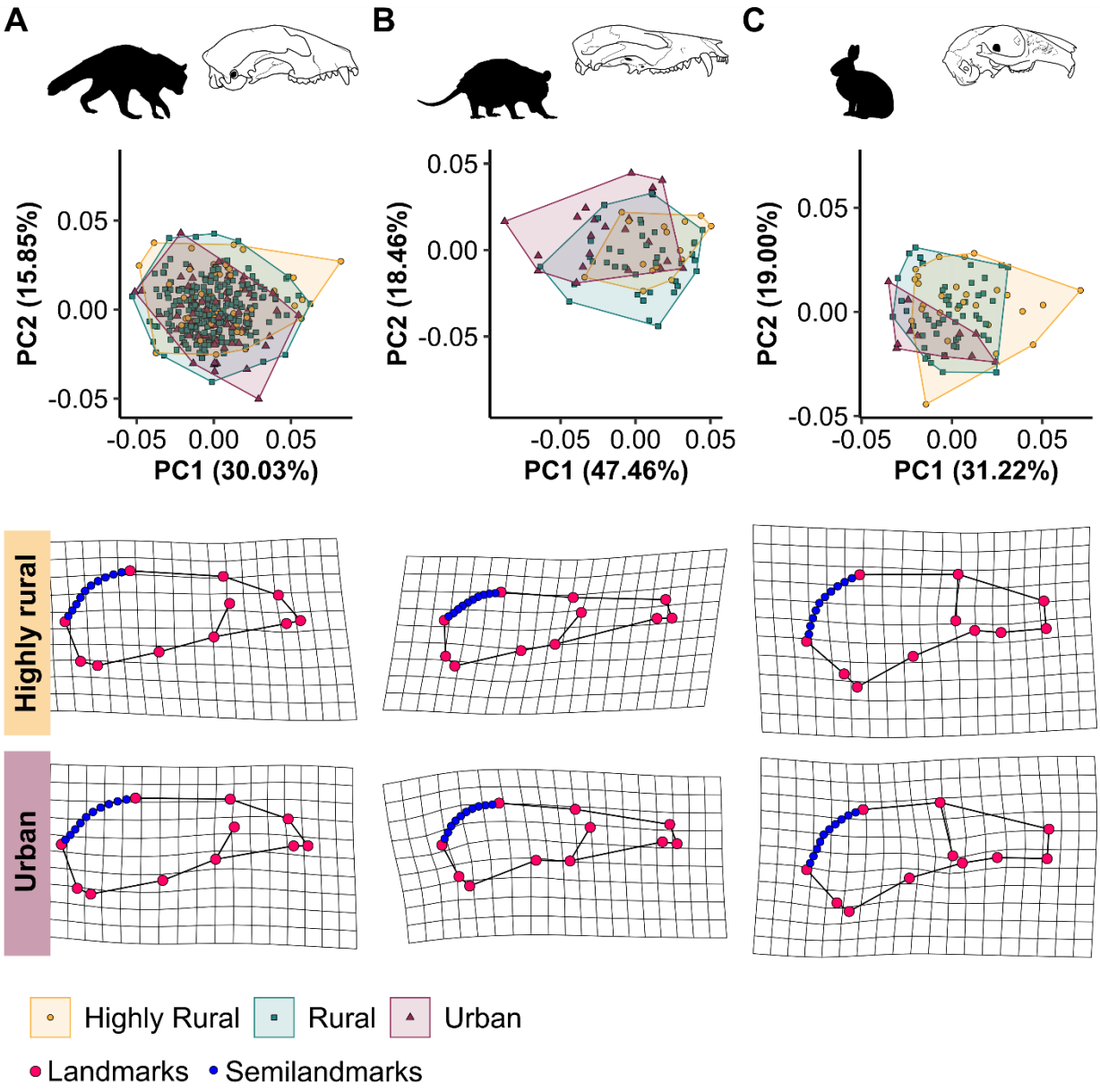


Figure 3. Skull shape differences across highly rural, rural, and urban habitat types categorized based on the county average human population density in the lateral skull aspect for Northern Raccoon (*Procyon lotor*) (A), Virginia Opossum (*Didelphis virginiana*) (B), and Eastern Cottontail (*Sylvilagus floridanus*) (C). Differences among individual specimens in morphospace are depicted in scatterplots of the first two principal component axes of Procrustes shape coordinates (top). Grid diagrams depict the relative displacement of landmarks (large pink points) and curves of semilandmarks (small blue points) in the mean shapes of the highly rural (yellow, middle) and urban (purple, bottom) groups compared to rural group (teal), which was used as the reference. Displacement is magnified 3x for clearer visualization.

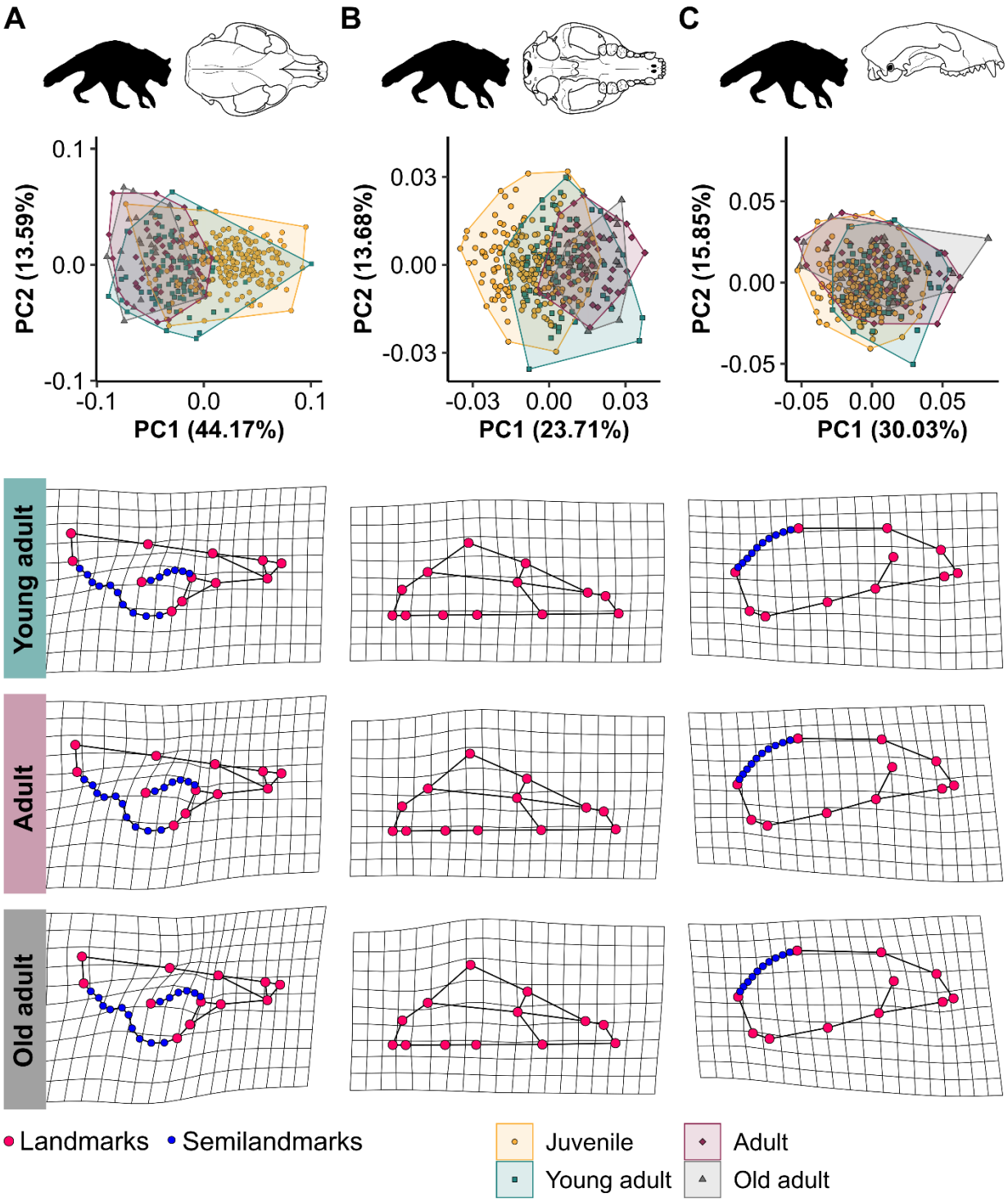


Figure 4. Shape differences by age class in Norther Raccoon (*Procyon lotor*) in the dorsal (A), ventral (B), and lateral (C) aspects. Differences among individuals in are depicted in scatterplots of the first two principal component axes of Procrustes shape coordinates (top). Grid diagrams depict (3x magnified) relative displacement of landmarks (large pink points) and semilandmarks (small blue points) in the mean shapes of young adults (teal, first row), adults (purple, second row), and old adults (gray, last row) compared to juveniles (yellow), the reference.

Juveniles had significantly lower morphological disparity compared to adults in the dorsal aspect (P=0.029) and young adults in the ventral aspect (P=0.015). Approximately 76-82% specimens were accurately grouped by age class in a CVA, depending on aspect, a slightly higher rate than when grouping by human-density based habitat category, but lower than by state.

Discussion

Anthropogenic habitats present numerous risks and rewards to wildlife which can subtly shape morphology. Quantifying these trends over spatial and temporal scales is an essential component to unraveling how wild mammals adapt and respond to urbanization. Domestication syndrome has garnered recent attention as a potentially important form of response to urbanization (Parsons et al. 2020, Apostolov et al. 2025); however, we found no evidence for such a phenomenon shared across taxonomically and ecologically disparate species. While raccoons, eastern cottontails, and opossums all exhibited some significant differences in skull shape across urban and rural habitat categories, these were not uniform across species and generally did not include clear indicators of domestication syndrome (i.e., decreased braincase size and shortened rostrum). This does not necessarily disprove domestication-like trends in some contexts but rather underscores that such effects act in concert with other behavioral, dietary, and demographic factors to produce complex variation in skull shape.

No evidence for widespread domestication syndrome in urban mammals

Trends in cranial morphology among our four urban mammal species generally did not conform with the predictions of domestication syndrome, indicating that this is not a widespread response to urbanization. The morphological divergence we did observe between urban and rural habitat categories did not follow any distinct patterns across species, and geography was generally a stronger contributor to skull shape variation than urbanization, consistent with previous findings (Sluka et al. 2025). This is not surprising, given that domestication syndrome does not even universally apply to domesticated mammals, such that the validity of the phenomenon and its proposed mechanisms have been challenged (Lord et al. 2020, 2025). Furthermore, although trends akin to domestication syndrome have been reported in some populations (Parsons et al. 2020, Apostalov et al. 2025, Sluka et al. 2025), it is important to recognize that the factors and processes influencing domesticated animals are not one-to-one with those experienced by wild human commensals. Our results suggest that morphology reflects these differences. For example, although responses to urbanization are generally not well studied in lagomorphs (Ritzel and Gallo 2020), domesticated European Rabbits (*Oryctolagus cuniculus*) have been shown to exhibit greater variation in skull shape as well as smaller braincases, as expected based on domestication syndrome, but longer faces, contrary to that hypothesis, when compared to feral and wild counterparts (Sherratt et al. 2025). In contrast, our results on wild Eastern Cottontails indicate a slight elongation in the skull but reduced shape variation (morphological disparity) in the urban category compared to more rural specimens. Moreover, although there is growing evidence for advantages conferred by behavioral boldness (Lowry et al. 2013, Ritzel and Gallo 2020), there is no single behavioral syndrome shared among all urban-dwelling animals with nuanced intra- and interspecific variation (Miranda et al. 2013, Padovani et al. 2021). Raccoons and opossums, despite sharing a reputation for garbage thievery, can differ greatly in their degree of human aversion, with raccoons tending to dominate anthropogenic habitats even compared to

other generalist mesopredators like opossums (Haverland and Veech 2017, Stark et al. 2020), which may be linked to observed differences in morphological trends. In fox squirrels, the slight but significant increase in morphological disparity but lack of a directional trend associated with urbanization observed here may reflect relaxed selection in the urban environment due to supplemental food sources and reduced predation (Fischer et al. 2012), permitting a broader range of foraging and threat assessment behaviors. There is evidence for such increased behavioral flexibility in urban squirrels (Bateman and Fleming 2014), and other mammals (Santini et al. 2019, Mazza et al. 2020). Connecting these diverse behavioral trends with other responses to urbanization, particularly morphology, is vital to understanding the diversity and combinations of traits that are conducive to thriving in anthropogenic environments.

Age distribution is a key component of morphological trends

Responses to the pressures of urban environments can vary by age and breeding status (e.g., (Biondi et al. 2010, Padovani et al. 2021), with effects on life history traits, such as litter size (Santini et al. 2019) and reproductive timing (Rodewald and Gehrt 2014, Sepp et al. 2018). Thus, differences in age structure may arise between rural and urban populations, in turn influencing variation in age-sensitive morphological traits.

Here, we found a significant effect of age class on skull shape in raccoons, regardless of urban or rural categorization; specifically, the zygomatic progressively broadens with age relative to the rest of the skull. Notably, this coincides with trends observed in highly rural habitats. There are a few possible explanations for this. First, our results indicate a higher proportion of juveniles in the urban category, consistent with observed trends (Prange et al. 2003), so these very young individuals are contributing more to the average skull shape in urban habitats compared to rural samples; however, the difference among habitat categories was still significant after accounting for age class, suggesting that other factors are at play. Second, although we cannot entirely rule out methodological factors, such as imprecision in landmark placement among older individuals (suture fusion can obscure boundaries between bones) overall shape variation was not significantly higher among older age classes, suggesting that variation simply due to error was not a likely cause of age-based differences. Finally, as animals age, they can experience shifts in diet and altered competitive interactions that favor more robust head musculature; it is possible that in the urban environment, these pressures are diminished due to both the availability of supplemental resources and the softness of human-processed foods—which can alter jaw morphology over development (Curtis et al. 2018, Puckett et al. 2020)—thereby producing a comparatively stronger trend across age groups among the most "wild" (i.e., highly rural) specimens.

These effects of age on morphology, when not accounted for, may alter or mask trends of interest. This could, at least in part, explain the discrepancies between our findings and those of other authors who concluded that urban raccoons are in fact subject to domestication syndrome (Apostalov et al. 2025, Sluka et al. 2025). Thus, these results highlight the importance of evaluating age effects to a complete and nuanced interpretation of morphological trends over space and time. To that end, developing reliable aging criteria as well as continued sampling effort, particularly in urban environments, is paramount to future studies.

Evolution and phenotypic plasticity

The degree to which phenotypic plasticity and microevolution drive morphological shifts in urban habitats remains elusive. While human activities present novel selection pressures—e.g., roadways—while relaxing others—e.g., predation—direct evidence for genetic change is still emerging (Lambert et al. 2021). Responses to urbanization may also arise rapidly due to phenotypic plasticity, which can be advantageous in new or rapidly changing environments (Ghalambor et al. 2007), which in the case of urbanization, can be highly region- or even city specific (Evans et al. 2009, Larson et al. 2024).

Although we could not test for genetic change, our results do suggest a central role of phenotypic plasticity. Among our focal species, geographic differences in skull shape were linked to local climate conditions, indicating that observed differences were not solely attributable to genetic differences among populations due to drift. Moreover, we found some trends in the breadth of phenotypic variation across habitat categories, though these differed among species; urban habitats were associated with reduced morphological disparity in raccoons and cottontails, possibly related to the homogenization of resources and strategies (e.g., reliance and garbage or lawns, respectively) for these species. Alternatively, morphological disparity was higher among urban fox squirrels, potentially linked to exploitation of diverse habitats that vary greatly in the type and availability of food, predation risk, exposure to humans and pets, and interspecific competition (van der Merwe et al. 2005, Larson et al. 2024). Unraveling the influence of plasticity, the potential evolution of urban forms, and what those forms may look and behave like in the future, will require more granular, multi-city studies (Fidino et al. 2021, Haight et al. 2023). Detecting phenotypic differences between rural and urban wildlife remains an essential step toward identifying traits of interest—i.e., those that may be highly plastic and/or under selection in urban environments—and predicting the direction of future responses to intensifying human activity.

The untapped potential of natural history collections in urban ecology

Natural history collections are a critical resource for tracking biodiversity patterns and responses to environmental change (MacLean et al. 2019, Sanders et al. 2023), yet they remain underutilized in the field of urban ecology (Shultz et al. 2021). A significant obstacle is limited sample sizes due to inconsistent collecting effort across both spatial and temporal dimensions, which adversely affects overall urban specimen representation. To address this shortcoming, various strategies—including salvage operations (e.g., roadkill), collaborations with pest removal personnel, specimen donations, and systematic surveys—can expand contemporary urban samples. When combined with modern methodologies—CT scanning, 3D morphometric techniques—and other data derived from museum specimens—occurrences, parasite and toxin loads, dietary indicators, hormone concentrations, and genetics—we can continue to advance a more complete picture of responses to urbanization across both spatial and temporal scales.

Conclusions

Responses to urbanization are highly variable, and the apparent absence of widespread domestication syndrome—or any universal trends across rural and urban habitats—highlighted by this study supports the notion that there are multiple emergent forms of successful urban

exploiters (Santini et al. 2019, Weiss et al. 2023). Our understanding of the future of biodiversity in human-dominated habitats depends on teasing apart common patterns of response for a given set of pressures. To that end, morphology lies at the confluence of behavioral, dietary, and ontogenetic factors, thus continuing to leverage museum specimens offers a means to identify rapid responses to urbanization across space, time, and taxa. Critically, in better understanding "urban exploiters," we can build a picture of what's missing from these environments, i.e., determining the intrinsic and environmental factors that lead to the displacement or exclusion of "urban avoiders." Beyond repairing and restoring ecosystems at the landscape level, as human populations continue to grow and condense into cities, bolstering biodiversity in our immediate surroundings is critical to human health and wellbeing (Keesing et al. 2010, Aerts et al. 2018). Armed with knowledge of the ways in which urbanization shapes populations, species, and communities, we can conserve and promote healthy biodiversity, benefiting humans and wildlife alike in the habitats we share.

Acknowledgements

We would like to thank the numerous collectors and museum personnel that made this work possible. We are especially grateful to Rebecca Hawkins at the Sam Noble Oklahoma Museum of Natural History, as well as Kayce Bell and Shannen Robson at the Natural History Museum of Los Angeles County. We would also like to thank Cameron Siler for loaning the camera and equipment, Jacqueline Lungmus for providing training in geometric morphometrics techniques, as well as our undergraduate research assistants, Andrew Hughes and Noah Lemons, for their contributions to early versions of this project. Finally, we extend our gratitude to the PhD committee for feedback on this manuscript.

Author Contributions

MKT conceptualized the ideas and methodology, collected and analyzed data, and led the writing of the manuscript. EJG obtained and cleaned GIS data. HCL supervised the project and provided critical feedback on the methodology and manuscript.

Funding

This work was supported in part by a Student Collections Study Award from the Natural History Museum of Los Angeles County as well as a Dissertation Completion Fellowship from the Dodge Family College of Arts and Sciences and the Eddie Carol Smith Scholarship from the Graduate College at the University of Oklahoma.

Data Availability

Data and analysis files are available at
https://osf.io/kma6j/overview?view_only=b70bcec4712e4f8b9104a110c356ebdc

References

Adams, D. C., Collyer, M. L., Kaliontzopoulou, A. and Baken, E. K. 2022. Geomorph: Software for geometric morphometric analyses. – < https://cran.r-project.org/package=geomorph>.

Aerts, R., Honnay, O. and Van Nieuwenhuyse, A. 2018. Biodiversity and human health: mechanisms and evidence of the positive health effects of diversity in nature and green spaces. – *Br. Med. Bull.* **127**: 5–22.

Apfelbeck, B., Snep, R. P. H., Hauck, T. E., Ferguson, J., Holy, M., Jakoby, C., Scott MacIvor, J., Schär, L., Taylor, M. and Weisser, W. W. 2020. Designing wildlife-inclusive cities that support human-animal co-existence. – *Landsc. Urban Plan*. **200**: 103817.

Apostolov, A., Bradley, A., Dreher, S., Dwyer, C., Edwards, J., Evans, M. E., Gu, N., Hansen, J., Lewis, J. D., Mashburn, A. T., Miller, K., Richardson, E., Roller, W., Stark, A., Swift, J., Zuniga, O. and Lesch, R. 2025. Tracking domestication signals across populations of North American raccoons (*Procyon lotor*) via citizen science-driven image repositories. – *Front. Zool.* **22**: 28.

Baken, E. K., Collyer, M. L., Kaliontzopoulou, A. and Adams, D. C. 2021. geomorph v4.0 and gmShiny: Enhanced analytics and a new graphical interface for a comprehensive morphometric experience. – *Methods Ecol. Evol.* **12**: 2355–2363.

Bateman, P. W. and Fleming, P. A. 2014. Does human pedestrian behaviour influence risk assessment in a successful mammal urban adapter? – *J. Zool.* **294**: 93–98.

Biondi, L. M., Bó, M. S. and Vassallo, A. I. 2010. Inter-individual and age differences in exploration, neophobia and problem-solving ability in a Neotropical raptor (*Milvago chimango*). – *Anim. Cogn.* **13**: 701–710.

Blair, R. B. 1996. Land use and avian species diversity along an urban gradient. – *Ecol. Appl.* **6**: 506–519.

Collyer, M. L. and Adams, D. C. 2018. RRPP: An R package for fitting linear models to high-dimensional data using residual randomization. – *Methods Ecol. Evol.* **9**: 1772–1779.

Collyer, M. L. and Adams, D. C. 2021. RRPP: Linear Model Evaluation with Randomized Residuals in a Permutation Procedure. – < https://cran.r-project.org/web/packages/RRPP>

Curtis, A. A., Orke, M., Tetradis, S. and Van Valkenburgh, B. 2018. Diet-related differences in craniodental morphology between captive-reared and wild coyotes, *Canis latrans* (Carnivora: Canidae). – *Biol. J. Linn. Soc.* **123**: 677–693.

Drake, A. G. and Klingenberg, C. P. 2010. Large-scale diversification of skull shape in domestic dogs: disparity and modularity. – *Am. Nat.* **175**: 289–301.

Elbroch, M. 2006. *Animal skulls: A Guide to North American Species*. – Stackpole Books.

Evans, K. L., Gaston, K. J., Sharp, S. P., McGowan, A. and Hatchwell, B. J. 2009. The effect of urbanisation on avian morphology and latitudinal gradients in body size. – *Oikos* **118**: 251–259.

Fidino, M., Gallo, T., Lehrer, E. W., Murray, M. H., Kay, C. A. M., Sander, H. A., MacDougall, B., Salsbury, C. M., Ryan, T. J., Angstmann, J. L., Amy Belaire, J., Dugelby, B., Schell,

C. J., Stankowich, T., Amaya, M., Drake, D., Hursh, S. H., Ahlers, A. A., Williamson, J., Hartley, L. M., Zellmer, A. J., Simon, K. and Magle, S. B. 2021. Landscape-scale differences among cities alter common species' responses to urbanization. – *Ecol. Appl.* **31**: e02253.

Fischer, J. D., Cleeton, S. H., Lyons, T. P. and Miller, J. R. 2012. Urbanization and the predation paradox: the role of trophic dynamics in structuring vertebrate communities. – *BioScience* **62**: 809–818.

Ghalambor, C. K., McKay, J. K., Carroll, S. P. and Reznick, D. N. 2007. Adaptive versus non-adaptive phenotypic plasticity and the potential for contemporary adaptation in new environments. – *Funct. Ecol.* **21**: 394–407.

Grau, G. A., Sanderson, G. C. and Rogers, J. P. 1970. Age Determination of Raccoons. – *J. Wildl. Manag.* **34**: 364.

Green, D. S., Tongue, A. D. W. and Boots, B. 2022. The ecological impacts of discarded cigarette butts. – *Trends Ecol. Evol.* **37**: 183–192.

Grimm, N. B., Faeth, S. H., Golubiewski, N. E., Redman, C. L., Wu, J., Bai, X. and Briggs, J. M. 2008. Global change and the ecology of cities. – *Science* **319**: 756–760.

Haight, J. D., Hall, S. J., Fidino, M., Adalsteinsson, S. A., Ahlers, A. A., Angstmann, J., Anthonysamy, W. J. B., Biro, E., Collins, M. K., Dugelby, B., Gallo, T., Green, A. M., Hartley, L., Jordan, M. J., Kay, C. A. M., Lehrer, E. W., Long, R. A., MacDougall, B., Magle, S. B., Minier, D. E., Mowry, C., Murray, M., Nininger, K., Pendergast, M. E., Remine, K. R., Ryan, T., Salsbury, C., Sander, H. A., Schell, C. J., Şekercioğlu, Ç. H., Shier, C. J., Simon, K. C., St. Clair, C. C., Stankowich, T., Stevenson, C. J., Wayne, L., Will, D., Williamson, J., Wilson, L., Zellmer, A. J. and Lewis, J. S. 2023. Urbanization, climate and species traits shape mammal communities from local to continental scales. - *Nat. Ecol. Evol.* **7**: 1654–1666.

Hansen, C. P., Kays, R. and Millspaugh, J. J. 2024. From backyard to backcountry: changes in mammal communities across an urbanization gradient (J Goheen, Ed.). – *J. Mammal.* **105**: 175–191.

Haverland, M. B. and Veech, J. A. 2017. Examining the occurrence of mammal species in natural areas within a rapidly urbanizing region of Texas, USA. – *Landsc. Urban Plan.* **157**: 221–230.

Hof, A. R., Snellenberg, J. and Bright, P. W. 2012. Food or fear? Predation risk mediates edge refuging in an insectivorous mammal. – *Anim. Behav.* **83**: 1099–1106.

Junge, R. and Hoffmeister, D. F. 1980. Age Determination in Raccoons from Cranial Suture Obliteration. – *J. Wildl. Manag.* **44**: 725.

Keesing, F., Belden, L. K., Daszak, P., Dobson, A., Harvell, C. D., Holt, R. D., Hudson, P., Jolles, A., Jones, K. E., Mitchell, C. E., Myers, S. S., Bogich, T. and Ostfeld, R. S. 2010. Impacts of biodiversity on the emergence and transmission of infectious diseases. - *Nature* **468**: 647–652.

Kent, E., Schwartz, A. L. W. and Perkins, S. E. 2021. Life in the fast lane: roadkill risk along an urban–rural gradient. – *J. Urban Ecol.* **7**: juaa039.

Lambert, M. R., Brans, K. I., Des Roches, S., Donihue, C. M. and Diamond, S. E. 2021. Adaptive Evolution in Cities: Progress and Misconceptions. – *Trends Ecol. Evol.* **36**: 239–257.

Larson, R. N., Sander, H. A., Fidino, M., Angstmann, J. L., Hayes Hursh, S., Magle, S. B., Moore, K., Salsbury, C. M., Stankowich, T., Tombs, K., Barczak, L., Davidge, A. M., Drake, D., Hartley, L., Reed Sanchez, P., Robey, A., Snyder, T., Williamson, J. and Zellmer, A. J. 2024. Patterns in tree squirrel co-occurrence vary with responses to local land cover in US cities. – *Urban Ecosyst.* **27**: 2121–2133.

Laundré, J. W., Hernández, L. and Altendorf, K. B. 2001. Wolves, elk, and bison: reestablishing the "landscape of fear" in Yellowstone National Park, U.S.A. – *Can. J. Zool.* **79**: 1401–1409.

Lord, K. A., Larson, G., Coppinger, R. P. and Karlsson, E. K. 2020. The history of farm foxes undermines the animal domestication syndrome. – *Trends Ecol. Evol.* **35**: 125–136.

Lord, K. A., Larson, G., Allaby, R. G. and Karlsson, E. K. 2025. A universally applicable definition for domestication. – *Proc. Natl. Acad. Sci. U.S.A.* **122**: e2413207122.

Lotze, J.-H. and Anderson, S. 1979. *Procyon lotor*. – *Mamm. Species* **119**: 1–8.

Lowry, H., Lill, A. and Wong, B. B. M. 2013. Behavioural responses of wildlife to urban environments. – *Biol. Rev.* **88**: 537–549.

MacLean, H. J., Nielsen, M. E., Kingsolver, J. G. and Buckley, L. B. 2019. Using museum specimens to track morphological shifts through climate change. – *Phil. Trans. R. Soc. B* **374**: 20170404.

Marcus, L. F., Hingst-Zaher, E. and Zaher, H. 2000. Application of landmark morphometrics to skulls representing the orders of living mammals. – *Hystrix* **11**: 27–47.

Mazza, V., Dammhahn, M., Lösche, E. and Eccard, J. A. 2020. Small mammals in the big city: Behavioural adjustments of non-commensal rodents to urban environments. – *Glob. Change Biol.* **26**: 6326–6337.

McDonnell, M. J. 2011. The history of urban ecology: An ecologist's perspective. – In: Niemelä, J. et al. (eds), *Urban Ecology: Patterns, Processes, and Applications* – Oxford University Press, pp. 5–13.

McKinney, M. L. 2002. Urbanization, Biodiversity, and Conservation. – *BioScience* **52**: 883.

Miranda, A. C., Schielzeth, H., Sonntag, T. and Partecke, J. 2013. Urbanization and its effects on personality traits: a result of microevolution or phenotypic plasticity? – *Glob. Change Biol.* **19**: 2634–2644.

Moncrief, N. D., Hightower, L., Mead, A. J. and Ivanov, K. 2022. Prevalence and location of survivable skeletal injuries in two North American tree squirrels (*Sciurus*). – *J. Mammal.* **103**: 663–671.

Morris, P. 1972. A review of mammalian age determination methods. – *Mammal Rev*. **2**: 69–104.

Murray, M. H., Sánchez, C. A., Becker, D. J., Byers, K. A., Worsley-Tonks, K. E. and Craft, M. E. 2019. City sicker? A meta-analysis of wildlife health and urbanization. – *Front. Ecol. Environ.* **17**: 575–583.

Padovani, R., Shi, Z. and Harris, S. 2021. Are British urban foxes (*Vulpes vulpes*) "bold"? The importance of understanding human–wildlife interactions in urban areas. – *Ecol. Evol.* **11**: 835–851.

Paniw, M., James, T. D., Ruth Archer, C., Römer, G., Levin, S., Compagnoni, A., Che-Castaldo, J., Bennett, J. M., Mooney, A., Childs, D. Z., Ozgul, A., Jones, O. R., Burns, J. H., Beckerman, A. P., Patwary, A., Sanchez-Gassen, N., Knight, T. M. and Salguero-Gómez, R. 2021. The myriad of complex demographic responses of terrestrial mammals to climate change and gaps of knowledge: A global analysis. – *J. Anim. Ecol.* **90**: 1398–1407.

Parsons, K. J., Rigg, A., Conith, A. J., Kitchener, A. C., Harris, S. and Zhu, H. 2020. Skull morphology diverges between urban and rural populations of red foxes mirroring patterns of domestication and macroevolution. – *Proc. R. Soc. B.* **287**: 20200763.

Peplinski, J. and Brown, J. S. 2020. Distribution and diversity of squirrels on university and college campuses of the United States and Canada. – *J. Mammal.* **101**: 930–940.

Prange, S., Gehrt, S. D. and Wiggers, E. P. 2003. Demographic factors contributing to high raccoon densities in urban landscapes. – *J. Wildl. Manag.* **67**: 324–333.

Puckett, E. E., Sherratt, E., Combs, M., Carlen, E. J., Harcourt-Smith, W. and Munshi-South, J. 2020. Variation in brown rat cranial shape shows directional selection over 120 years in New York City. – *Ecol. Evol.* **10**: 4739–4748.

R Core Team 2025. R: A language and environment for statistical computing. – < https://www.R-project.org/>.

Ratcliffe, M., Burd, C., Holder, K. and Fields, A. 2016. Defining Rural at the U.S. Census Bureau. ACSGEO-1, U.S. Census Bureau, Washington, DC.

Ritzel, K. and Gallo, T. 2020. Behavior Change in Urban Mammals: A Systematic Review. – *Front. Ecol. Evol.* **8**: 576665.

Rodewald, A. D. and Gehrt, S. D. 2014. Wildlife Population Dynamics in Urban Landscapes. – In: McCleery, R. A. et al. (eds), *Urban Wildlife* – Springer US, pp. 117–147.

Rohlf, F. J. 2021. tpsDig2. – < https://sbmorphometrics.org/>.

Rohlf, F. J. 2022. tpsUtil. – < https://sbmorphometrics.org/>.

Sanders, N. J., Cooper, N., Davis Rabosky, A. R. and Gibson, D. J. 2023. Leveraging natural history collections to understand the impacts of global change. – *J. Anim. Ecol.* **92**: 232–236.

Santini, L., González-Suárez, M., Russo, D., Gonzalez-Voyer, A., Von Hardenberg, A. and Ancillotto, L. 2019. One strategy does not fit all: determinants of urban adaptation in mammals. – *Ecol. Lett.* **22**: 365–376.

Schlager, S. 2017. Morpho and Rvcg - Shape Analysis in R. – In: Zheng, G. et al. (eds), *Statistical Shape and Deformation Analysis* – Academic Press, pp. 217–256.

Schroeder, J., Van Riper, D., Manson, S., Knowles, K., Kugler, T., Roberts, F. and Ruggles, S. 2025. IPUMS National Historical Geographic Information System: Version 20.0 [dataset]. < http://doi.org/10.18128/D050.V20.0>.

Sepp, T., McGraw, K. J., Kaasik, A. and Giraudeau, M. 2018. A review of urban impacts on avian life-history evolution: Does city living lead to slower pace of life? – *Glob. Change Biol.* **24**: 1452–1469.

Sherratt, E., Böhmer, C., Callou, C., Nelson, T. J., Pillai, R., Ruf, I., Sanger, T. J., Schaar, J., Le Verger, K., Kraatz, B. and Geiger, M. 2025. From wild to domestic and in between: how domestication and feralization changed the morphology of rabbits. – *Proc. R. Soc. B.* **292**: 20251150.

Shochat, E., Warren, P., Faeth, S., Mcintyre, N. and Hope, D. 2006. From patterns to emerging processes in mechanistic urban ecology. – *Trends Ecol. Evol.* **21**: 186–191.

Shultz, A. J., Adams, B. J., Bell, K. C., Ludt, W. B., Pauly, G. B. and Vendetti, J. E. 2021. Natural history collections are critical resources for contemporary and future studies of urban evolution. – *Evol. Appl.* **14**: 233–247.

Sluka, C. M., Clementz, M. T., Benson-Amram, S. and Ben-David, M. 2025. Patterns of raccoon craniodental morphology under urbanization. – *Integr. Comp. Biol*. **65**: 236–248.

Stark, J. R., Aiello-Lammens, M. and Grigione, M. M. 2020. The effects of urbanization on carnivores in the New York metropolitan area. – *Urban Ecosyst.* **23**: 215–225.

Tanner, C. J., Adler, F. R., Grimm, N. B., Groffman, P. M., Levin, S. A., Munshi-South, J., Pataki, D. E., Pavao-Zuckerman, M. and Wilson, W. G. 2014. Urban ecology: advancing science and society. – *Front. Ecol. Environ.* **12**: 574–581.

Theriot, M. K., Olson, L. E. and Lanier, H. C. 2024. Accounting for age: uncovering the nuanced drivers of mammal body-size responses to climate change. – *J. Mammal.* **105**: 512–523.

United Nations, Department of Economic and Social Affairs, Population Division 2019. World urbanization prospects: the 2018 revision (ST/ESA/SER.A/420). – United Nations.

van der Merwe, M., Brown, Joel. S. and Jackson, W. M. 2005. The coexistence of Fox (*Sciurus niger*) and gray (*S. caroliniensis*) squirrels in the Chicago metropolitan area. – *Urban Ecosyst.* **8**: 335–347.

Walsh, L. L. and Tucker, P. K. 2023. Evaluating anthropogenic influence on a mesopredator: opossum (*Didelphis virginiana*) isotope values influenced by corn agriculture more than urbanization. – *Can. J. Zool.* **101**: 307–316.

Wang, T., Hamann, A., Spittlehouse, D. and Carroll, C. 2016. Locally downscaled and spatially customizable climate data for historical and future periods for North America. – *PLoS ONE* **11**: e0156720.

Wang, T., Hamann, A. and Sang, Z. 2025. Monthly High-Resolution Historical Climate Data for North America Since 1901. – *Int. J. Climatol.* **45**: e8726.

Weiss, K. C. B., Green, A. M., Herrera, D. J., Hubbard, T. M., Rega-Brodsky, C. C. and Allen, M. L. 2023. Effect of species-level trait variation on urban exploitation in mammals. – *Ecology* **104**: e4055.

Wilkins, A. S., Wrangham, R. W. and Fitch, W. T. 2014. The “domestication syndrome” in mammals: A unified explanation based on neural crest cell behavior and genetics. – *Genetics* **197**: 795–808.

Zelditch, M., Swiderski, D. L. and Sheets, H. D. 2012. *Geometric morphometrics for biologists: a primer* – Elsevier/Academic Press.

Zhang, L., Yang, L., Zohner, C. M., Crowther, T. W., Li, M., Shen, F., Guo, M., Qin, J., Yao, L. and Zhou, C. 2022. Direct and indirect impacts of urbanization on vegetation growth across the world's cities. – *Sci. Adv.* **8**: eabo0095.

Supplementary Material

Supplemental methods

Landmark placement

Dorsal	
D1	Most anterior point of the skull—anteriormost point of the premaxillae along the midline. *Raccoons and opossums only*.
D2	Most anterior point of the rostrum—anteriormost point between the nasals along the midline.
D3	Lateral boundary of the rostrum—anteriormost point of the suture between premaxilla and maxilla.
D4	Posterior boundary of the rostrum—suture between nasals and frontals along the midline.
D5	Anteriormost boundary of orbit.
D6	Medial boundary of orbit—tip of the postorbital process, or lateralmost point of the frontal along the boundary of the orbit when the postorbital process is not prominent. *In cottontails, two points were placed at the anterior and posterior tips of the supraorbital process (points D6 and D9).*
D7	Lateral boundary of the orbit—medial most point of the zygomatic arch along the boundary of the orbit.
D8	Lateral boundary of the zygomatic arch—anteriormost point of the zygomatic portion of the squamosal along the squamosal-jugal suture.
D9	Lateral boundary of the braincase—posteromedial point where zygomatic arch joints with the braincase. *In cottontails, posterior tip of supraorbital process (a) and most medial point at the constriction in the skull just posterior to supraorbital process (b).*
D10	Crown of the braincase—posteriormost point of frontal-parietal suture along the midline.
D11	Posterior boundary of braincase—posteriormost point along the midline between the parietals.
D12	Lateral, posterior boundary of the braincase—posterolateral edge along the occipital-parietal-squamosal suture.
Dc1	Inner curve of braincase—6 semilandmarks evenly spaced between landmarks D6 and D9. *In cottontails, following the curve of the supraorbital process.*
Dc2	Outer curve of zygomatic arch and braincase—10 semilandmarks evenly spaced between landmarks D8 and D11.
Ventral	
V1	Most anterior point of the skull—anteriormost point of the premaxillae along the midline.

V2	Lateral boundary of the rostrum—premaxillary-maxillary suture along lateral edge.
V3	Anterior boundary of zygomatic arch—Anteriormost point of the jugal. *In cottontails, anteriormost point of zygomatic arch (jugal-maxillary suture not distinct).*
V4	Anterior boundary of cheek teeth—anteriormost point of the alveolus holding the first premolar.
V5	Posterior boundary of cheek teeth—posteriormost point of the alveolus holding the last molar.
V6	Center of hard palate—posteriormost point of maxillary-palatine suture along the midline
V7	End of palate—posteriormost point of palatines along the midline
V8	Posterior of the zygomatic arch—posteriormost point of the jugal-squamosal suture.
V9	Posterior, lateral boundary of braincase—posterolateral tip of the auditory bulla.
V10	Lateralmost point of the occipital condyle.
V11	Center of braincase floor—basisphenoid-basioccipital suture along midline.
V12	Anterior margin of foramen magnum along the midline.
V13	Posterior margin of foramen magnum along the midline.
Lateral	
L1	Anteriormost point of the nasals.
L2	Anteriormost point of the premaxillae.
L3	Premaxillary-maxillary suture along ventral edge. *In raccoons, meeting the anterior edge of the canine alveolus. In opossums, meeting the posterior edge of the fifth incisor alveolus.*
L4	Anteriormost point of the jugal on the ventral surface where it meets the maxilla. *In cottontails, anteriormost point of zygomatic arch.*
L5	Anterior boundary of the orbit.
L6	Dorsal boundary of the rostrum—frontal nasal suture along dorsal edge.
L7	Ventral boundary of the palate—palatine-pterygoid suture along ventral edge.
L8	Ventral, posterior boundary of the skull—tip of the paroccipital process.
L9	Posteriormost point of the occipital condyle. *In cottontails, posterior margin of the occipital bone dorsal to the auditory bulla (occipital condyles not visible in lateral view).*
L10	Frontal-parietal suture along the dorsal edge.
L11	Posteriormost point of interparietal.
Lc1	Dorsal curve of braincase and sagittal crest—10 semilandmarks evenly spaced between landmarks L10 and L11.

Table S1. Detailed descriptions of landmarks placed in the dorsal, ventral, and lateral skull aspects. These include sets of semilandmarks, or curves (two in the dorsal aspect, one in the lateral, none in the ventral). Slight variations in placement among species are also noted.

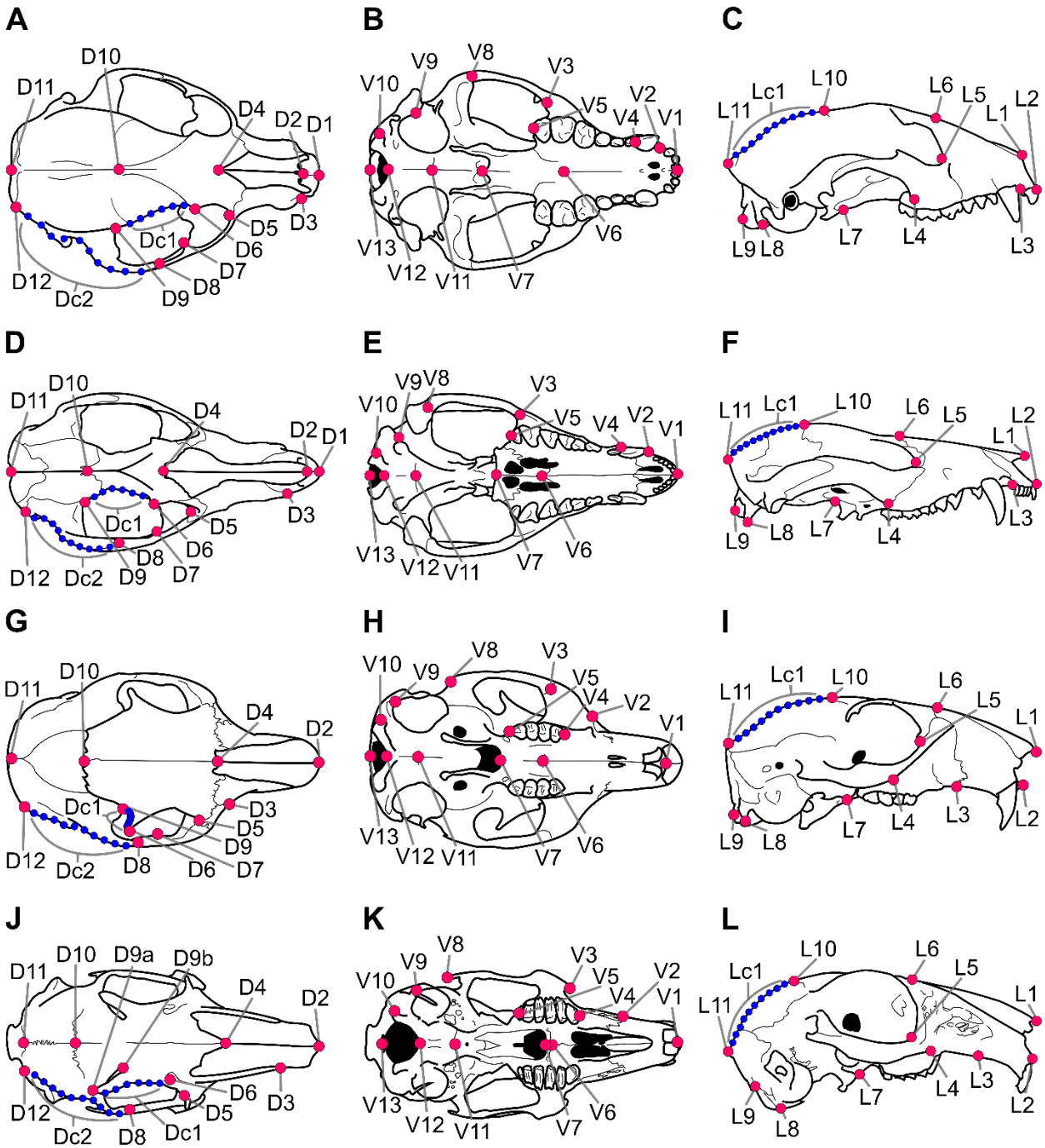
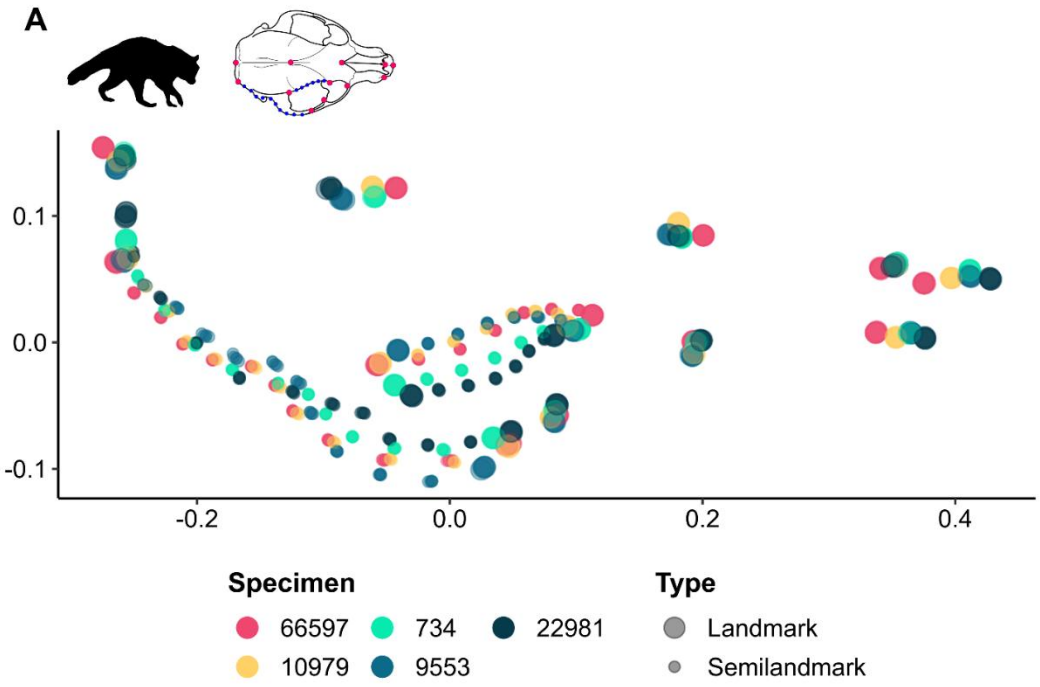
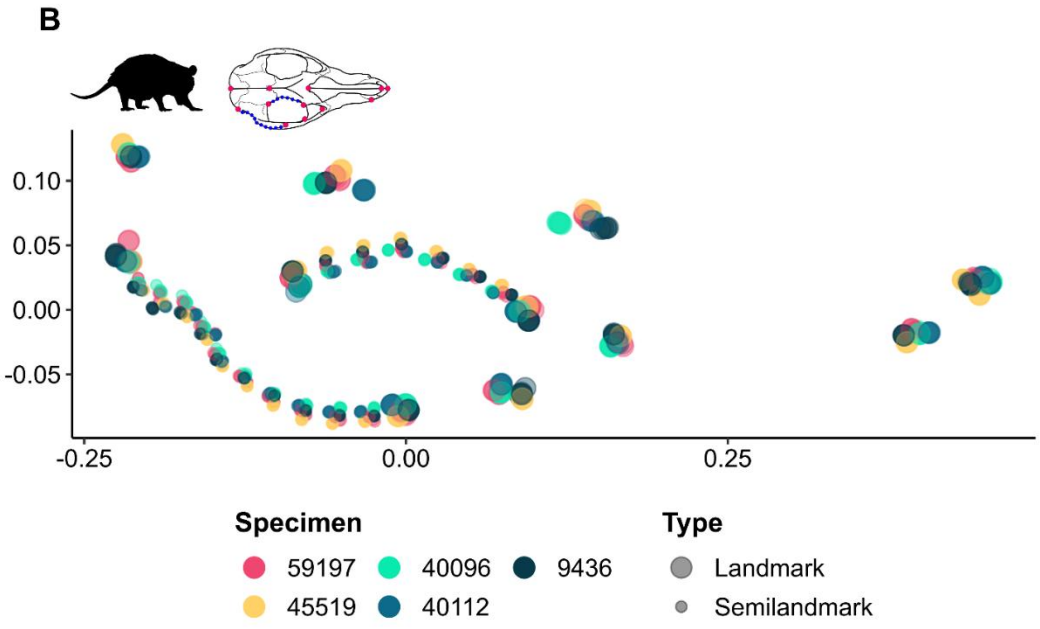


Figure S1. Landmarks for geometric morphometric analysis on Northern Raccoon (*Procyon lotor*) (A-C), Virginia Opossum (*Didelphis virginiana*) (D-F), Eastern Fox Squirrel (*Sciurus niger*) (G-I), and Eastern Cottontails (*Sylvilagus floridanus*) (J-L) skulls in the dorsal (left column), ventral (middle column), and lateral (right column) aspects. Landmarks are represented by large pink circles, semilandmarks (curves, denoted by "c" in the labels) small blue circles. For full descriptions of each landmark, see Table S1.

Repeatability

To visualize repeatability in the landmarking procedure, one researcher repeated the entire set of dorsal landmarks on five randomly selected specimens—excluding those with partially broken skulls—for each species five times each. For a given species, replicates were always performed in same order, i.e., the first specimen was fully landmarked once, followed by the second specimen, and so on, starting again at the first specimen until each had been completed five times. Procrustes coordinates are plotted below.





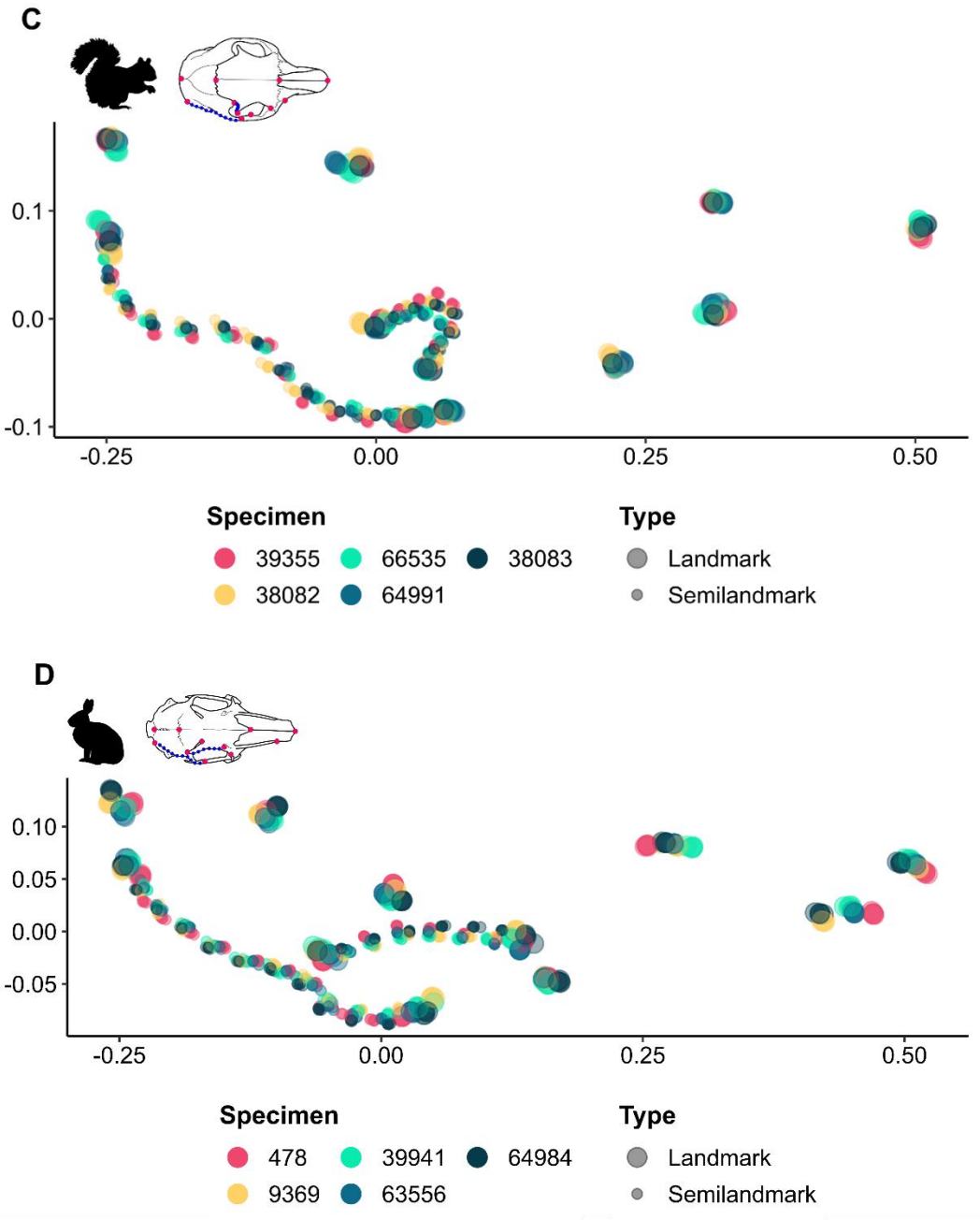


Figure S2. Repeatability of landmarking in the dorsal aspect for raccoons (*Procyon lotor*) (A), opossums (*Didelphis virginiana*) (B), fox squirrels (*Sciurus niger*) (C), and cottontails (*Sylvilagus floridanus*) (D). Within each plot, specimens are represented by different colors, each of which were repeated five times. The points are semitransparent such that darker spots of one color indicate overlap in placement of the same landmark on the same specimen. The specimen identifiers in the legend are Oklahoma Museum of Natural History (OMNH) Mammal Collection catalog numbers.

Aging in Raccoons (*Procyon lotor*)

Age classes were assigned based on the progression of suture closure, as described by Junge and Hoffmeister (1980). While these authors categorized specimens in 18 age groups, each approximately 2-6 months apart, the low sample sizes among older individuals leads us to question the precision of this method. Instead, we collapsed those authors' age categories into four classes based on relative signs of aging. We also evaluated the degree of tooth wear, but as it is more difficult to define discrete age classes based on this metric (Grau et al. 1970), we considered it a secondary criterion to suture closure. Based on the age descriptions by Junge and Hoffmeister (1980) and Grau et al. (1970), we used the following age classes:

Juvenile: Approximately < 1 year old. In addition to the following, the maxillary-palatine, squamosal-parietal, interpalatine, and squamosal-mastoid sutures are still open. There is little-to-no tooth wear, and some molars may still be erupting.

Young adult: Approximately 1-2 years old. Minimal signs of aging; in addition to the following, the squamosal-jugal, pterygoid-palatine, and internasal sutures are still open. The open sutures in the juvenile age class show a partial or intermediate state of closure. There is little-to-no tooth wear.

Adult: Approximately 3-5 years old. Moderate signs of aging; no sutures are fully open. The squamosal-mastoid is completely obliterated (not visible), while the remainder of sutures listed for the juvenile and young adult age classes may show partial or intermediate state of closure. There is wear to the molars but only some cones are worn down completely. Slight wear to premolars.

Old adult: Approximately 5+ years old. Advanced signs of aging; all sutures are obliterated, but the internasal may still be partially visible. The molars are worn flat.

Repeatability of age assignments was verified by estimating age class for 30 randomly selected specimens and repeating the aging procedure several days later, with the order of specimens randomized. The second round matched the first for 24 specimens (80%), and the remaining 6 were examined in a third round to refine the aging criteria. However, it should be noted that these categories are only rough estimates of age that cannot quantify or account for individual variation in ontogeny.

Urban/rural habitat category assignments

Habitat category (urban or rural) was assigned using two methods. The first was based on the verbatim locality in the specimen record. Those that were described relative to a town in a general fashion (e.g., "ca 9 mi S Stillwater, Hwy 33") were considered rural, while those including specific street names (e.g., 2101 NE 50th St, Oklahoma City) were categorized as urban. When coordinates were available, we used satellite imagery (Google Earth 2025) of the collection locality to further distinguish rural from urban, with the former dominated by trees or cropland and the latter by buildings. Specimens lacking a specific verbatim locality, such as those only recorded to county, were designated as "unknown" and excluded from analyses. The drawback to this approach is that it relies upon the landscape as it exists today and not necessarily at the time of collection, but the majority of specimens were collected before extensive satellite imagery was widely available. Therefore, we also categorized rural versus urban based on human population density around the time of collection, a common metric of

urbanization in ecological research (Rega-Brodsky et al. 2022). This approach permitted us to retain specimens with only county-level locality information in these models. Species were grouped by decade (1920 = collection year 1920-1929, 1930 = collection year 1930-1939, etc.) and county, for which human population size was obtained from US Census records via the National Historical Geographic Information System (Schroeder et al. 2025). Average county-level human population density was calculated by dividing population size by county size in km^2. At the census block level, urban areas are those containing at least 1,000 people/mi^2 (~380 people/ km^2) surrounded by areas of 500 people/mi^2 (~190 people/ km^2) (Ratcliffe et al. 2016). Using a conservative benchmark, we considered counties with > 200 people/ km^2 as urban, 10-200 people/ km^2 as rural, and <10 people/ km^2 as highly rural.

Supplemental results

Procrustes ANOVA

Here, the ProcD.lm function in the geomorph package (Baken et al. 2021, Adams et al. 2022) was used to run Procrustes ANOVA, a permutation-based method for conducting statistical tests to assess variance in Procrustes-aligned shape data. Random resampling of the data generates a probability distribution from which the *F*-statistic is derived. The analyses herein employ a residual randomization permutation procedure (Collyer and Adams 2018, 2021). The effect sizes (Z-scores) are based on the difference between the observed *F* value and the expected *F* value under the null hypothesis derived from the mean of the distribution of *F* values generated through permutation, relative to the standard deviation of that distribution. A larger Z-score indicates a larger difference among groups in the observed data than what is expected from random sampling, whereas values closer to 0 indicate little to no difference (a negative value suggests a weaker difference among groups than expected under the null).

Full results for Procrustes ANOVA are detailed below, organized by species, aspect, and the method used to categorize urban/rural (either based on verbatim locality or on county average human population density by decade, unknowns are excluded in both cases). Results include degrees of freedom (df), sum of squares (SS), mean squares (MS), R^2 (Rsq), *F*-statistic (F), Z score (Z), and *P*-value (Pr(>F).

	Verbatim locality habitat assignment							Human population density habitat assignment						
Variable	Df	SS	MS	Rsq	F	Z	Pr(>F)	Df	SS	MS	Rsq	F	Z	Pr(>F)
Csize	1	0.054	0.054	0.054	22.024	7.546	**0.001**	1	0.083	0.083	0.059	34.619	7.543	**0.001**
Sex	1	0.004	0.004	0.004	1.583	1.216	0.108	1	0.005	0.005	0.003	1.963	1.641	0.052
Age	3	0.129	0.043	0.126	17.335	7.993	**0.001**	3	0.170	0.057	0.121	23.625	9.973	**0.001**
State	2	0.021	0.011	0.021	4.269	4.503	**0.001**	2	0.023	0.011	0.016	4.746	4.813	**0.001**
Habitat	1	0.007	0.007	0.007	2.791	2.451	**0.010**	2	0.012	0.006	0.008	2.441	2.778	**0.003**
Residuals	245	0.605	0.002	0.596				366	0.877	0.002	0.626			
Total	253	1.017						375	1.401					

Table S2. Racoon (*Procyon lotor*) dorsal aspect Procrustes ANOVA model results, using verbatim locality and human population density to assign urban and rural habitat categories.

	Verbatim locality habitat assignment							Human population density habitat assignment						
Variable	Df	SS	MS	Rsq	F	Z	Pr(>F)	Df	SS	MS	Rsq	F	Z	Pr(>F)
Csize	1	0.011	0.011	0.048	15.399	6.878	**0.001**	1	0.014	0.014	0.044	20.006	7.313	**0.001**
Sex	1	0.002	0.002	0.011	3.587	3.479	**0.001**	1	0.004	0.004	0.011	5.076	4.402	**0.001**
Age	3	0.021	0.007	0.096	10.167	10.031	**0.001**	3	0.026	0.009	0.080	12.180	11.213	**0.001**
State	2	0.006	0.003	0.025	4.032	5.165	**0.001**	2	0.005	0.002	0.015	3.335	4.883	**0.001**
Habitat	1	0.003	0.003	0.013	4.025	3.675	**0.001**	2	0.003	0.001	0.009	1.945	2.416	**0.012**
Residuals	238	0.166	0.001	0.749				358	0.252	0.001	0.783			
Total	246	0.221						367	0.322					

Table S3. Racoon (*Procyon lotor*) ventral aspect Procrustes ANOVA model results, using verbatim locality and human population density to assign urban and rural habitat categories.

	Verbatim locality habitat assignment							Human population density habitat assignment						
Variable	Df	SS	MS	Rsq	F	Z	Pr(>F)	Df	SS	MS	Rsq	F	Z	Pr(>F)
Csize	1	0.020	0.020	0.053	16.043	4.958	**0.001**	1	0.026	0.026	0.048	21.348	6.770	**0.001**
Sex	1	0.002	0.002	0.006	1.791	1.415	0.087	1	0.002	0.002	0.004	1.920	1.612	0.052
Age	3	0.011	0.004	0.031	3.078	3.870	**0.001**	3	0.017	0.006	0.032	4.682	5.394	**0.001**
State	2	0.031	0.015	0.082	12.417	6.557	**0.001**	2	0.029	0.014	0.054	11.923	6.473	**0.001**
Habitat	1	0.004	0.004	0.010	3.156	2.591	**0.006**	2	0.008	0.004	0.015	3.279	3.532	**0.001**
Residuals	239	0.297	0.001	0.791				359	0.431	0.001	0.814			
Total	247	0.376						368	0.530					

Table S4. Racoon (*Procyon lotor*) lateral aspect Procrustes ANOVA model results, using verbatim locality and human population density to assign urban and rural habitat categories.

	Verbatim locality habitat assignment							Human population density habitat assignment						
Variable	Df	SS	MS	Rsq	F	Z	Pr(>F)	Df	SS	MS	Rsq	F	Z	Pr(>F)
Csize	1	0.026	0.026	0.145	18.763	5.009	**0.001**	1	0.025	0.025	0.135	17.888	5.316	**0.001**
Sex	1	0.005	0.005	0.027	3.515	2.495	**0.008**	1	0.005	0.005	0.024	3.205	2.479	**0.008**
State	2	0.009	0.005	0.050	3.230	3.129	**0.002**	2	0.011	0.005	0.058	3.834	3.623	**0.001**
Habitat	1	0.001	0.001	0.008	1.018	0.271	0.388	2	0.002	0.001	0.012	0.804	-0.381	0.646
Residuals	86	0.120	0.001	0.665				90	0.127	0.001	0.677			
Total	91	0.181						96	0.187					

Table S5. Opossum (*Didelphis virginiana*) dorsal aspect Procrustes ANOVA model results, using verbatim locality and human population density to assign urban and rural habitat categories.

	Verbatim locality habitat assignment							Human population density habitat assignment						
Variable	Df	SS	MS	Rsq	F	Z	Pr(>F)	Df	SS	MS	Rsq	F	Z	Pr(>F)
Csize	1	0.017	0.017	0.272	33.654	5.380	**0.001**	1	0.018	0.018	0.258	32.861	5.422	**0.001**
Sex	1	0.002	0.002	0.033	4.117	3.874	**0.001**	1	0.002	0.002	0.031	3.998	3.315	**0.001**
State	2	0.001	0.001	0.018	1.091	0.391	0.351	2	0.002	0.001	0.024	1.558	1.571	**0.044**
Habitat	1	0.001	0.001	0.013	1.586	1.253	0.101	2	0.001	0.001	0.016	1.007	0.148	0.432
Residuals	64	0.033	0.001	0.517				67	0.036	0.001	0.526			
Total	69	0.063						73	0.069					

Table S6. Opossum (*Didelphis virginiana*) ventral aspect Procrustes ANOVA model results, using verbatim locality and human population density to assign urban and rural habitat categories.

	Verbatim locality habitat assignment							Human population density habitat assignment						
Variable	Df	SS	MS	Rsq	F	Z	Pr(>F)	Df	SS	MS	Rsq	F	Z	Pr(>F)
Csize	1	0.015	0.015	0.113	12.267	4.317	0.001	1	0.015	0.015	0.109	12.654	4.456	**0.001**
Sex	1	0.005	0.005	0.035	3.796	2.684	0.004	1	0.004	0.004	0.031	3.564	2.610	**0.005**
State	2	0.003	0.002	0.027	1.445	1.099	0.135	2	0.005	0.002	0.035	2.020	2.010	**0.023**
Habitat	1	0.002	0.002	0.016	1.715	1.255	0.101	2	0.004	0.002	0.033	1.910	1.760	**0.041**
Residuals	64	0.076	0.001	0.591				68	0.079	0.001	0.588			
Total	69	0.129						74	0.135					

Table S7. Opossum (*Didelphis virginiana*) lateral aspect Procrustes ANOVA model results, using verbatim locality and human population density to assign urban and rural habitat categories.

	Verbatim locality habitat assignment							Human population density habitat assignment						
Variable	Df	SS	MS	Rsq	F	Z	Pr(>F)	Df	SS	MS	Rsq	F	Z	Pr(>F)
Csize	1	0.008	0.008	0.047	5.852	4.770	**0.001**	1	0.006	0.006	0.037	4.272	3.739	**0.001**
Sex	1	0.001	0.001	0.009	1.132	0.490	0.312	1	0.002	0.002	0.010	1.145	0.517	0.287
State	2	0.020	0.010	0.121	7.581	5.840	**0.001**	2	0.006	0.003	0.042	2.392	2.530	**0.012**
Habitat	1	0.002	0.002	0.012	1.443	0.991	0.163	2	0.003	0.001	0.017	1.001	0.259	0.399
Residuals	96	0.127	0.001	0.768				89	0.121	0.001	0.773			
Total	101	0.166						95	0.156					

Table S8. Fox squirrel (*Sciurus niger*) dorsal aspect Procrustes ANOVA model results, using verbatim locality and human population density to assign urban and rural habitat categories.

	Verbatim locality habitat assignment							Human population density habitat assignment						
Variable	Df	SS	MS	Rsq	F	Z	Pr(>F)	Df	SS	MS	Rsq	F	Z	Pr(>F)
Csize	1	0.012	0.012	0.118	14.861	5.578	**0.001**	1	0.008	0.008	0.087	10.105	5.187	**0.001**
Sex	1	0.001	0.001	0.007	0.838	-0.165	0.559	1	0.001	0.001	0.009	1.044	0.296	0.379
State	2	0.004	0.002	0.034	2.157	2.571	**0.006**	2	0.003	0.001	0.031	1.826	1.602	**0.040**
Habitat	1	0.001	0.001	0.011	1.390	0.999	0.159	2	0.003	0.001	0.030	1.728	1.418	0.072
Residuals	103	0.085	0.001	0.817				96	0.077	0.001	0.822			
Total	108	0.104						102	0.094					

Table S9. Fox squirrel (*Sciurus niger*) ventral aspect Procrustes ANOVA model results, using verbatim locality and human population density to assign urban and rural habitat categories.

	Verbatim locality habitat assignment							Human population density habitat assignment						
Variable	Df	SS	MS	Rsq	F	Z	Pr(>F)	Df	SS	MS	Rsq	F	Z	Pr(>F)
Csize	1	0.005	0.005	0.060	6.246	4.119	**0.001**	1	0.003	0.003	0.049	4.665	3.295	**0.002**
Sex	1	0.001	0.001	0.010	1.062	0.322	0.384	1	0.001	0.001	0.010	0.924	0.079	0.472
State	2	0.005	0.003	0.072	3.705	4.204	**0.001**	2	0.003	0.001	0.038	1.827	1.816	**0.041**
Habitat	1	0.001	0.001	0.016	1.676	1.303	0.101	2	0.002	0.001	0.026	1.246	0.776	0.226
Residuals	85	0.061	0.001	0.823				78	0.057	0.001	0.820			
Total	90	0.075						84	0.070					

Table S10. Fox squirrel (*Sciurus niger*) lateral aspect Procrustes ANOVA model results, using verbatim locality and human population density to assign urban and rural habitat categories.

	Verbatim locality habitat assignment							Human population density habitat assignment						
Variable	Df	SS	MS	Rsq	F	Z	Pr(>F)	Df	SS	MS	Rsq	F	Z	Pr(>F)
Csize	1	0.032	0.032	0.123	14.864	6.053	**0.001**	1	0.032	0.032	0.122	15.057	6.511	**0.001**
Sex	1	0.002	0.002	0.008	0.946	0.073	0.462	1	0.002	0.002	0.009	1.109	0.377	0.350
State	1	0.012	0.012	0.048	5.726	4.501	**0.001**	1	0.009	0.009	0.033	4.068	3.722	**0.001**
Habitat	1	0.002	0.002	0.006	0.772	-0.456	0.677	2	0.003	0.002	0.013	0.810	-0.587	0.715
Residuals	95	0.201	0.002	0.789				96	0.203	0.002	0.781			
Total	99	0.255						101	0.260					

Table S11. Eastern Cottontail (*Sylvilagus floridanus*) dorsal aspect Procrustes ANOVA model results, using verbatim locality and human population density to assign urban and rural habitat categories.

	Verbatim locality habitat assignment							Human population density habitat assignment						
Variable	Df	SS	MS	Rsq	F	Z	Pr(>F)	Df	SS	MS	Rsq	F	Z	Pr(>F)
Csize	1	0.015	0.015	0.142	16.372	7.150	**0.001**	1	0.016	0.016	0.150	17.890	6.777	**0.001**
Sex	1	0.001	0.001	0.005	0.614	-0.889	0.832	1	0.001	0.001	0.005	0.654	-0.743	0.777
State	1	0.008	0.008	0.073	8.363	5.016	**0.001**	1	0.005	0.005	0.051	6.047	4.483	**0.001**
Habitat	1	0.001	0.001	0.010	1.193	0.594	0.268	2	0.002	0.001	0.022	1.296	0.987	0.167
Residuals	90	0.081	0.001	0.781				91	0.082	0.001	0.762			
Total	94	0.104						96	0.107					

Table S12. Eastern Cottontail (*Sylvilagus floridanus*) ventral aspect Procrustes ANOVA model results, using verbatim locality and human population density to assign urban and rural habitat categories.

	Verbatim locality habitat assignment							Human population density habitat assignment						
Variable	Df	SS	MS	Rsq	F	Z	Pr(>F)	Df	SS	MS	Rsq	F	Z	Pr(>F)
Csize	1	0.015	0.015	0.135	14.757	5.583	**0.001**	1	0.016	0.016	0.141	15.830	5.613	**0.001**
Sex	1	0.001	0.001	0.009	0.950	0.058	0.483	1	0.001	0.001	0.007	0.800	-0.293	0.620
State	1	0.005	0.005	0.048	5.218	3.703	**0.001**	1	0.004	0.004	0.038	4.257	3.307	**0.001**
Habitat	1	0.003	0.003	0.023	2.504	2.200	**0.015**	2	0.004	0.002	0.039	2.190	2.527	**0.006**
Residuals	82	0.083	0.001	0.753				83	0.083	0.001	0.740			
Total	86	0.111						88	0.112					

Table S13. Eastern Cottontail (*Sylvilagus floridanus*) lateral aspect Procrustes ANOVA model results, using verbatim locality and human population density to assign urban and rural habitat categories.

Testing the role of climate in state-based shape differences

PCA of climate variables

Shape differences based on higher geography (state) may be attributed to genetic differences (including drift) among populations and environmental differences that influence how individuals grow. While we cannot assess genetic patterns using the present data, as a follow-up to the models describe above, we tested for the effects of including climate variables, specifically whether state and climate seemed to explain similar variation (suggesting climate as a driver of shape variation over geographic scales) or more separate components of skull shape (suggesting that state differences are more strongly determined by genetic diverge among populations that are largely isolated from one another due to distance).

We obtained seasonal climate data from ClimateNA, *version 7.60* (Wang et al. 2016, 2025). Data were calculated for all specimen locations based on latitude and longitude, when available. For Specimen locations listed only to county, we used the latitude and longitude of the centroid of that county, calculated using ArcGIS. We extracted the following seasonal climate variables by decade (note that ClimateNA's model groups decades from year 1 to 10, e.g., 1921-1930):

Tave_wt	winter mean temperature (°C)
Tave_sp	spring mean temperature (°C)
Tave_sm	summer mean temperature (°C)
Tave_at	autumn mean temperature (°C)
Tmax_wt	winter mean maximum temperature (°C)
Tmax_sp	spring mean maximum temperature (°C)
Tmax_sm	summer mean maximum temperature (°C)
Tmax_at	autumn mean maximum temperature (°C)
Tmin_wt	winter mean minimum temperature (°C)
Tmin_sp	spring mean minimum temperature (°C)
Tmin_sm	summer mean minimum temperature (°C)
Tmin_at	autumn mean minimum temperature (°C)
PPT_wt	winter precipitation (mm)
PPT_sp	spring precipitation (mm)
PPT_sm	summer precipitation (mm)
PPT_at	autumn precipitation (mm)
rsds_wt	winter solar radiation (MJ m-2 d-1)
rsds_sp	spring solar radiation (MJ m-2 d-1)
rsds_sm	summer solar radiation (MJ m-2 d-1)
rsds_at	autumn solar radiation (MJ m-2 d-1)

The first two components of a principal component analysis (PCA) together explained ~80% of the variance:

PC1 (53.25% total variation): generally most strongly associated with colder winter (negative correlation with max winter temp and average winter temp) and colder autumn (negative correlation with max autumn temp and average autumn temp). PC1 was positively correlated with solar radiation across all seasons, but the strongest relationship in winter. PC1 was also positively correlated with precipitation across all seasons, but these variables are slightly less important than those above.

PC2 (27.28% total variation): generally most strongly associated with cooler spring and summer (strongest negative correlation with average summer temperature, followed by minimum summer temperature, max summer temperature, max spring temperature, average spring temperature, minimum spring temperature). PC2 is negatively but weakly correlated with solar radiation and precipitation across seasons (except winter, which is positively associated).

As expected, California specimens stand out more starkly along these climate axes, whereas Oklahoma, Tennessee, and Mississippi specimens (although not the latter are only represented by a small sample of fox squirrels), are more similar:

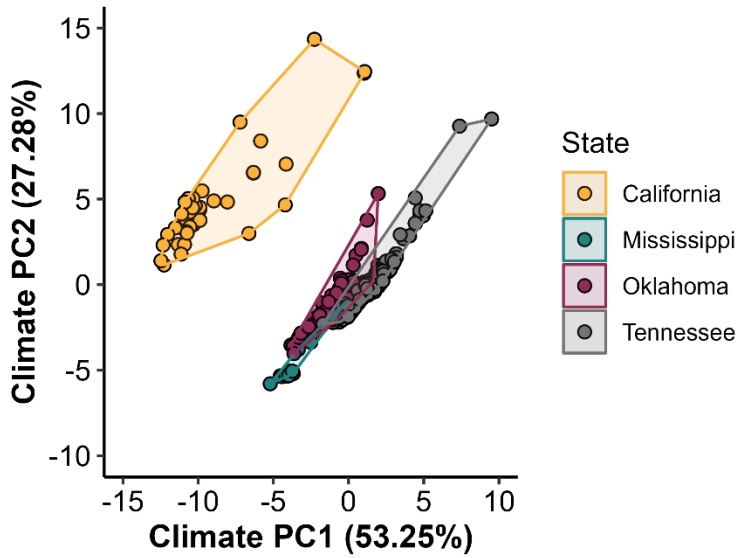


Figure S3. Principal component analysis plot of climate variables by state.

We added Climate PC1 and PC2 to the models above (with urban/rural based on human density), both with and without state, full results below.

	Including state							Excluding state						
Variable	Df	SS	MS	Rsq	F	Z	Pr(>F)	Df	SS	MS	Rsq	F	Z	Pr(>F)
Csize	1	0.080	0.080	0.057	33.414	7.765	**0.001**	1	0.090	0.090	0.064	37.362	8.164	**0.001**
Sex	1	0.005	0.005	0.003	1.959	1.650	**0.050**	1	0.005	0.005	0.004	2.217	1.888	**0.025**
Age	3	0.167	0.056	0.119	23.259	9.820	**0.001**	3	0.169	0.056	0.120	23.343	10.063	**0.001**
State	2	0.011	0.005	0.008	2.263	2.637	**0.006**	-	-	-	-	-	-	-
Habitat	2	0.012	0.006	0.008	2.405	2.769	**0.003**	2	0.015	0.007	0.010	3.030	3.463	**0.001**
Clim.PC1	1	0.004	0.004	0.003	1.525	1.093	0.147	1	0.013	0.013	0.009	5.433	4.024	**0.001**
Clim.PC2	1	0.004	0.004	0.003	1.715	1.367	0.082	1	0.007	0.007	0.005	2.794	2.480	**0.005**
Residuals	364	0.870	0.002	0.621				366	0.881	0.002	0.629			
Total	375	1.401						375	1.401					

Table S14. Racoon (*Procyon lotor*) dorsal aspect Procrustes ANOVA model results incorporating climate PC1 and PC2, with and without state. Human population density was used to assign urban and rural habitat categories.

	Including state							Excluding state						
Variable	Df	SS	MS	Rsq	F	Z	Pr(>F)	Df	SS	MS	Rsq	F	Z	Pr(>F)
Csize	1	0.014	0.014	0.043	19.828	7.929	**0.001**	1	0.013	0.013	0.042	19.201	7.432	**0.001**
Sex	1	0.004	0.004	0.012	5.417	4.693	**0.001**	1	0.004	0.004	0.012	5.540	4.523	**0.001**
Age	3	0.026	0.009	0.080	12.349	10.960	**0.001**	3	0.027	0.009	0.083	12.628	11.503	**0.001**
State	2	0.003	0.001	0.009	2.097	2.648	**0.003**	-	-	-	-	-	-	-
Habitat	2	0.003	0.002	0.010	2.396	2.980	**0.003**	2	0.003	0.002	0.010	2.259	2.798	**0.003**
Clim.PC1	1	0.001	0.001	0.005	2.113	2.044	**0.019**	1	0.003	0.003	0.009	4.237	4.222	**0.001**
Clim.PC2	1	0.001	0.001	0.003	1.498	1.183	0.129	1	0.003	0.003	0.008	3.807	4.096	**0.001**
Residuals	356	0.249	0.001	0.772				358	0.251	0.001	0.781			
Total	367	0.322						367	0.322					

Table S15. Racoon (*Procyon lotor*) ventral aspect Procrustes ANOVA model results incorporating climate PC1 and PC2, with and without state. Human population density was used to assign urban and rural habitat categories.

	Including state							Excluding state						
Variable	Df	SS	MS	Rsq	F	Z	Pr(>F)	Df	SS	MS	Rsq	F	Z	Pr(>F)
Csize	1	0.025	0.025	0.047	20.637	6.746	0.001	1	0.023	0.023	0.043	18.937	6.291	0.001
Sex	1	0.003	0.003	0.005	2.202	1.875	0.031	1	0.002	0.002	0.003	1.431	1.027	0.161
Age	3	0.017	0.006	0.032	4.706	5.406	0.001	3	0.017	0.006	0.033	4.721	5.464	0.001
State	2	0.009	0.004	0.016	3.552	3.749	0.001	-	-	-	-	-	-	-
Habitat	2	0.006	0.003	0.012	2.613	2.939	0.001	2	0.008	0.004	0.016	3.473	3.825	0.001
Clim.PC1	1	0.001	0.001	0.002	0.955	0.172	0.427	1	0.014	0.014	0.026	11.308	4.908	0.001
Clim.PC2	1	0.001	0.001	0.002	0.838	-0.039	0.512	1	0.013	0.013	0.025	10.714	4.279	0.001
Residuals	357	0.428	0.001	0.808				359	0.436	0.001	0.824			
Total	368	0.530						368	0.530					

Table S16. Racoon (*Procyon lotor*) lateral aspect Procrustes ANOVA model results incorporating climate PC1 and PC2, with and without state. Human population density was used to assign urban and rural habitat categories.

	Including state							Excluding state						
Variable	Df	SS	MS	Rsq	F	Z	Pr(>F)	Df	SS	MS	Rsq	F	Z	Pr(>F)
Csize	1	0.024	0.024	0.131	17.277	4.368	**0.001**	1	0.026	0.026	0.138	17.863	4.856	**0.001**
Sex	1	0.005	0.005	0.025	3.231	2.386	**0.010**	1	0.005	0.005	0.025	3.259	2.472	**0.008**
State	2	0.005	0.003	0.028	1.869	1.755	**0.042**	-	-	-	-	-	-	-
Habitat	2	0.002	0.001	0.012	0.769	-0.509	0.698	2	0.003	0.002	0.018	1.137	0.520	0.293
Clim.PC1	1	0.003	0.003	0.015	1.940	1.508	0.067	1	0.008	0.008	0.044	5.681	3.361	**0.001**
Clim.PC2	1	0.002	0.002	0.011	1.486	1.009	0.176	1	0.001	0.001	0.008	1.002	0.290	0.381
Residuals	86	0.121	0.001	0.652				88	0.126	0.001	0.681			
Total	94	0.185						94	0.185					

Table S17. Opossum (*Didelphis virginiana*) dorsal aspect Procrustes ANOVA model results incorporating climate PC1 and PC2, with and without state. Human population density was used to assign urban and rural habitat categories.

	Including state							Excluding state						
Variable	Df	SS	MS	Rsq	F	Z	Pr(>F)	Df	SS	MS	Rsq	F	Z	Pr(>F)
Csize	1	0.017	0.017	0.249	31.559	5.367	**0.001**	1	0.017	0.017	0.254	31.916	5.556	**0.001**
Sex	1	0.002	0.002	0.034	4.273	3.633	**0.001**	1	0.002	0.002	0.033	4.199	3.617	**0.001**
State	2	0.001	0.001	0.020	1.272	0.870	0.191	-	-	-	-	-	-	-
Habitat	2	0.002	0.001	0.023	1.457	1.340	0.094	2	0.001	0.001	0.019	1.202	0.690	0.251
Clim.PC1	1	0.001	0.001	0.008	0.988	0.218	0.417	1	0.001	0.001	0.015	1.877	1.660	**0.047**
Clim.PC2	1	0.000	0.000	0.005	0.684	-0.577	0.724	1	0.001	0.001	0.007	0.927	0.035	0.491
Residuals	64	0.035	0.001	0.504				66	0.036	0.001	0.525			
Total	72	0.068						72	0.068					

Table S18. Opossum (*Didelphis virginiana*) ventral aspect Procrustes ANOVA model results incorporating climate PC1 and PC2, with and without state. Human population density was used to assign urban and rural habitat categories.

	Including state							Excluding state						
Variable	Df	SS	MS	Rsq	F	Z	Pr(>F)	Df	SS	MS	Rsq	F	Z	Pr(>F)
Csize	1	0.015	0.015	0.109	12.146	4.802	**0.001**	1	0.015	0.015	0.111	12.504	4.830	**0.001**
Sex	1	0.004	0.004	0.030	3.331	2.486	**0.009**	1	0.004	0.004	0.030	3.337	2.469	**0.008**
State	2	0.001	0.001	0.010	0.550	-1.268	0.898	-	-	-	-	-	-	-
Habitat	2	0.003	0.001	0.022	1.208	0.719	0.239	2	0.003	0.002	0.023	1.273	0.848	0.193
Clim.PC1	1	0.001	0.001	0.006	0.621	-0.616	0.728	1	0.003	0.003	0.020	2.227	1.724	**0.043**
Clim.PC2	1	0.001	0.001	0.005	0.550	-0.813	0.790	1	0.001	0.001	0.004	0.491	-1.017	0.852
Residuals	64	0.077	0.001	0.575				66	0.078	0.001	0.585			
Total	72	0.134						72	0.134					

Table S19. Opossum (*Didelphis virginiana*) lateral aspect Procrustes ANOVA model results incorporating climate PC1 and PC2, with and without state. Human population density was used to assign urban and rural habitat categories.

	Including state							Excluding state						
Variable	Df	SS	MS	Rsq	F	Z	Pr(>F)	Df	SS	MS	Rsq	F	Z	Pr(>F)
Csize	1	0.006	0.006	0.037	4.329	4.018	**0.001**	1	0.006	0.006	0.039	4.439	3.787	**0.001**
Sex	1	0.002	0.002	0.011	1.257	0.731	0.228	1	0.002	0.002	0.012	1.345	0.902	0.182
State	2	0.005	0.003	0.034	2.006	2.341	**0.013**	-	-	-	-	-	-	-
Habitat	2	0.003	0.001	0.017	0.984	0.197	0.423	2	0.003	0.002	0.020	1.150	0.628	0.261
Clim.PC1	1	0.002	0.002	0.013	1.565	1.274	0.091	1	0.003	0.003	0.021	2.362	1.993	**0.023**
Clim.PC2	1	0.003	0.003	0.017	1.989	1.844	**0.030**	1	0.002	0.002	0.010	1.112	0.442	0.333
Residuals	87	0.117	0.001	0.748				89	0.122	0.001	0.782			
Total	95	0.156						95	0.156					

Table S20. Fox squirrel (*Sciurus niger*) dorsal aspect Procrustes ANOVA model results incorporating climate PC1 and PC2, with and without state. Human population density was used to assign urban and rural habitat categories.

	Including state							Excluding state						
Variable	Df	SS	MS	Rsq	F	Z	Pr(>F)	Df	SS	MS	Rsq	F	Z	Pr(>F)
Csize	1	0.008	0.008	0.080	9.465	5.259	**0.001**	1	0.008	0.008	0.090	10.544	5.174	**0.001**
Sex	1	0.001	0.001	0.008	0.953	0.091	0.461	1	0.001	0.001	0.009	1.094	0.398	0.364
State	2	0.002	0.001	0.021	1.247	0.802	0.209	-	-	-	-	-	-	-
Habitat	2	0.003	0.001	0.029	1.720	1.409	0.059	2	0.003	0.001	0.028	1.660	1.368	0.067
Clim.PC1	1	0.001	0.001	0.012	1.397	0.918	0.178	1	0.002	0.002	0.019	2.196	1.552	0.053
Clim.PC2	1	0.001	0.001	0.011	1.250	0.718	0.248	1	0.001	0.001	0.013	1.500	1.074	0.128
Residuals	94	0.075	0.001	0.798				96	0.077	0.001	0.819			
Total	102	0.094						102	0.094					

Table S21. Fox squirrel (*Sciurus niger*) ventral aspect Procrustes ANOVA model results incorporating climate PC1 and PC2, with and without state. Human population density was used to assign urban and rural habitat categories.

	Including state							Excluding state						
Variable	Df	SS	MS	Rsq	F	Z	Pr(>F)	Df	SS	MS	Rsq	F	Z	Pr(>F)
Csize	1	0.004	0.004	0.054	5.206	3.550	**0.001**	1	0.003	0.003	0.045	4.286	3.236	**0.002**
Sex	1	0.000	0.000	0.006	0.618	-0.743	0.771	1	0.001	0.001	0.010	0.910	0.051	0.489
State	2	0.003	0.001	0.036	1.770	1.747	**0.039**	-	-	-	-	-	-	-
Habitat	2	0.002	0.001	0.024	1.168	0.600	0.274	2	0.002	0.001	0.027	1.268	0.808	0.206
Clim.PC1	1	0.001	0.001	0.011	1.077	0.388	0.344	1	0.001	0.001	0.013	1.260	0.650	0.245
Clim.PC2	1	0.001	0.001	0.018	1.765	1.419	0.084	1	0.001	0.001	0.015	1.437	0.960	0.164
Residuals	76	0.055	0.001	0.782				78	0.057	0.001	0.818			
Total	84	0.070						84	0.070					

Table S22. Fox squirrel (*Sciurus niger*) lateral aspect Procrustes ANOVA model results incorporating climate PC1 and PC2, with and without state. Human population density was used to assign urban and rural habitat categories.

	Including state							Excluding state						
Variable	Df	SS	MS	Rsq	F	Z	Pr(>F)	Df	SS	MS	Rsq	F	Z	Pr(>F)
Csize	1	0.032	0.032	0.122	14.967	6.340	**0.001**	1	0.032	0.032	0.125	15.196	6.407	**0.001**
Sex	1	0.002	0.002	0.009	1.126	0.413	0.348	1	0.002	0.002	0.009	1.098	0.372	0.354
State	1	0.003	0.003	0.010	1.277	0.756	0.227	-	-	-	-	-	-	-
Habitat	2	0.003	0.002	0.013	0.800	-0.596	0.732	2	0.004	0.002	0.017	1.038	0.237	0.408
Clim.PC1	1	0.002	0.002	0.008	0.969	0.148	0.440	1	0.005	0.005	0.019	2.332	2.311	**0.012**
Clim.PC2	1	0.002	0.002	0.007	0.865	-0.124	0.545	1	0.002	0.002	0.008	1.037	0.274	0.397
Residuals	94	0.200	0.002	0.768				95	0.203	0.002	0.779			
Total	101	0.260						101	0.260					

Table S23. Eastern cottontail (*Sylvilagus floridanus*) dorsal aspect Procrustes ANOVA model results incorporating climate PC1 and PC2, with and without state. Human population density was used to assign urban and rural habitat categories.

	Including state							Excluding state						
Variable	Df	SS	MS	Rsq	F	Z	Pr(>F)	Df	SS	MS	Rsq	F	Z	Pr(>F)
Csize	1	0.016	0.016	0.146	17.536	7.159	**0.001**	1	0.015	0.015	0.145	17.023	6.536	**0.001**
Sex	1	0.001	0.001	0.005	0.642	-0.776	0.795	1	0.001	0.001	0.005	0.644	-0.747	0.781
State	1	0.002	0.002	0.022	2.601	2.365	**0.014**	-	-	-	-	-	-	-
Habitat	2	0.002	0.001	0.021	1.245	0.878	0.189	2	0.002	0.001	0.020	1.190	0.741	0.217
Clim.PC1	1	0.001	0.001	0.009	1.026	0.270	0.397	1	0.003	0.003	0.032	3.756	3.176	**0.002**
Clim.PC2	1	0.001	0.001	0.006	0.777	-0.352	0.631	1	0.002	0.002	0.020	2.391	2.241	**0.015**
Residuals	89	0.079	0.001	0.743				90	0.082	0.001	0.764			
Total	96	0.107						96	0.107					

Table S24. Eastern cottontail (*Sylvilagus floridanus*) ventral aspect Procrustes ANOVA model results incorporating climate PC1 and PC2, with and without state. Human population density was used to assign urban and rural habitat categories.

	Including state							Excluding state						
Variable	Df	SS	MS	Rsq	F	Z	Pr(>F)	Df	SS	MS	Rsq	F	Z	Pr(>F)
Csize	1	0.014	0.014	0.128	14.414	5.687	**0.001**	1	0.017	0.017	0.149	16.827	6.049	**0.001**
Sex	1	0.001	0.001	0.008	0.940	0.036	0.486	1	0.001	0.001	0.008	0.923	0.000	0.496
State	1	0.001	0.001	0.011	1.213	0.634	0.271	-	-	-	-	-	-	-
Habitat	2	0.003	0.002	0.029	1.667	1.636	0.058	2	0.004	0.002	0.040	2.232	2.553	**0.001**
Clim.PC1	1	0.001	0.001	0.013	1.484	1.079	0.137	1	0.004	0.004	0.036	4.041	3.110	**0.002**
Clim.PC2	1	0.002	0.002	0.016	1.801	1.512	0.066	1	0.003	0.003	0.028	3.138	2.671	**0.003**
Residuals	81	0.080	0.001	0.717				82	0.081	0.001	0.727			
Total	88	0.112						88	0.112					

Table S25. Eastern cottontail (*Sylvilagus floridanus*) lateral aspect Procrustes ANOVA model results incorporating climate PC1 and PC2, with and without state. Human population density was used to assign urban and rural habitat categories.

Morphological disparity

Morphological disparity describes differences in the degree of variation among groups. We used the 'morphol.disparity' function in the *geomorph* package, which estimates Procrustes variance within groups based on the residuals of a model fit with ProcD.lm as described above, then evaluates statistically significant differences among groups through randomized permutation (Baken et al. 2021; Adams et al. 2022).

Below, we report the Procrustes variances and p-values for all pairwise comparisons for urban and rural groups (both based on verbatim locality and human density), state, sex, and age class (raccoons). For all but verbatim-locality urban/rural, results are based on models incorporating human-density urban/rural.

Aspect	Procrustes Variance		Differences
	Female	Male	
Dorsal	2.42×10^{-3}	2.27×10^{-3}	none (P=0.363)
Ventral	6.43×10^{-4}	7.17×10^{-4}	none (P=0.069)
Lateral	1.07×10^{-3}	1.24×10^{-3}	none (P=0.123)

Table S26. Raccoon (*Procyon lotor*) morphological disparity between sexes.

Aspect	Procrustes Variance				Differences
	Juvenile	Young Adult	Adult	Old Adult	
Dorsal	2.13×10^{-3} *	2.51×10^{-3}	2.69×10^{-3} *	2.66×10^{-3}	***P*=0.029**
Ventral	6.54×10^{-4} *	7.68×10^{-4} *	6.96×10^{-4}	5.99×10^{-4}	***P*=0.015**
Lateral	1.09×10^{-3} *	1.13×10^{-3}	1.37×10^{-3}	1.59×10^{-3} *	***P*=0.050**

Table S27. Raccoon (*Procyon lotor*) morphological disparity among age classes.

	Procrustes Variance			Differences
	California	Oklahoma	Tennessee	
Dorsal	2.81×10^{-3}	2.95×10^{-3} *	2.25×10^{-3} *	***P*=0.017**
Ventral	5.72×10^{-4}	7.44×10^{-4}	6.85×10^{-4}	none
Lateral	1.24×10^{-3}	1.09×10^{-3}	1.17×10^{-3}	none

Table S28. Raccoon (*Procyon lotor*) morphological disparity among states.

Aspect	Procrustes Variance		Differences
	Rural	Urban	
Dorsal	2.36×10^{-3}	2.46×10^{-3}	none (*P*=0.735)
Ventral	6.63×10^{-4}	7.02×10^{-4}	none (*P*=0.496)
Lateral	1.20×10^{-3}	1.20×10^{-3}	none (*P*=0.926)

Table S29. Raccoon (*Procyon lotor*) morphological disparity between habitat categories (based on verbatim locality)

Aspect	Procrustes Variance			Differences
	Highly Rural	Rural	Urban	
Dorsal	3.25×10^{-3} *†	2.21×10^{-3} †	2.23×10^{-3} *	***P*=0.001; †*P*=0.001**
Ventral	7.04×10^{-4}	6.75×10^{-4}	7.08×10^{-4}	none
Lateral	1.27×10^{-3}	1.16×10^{-3}	1.12×10^{-3}	none

Table S30. Raccoon (*Procyon lotor*) morphological disparity between habitat categories (based on human population density).

Aspect	Procrustes Variance		Differences
	Female	Male	
Dorsal	1.12×10^{-3}	1.48×10^{-3}	***P*=0.029**
Ventral	4.56×10^{-4}	5.22×10^{-4}	none (*P*=0.507)
Lateral	9.92×10^{-4}	1.13×10^{-3}	none (*P*=0.313)

Table S31. Opossum (*Didelphis virginiana*) morphological disparity between sexes.

	Procrustes Variance			Differences
	California	Oklahoma	Tennessee	
Dorsal	1.83×10^{-3} *†	1.23×10^{-3} *	1.24×10^{-3} †	***P*=0.036; †*P*=0.022**
Ventral	4.81×10^{-4}	4.28×10^{-4}	5.11×10^{-4}	none
Lateral	1.25×10^{-3}	1.10×10^{-3}	1.01×10^{-3}	none

Table S32. Opossum (*Didelphis virginiana*) morphological disparity among states.

Aspect	Procrustes Variance		Differences
	Rural	Urban	
Dorsal	1.25×10^{-3}	1.47×10^{-3}	none (*P*=0.243)
Ventral	4.57×10^{-4}	4.87×10^{-4}	none (*P*=0.672)
Lateral	1.09×10^{-3}	1.07×10^{-3}	none (*P*=0.916)

Table S33. Opossum (*Didelphis virginiana*) morphological disparity between habitat categories (based on verbatim locality).

Aspect	Procrustes Variance			Differences
	Highly Rural	Rural	Urban	
Dorsal	1.17×10^{-3}	1.26×10^{-3}	1.55×10^{-3}	none
Ventral	4.48×10^{-4}	5.42×10^{-4}	4.28×10^{-4}	none
Lateral	9.57×10^{-4}	1.10×10^{-3}	1.05×10^{-3}	none

Table S34. Opossum (*Didelphis virginiana*) morphological disparity between habitat categories (based on human population density).

Aspect	Procrustes Variance		Differences
	Female	Male	
Dorsal	1.19×10^{-3}	1.31×10^{-3}	none (*P*= 0.447)
Ventral	7.68×10^{-4}	7.38×10^{-4}	none (*P*= 0.831)
Lateral	6.71×10^{-4}	6.75×10^{-4}	none (*P*= 0.976)

Table S35. Fox squirrels (*Sciurus niger*) morphological disparity between sexes.

	Procrustes Variance			Differences
	California	Mississippi	Oklahoma	
Dorsal	1.60×10^{-3} *	1.32×10^{-3}	1.10×10^{-3} *	***P*=0.007**
Ventral	6.62×10^{-4}	6.76×10^{-4}	8.29×10^{-4}	none
Lateral	6.84×10^{-4}	6.84×10^{-4}	6.16×10^{-4}	none

Table S36. Fox squirrels (*Sciurus niger*) morphological disparity among states.

Aspect	Procrustes Variance		Differences
	Rural	Urban	
Dorsal	1.18×10^{-3}	1.32×10^{-3}	none (*P*=0.355)
Ventral	7.44×10^{-4}	8.25×10^{-4}	none (*P*=0.0.594)
Lateral	6.94×10^{-4}	6.54×10^{-4}	none (*P*=0.0.627)

Table S37. Fox squirrels (*Sciurus niger*) morphological disparity between habitat categories (based on verbatim locality).

Aspect	Procrustes Variance			Differences
	Highly Rural	Rural	Urban	
Dorsal	1.20×10^{-3}	1.15×10^{-3} *	1.54×10^{-3} *	***P*=0.048**
Ventral	7.54×10^{-4}	8.17×10^{-4}	6.36×10^{-4}	none
Lateral	6.72×10^{-4}	6.85×10^{-4}	6.53×10^{-4}	none

Table S38. Fox squirrels (*Sciurus niger*) morphological disparity between habitat categories (based on human population density).

Aspect	Procrustes Variance		Differences
	Female	Male	
Dorsal	2.11×10^{-3}	1.88×10^{-3}	none (*P*= 0.208)
Ventral	8.21×10^{-4}	8.57×10^{-4}	none (*P*= 0.646)
Lateral	1.08×10^{-3}	7.96×10^{-4}	***P*=0.003**

Table S39. Eastern cottontail (*Sylvilagus floridanus*) morphological disparity between sexes.

Aspect	Procrustes Variance		Differences
	Oklahoma	Tennessee	
Dorsal	2.17×10^{-3}	1.77×10^{-3}	***P*=0.038**
Ventral	8.86×10^{-4}	7.85×10^{-4}	none (*P*= 0.201)
Lateral	9.53×10^{-4}	8.98×10^{-4}	none (*P*= 0.534)

Table S40. Eastern cottontail (*Sylvilagus floridanus*) morphological disparity among states.

Aspect	Procrustes Variance		Differences
	Rural	Urban	
Dorsal	2.01×10^{-3}	2.03×10^{-3}	none (*P*=0.0.893)
Ventral	8.44×10^{-4}	8.76×10^{-4}	none (*P*=0.0.774)
Lateral	9.21×10^{-4}	1.10×10^{-3}	none (*P*=0.0.115)

Table S41. Eastern cottontail (*Sylvilagus floridanus*) morphological disparity between habitat categories (based on verbatim locality).

Aspect	Procrustes Variance			Differences
	Highly Rural	Rural	Urban	
Dorsal	2.13×10^{-3} *	2.15×10^{-3} †	1.19×10^{-3} *†	***P*=0.004; †*P*=0.003**
Ventral	9.94×10^{-4} *	7.58×10^{-4} *	7.92×10^{-4}	***P*=0.010**
Lateral	9.42×10^{-4}	9.63×10^{-4}	7.43×10^{-4}	none

Table S42. Eastern cottontail (*Sylvilagus floridanus*) morphological disparity between habitat categories (based on human population density).

Canonical Variate Analysis

Canonical variate analysis is an ordination method that optimizes differences between groups (as opposed to differences among individuals, as in PCA), which are designated *a priori*. The canonical variates (CVs) are the new axes along which differences in group means are maximized. Notably, this method does not test statistical significance among groups. How well the CVs discriminate among groups was assessed by calculating Mahalanobis distance between each specimen and the group means, such that each specimen is assigned to the group it is closest to, providing accuracy as a percentage of total specimens that were placed in the correct group. The following table provides these accuracy ratings for each species and aspect when using verbatim-locality urban/rural categories, human-density urban/rural categories, state of collection, or age class (raccoons only) as the grouping variable.

Species	**Aspect**	**Urban/Rural (verbatim locality)**	**Urban/Rural (human density)**	**State**	**Age**
Raccoons (*P. lotor*)	Dorsal	89.0%	78.5%	95.3%	81.5%
	Ventral	83.4%	69.3%	89.5%	75.8%
	Lateral	86.3%	75.6%	93.6%	76.1%
Opossums (*D. virginiana*)	Dorsal	97.8%	83.5%	96.9%	
	Ventral	79.0%	68.9%	79.7%	
	Lateral	95.7%	93.3%	100%	
Fox squirrels (*S. niger*)	Dorsal	92.1%	93.8%	96.1%	
	Ventral	77.1%	70.9%	78.0%	
	Lateral	79.1%	89.4%	96.7%	
Cottontails (*S. floridanus*)	Dorsal	90.0%	86.3%	94.2%	
	Ventral	86.3%	70.1%	96.9%	
	Lateral	94.3%	86.5%	96.7%	

Table S43. Accurate classification of specimens based on canonical variate analysis for each species, aspect, and grouping variable.

References

Adams, D. C., Collyer, M. L., Kaliontzopoulou, A. and Baken, E. K. 2022. Geomorph: Software for geometric morphometric analyses. – < https://cran.r-project.org/package=geomorph>.

Baken, E. K., Collyer, M. L., Kaliontzopoulou, A. and Adams, D. C. 2021. geomorph v4.0 and gmShiny: Enhanced analytics and a new graphical interface for a comprehensive morphometric experience. – *Methods Ecol. Evol.* **12**: 2355–2363.

Collyer, M. L. and Adams, D. C. 2018. RRPP: An r package for fitting linear models to high-dimensional data using residual randomization. – *Methods Ecol. Evol.* **9**: 1772–1779.

Collyer, M. L. and Adams, D. C. 2021. RRPP: Linear Model Evaluation with Randomized Residuals in a Permutation Procedure. – < https://cran.r-project.org/web/packages/RRPP>

Google Earth. 2025. Satellite imagery of North America. (Version 7.3.6). Google. https://earth.google.com/ Imagery date: June 14, 2024; Accessed March 12-13, 2025.

Grau, G. A., Sanderson, G. C. and Rogers, J. P. 1970. Age Determination of Raccoons. – *J. Wildl. Manag.* **34**: 364.

Junge, R. and Hoffmeister, D. F. 1980. Age Determination in Raccoons from Cranial Suture Obliteration. – *J. Wildl. Manag.* **44**: 725.

R Core Team 2025. R: A language and environment for statistical computing. – < https://www.R-project.org/>.

Ratcliffe, M., Burd, C., Holder, K. and Fields, A. 2016. Defining Rural at the U.S. Census Bureau. ACSGEO-1, U.S. Census Bureau, Washington, DC.

Rega-Brodsky, C. C., Aronson, M. F. J., Piana, M. R., Carpenter, E.-S., Hahs, A. K., Herrera-Montes, A., Knapp, S., Kotze, D. J., Lepczyk, C. A., Moretti, M., Salisbury, A. B., Williams, N. S. G., Jung, K., Katti, M., MacGregor-Fors, I., MacIvor, J. S., La Sorte, F. A., Sheel, V., Threfall, C. G. and Nilon, C. H. 2022. Urban biodiversity: State of the science and future directions. – *Urban. Ecosyst.* **25**: 1083–1096.

Rohlf, F. J. 2021. tpsDig2. – < https://sbmorphometrics.org/>.

Rohlf, F. J. 2022. tpsUtil. – < https://sbmorphometrics.org/>.

Schroeder, J., Van Riper, D., Manson, S., Knowles, K., Kugler, T., Roberts, F. and Ruggles, S. 2025. IPUMS National Historical Geographic Information System: Version 20.0 [dataset]. < http://doi.org/10.18128/D050.V20.0>.

Wang, T., Hamann, A., Spittlehouse, D. and Carroll, C. 2016. Locally downscaled and spatially customizable climate data for historical and future periods for North America. – *PLoS ONE* **11**: e0156720.

Wang, T., Hamann, A. and Sang, Z. 2025. Monthly High-Resolution Historical Climate Data for North America Since 1901. – *Int. J. Climatol.* **45**: e8726.

CONCLUSION

Humans are driving and suffering the consequences of a global biodiversity crisis. Time, money, and resources are limited, therefore conservation strategies must be targeted and data driven. Natural history collections uniquely provide a material history of biodiversity on our planet; each specimen represents an irreplaceable record of a given species at a given place and time that will never again be repeated. These collections provide information not only on where we have been, but can offer foresight into where we are headed: which species will be "winners" and "losers" under future climate scenarios and, importantly, *why*? What traits and environmental conditions are associated with particular responses, and what interventions may be more or less impactful? To that end, this dissertation highlights the diverse ways in which natural history collections can be used to track ongoing environmental change.

My first chapter demonstrated how the inclusion of age—an oft-overlooked aspect of morphology in mammals—can refine our understanding of body-size variation and demographic change through time. This work contributes to an improved understanding of global-change responses, both by encouraging interpretation of previous body-size research through a new lens and in highlighting the essential, but largely untapped, connections between morphology and demographic data in museum specimens. In future work, I aim to contribute to the development and assessment of age-determination methods across a broader range of mammal species and to further investigate the extent and effects of population age structure shifts as a response to global change. My second chapter focuses on nutrient dilution, a consequence of climate change that is global in scope but still understudied in the realm of organismal responses to climate change. My work provides evidence of widespread body-size decline in a small herbivore paired with an apparent shift in forage selection, potentially to compensate for a changing nutritional landscape. Building on this work will lead to refinement of methods for detecting the signatures of nutrient dilution in museum specimens to better understand the extent and effects of widespread nutritional deficits across taxa and through trophic levels. Finally, my third chapter shows that the morphological signal of responses to urbanization are not consistent across species. While behavior-mediated change—i.e., domestication syndrome—has been proposed as an overarching driver of responses to urbanization, my research suggests a higher importance of ecological and city-specific factors. My future work on this topic will target community-level size and shape distributions along urban-rural gradients, testing for patterns within guilds, across trophic levels, and/or between competitors, to construct a clearer image of the traits and habitat context that led to morphological change with urbanization.

My proposed extensions to this dissertation research share one fundamental requirement: the continued maintenance and growth of natural history collections. The modern museum must continue to serve its traditional research purposes, e.g., proving the physical material needed to study species delineations and relationships, while opening a wealth of possibilities for answering ecological questions. In that regard, a few representatives of each species are not enough, a fact that has gained widespread recognition, as resurvey projects—from single sites to entire states—are on the rise. Even in showcasing only a subset of the potential applications for museum specimens, this dissertation emphasizes that the ongoing documentation of biodiversity (even, and perhaps especially, in places that already seem well explored, including our own backyards) and safeguarding of those data are paramount to understanding our past, present, and future in a changing world. This work is only possible thanks to the countless curators,

collections managers, researchers, and preparators who create and care for these resources and advocate for the critical role of museum in science and society.

REFERENCES

Abrahms B, Carter NH, Clark-Wolf TJ, Gaynor KM, Johansson E, McInturff A, Nisi AC, Rafiq K, West L. 2023. Climate change as a global amplifier of human–wildlife conflict. Nature Climate Change 13(3):224–234. https://doi.org/10.1038/s41558-023-01608-5

Bergmann C. 1847. Über die Verhältnisse der Wärmeökonomie der Thiere zu ihrer Grösse. Göttinger Studien 1:595–708.

Calvin K, Dasgupta D, Krinner G, Mukherji A, Thorne PW, Trisos C, Romero J, Aldunce P, Barrett K, Blanco G *et al.* 2023. IPCC, 2023: Climate Change 2023: Synthesis Report. Contribution of Working Groups I, II and III to the Sixth Assessment Report of the Intergovernmental Panel on Climate Change [Core Writing Team, H. Lee and J. Romero (eds.)]. IPCC, Geneva, Switzerland. First. Arias P, Bustamante M, Elgizouli I, Flato G, Howden M, Méndez-Vallejo C, Pereira JJ, Pichs-Madruga R, Rose SK, Saheb Y, et al., editors. Intergovernmental Panel on Climate Change (IPCC). https://doi.org/10.59327/IPCC/AR6-9789291691647

Cardillo M, Mace GM, Jones KE, Bielby J, Bininda-Emonds ORP, Sechrest W, Orme CDL, Purvis A. 2005. Multiple causes of high extinction risk in large mammal species. Science 309(5738):1239–1241. https://doi.org/10.1126/science.1116030

Cohen JE. 2003. Human Population: The Next Half Century. Science 302(5648):1172–1175. https://doi.org/10.1126/science.1088665

Correll RA, Prowse TAA, Prideaux GJ. 2016. Lean-season primary productivity and heat dissipation as key drivers of geographic body-size variation in a widespread marsupial. Ecography 39(1):77–86. https://doi.org/10.1111/ecog.01243

Cowie RH, Bouchet P, Fontaine B. 2022. The Sixth Mass Extinction: fact, fiction or speculation? Biological Reviews 97(2):640–663. https://doi.org/10.1111/brv.12816

Crutzen PJ, Stoermer EF. 2021. The ‘Anthropocene’ (2000). In: Benner S, Lax G, Crutzen PJ, Pöschl U, Lelieveld J, Brauch HG, editors. *Paul J. Crutzen and the Anthropocene: A New Epoch in Earth’s History*. Vol. 1, The Anthropocene: Politik—Economics—Society—Science. Cham: Springer International Publishing; p. 19–21. https://doi.org/10.1007/978-3-030-82202-6_2

Curtis AA, Orke M, Tetradis S, Van Valkenburgh B. 2018. Diet-related differences in craniodental morphology between captive-reared and wild coyotes, Canis latrans (Carnivora: Canidae). Biological Journal of the Linnean Society 123(3):677–693. https://doi.org/10.1093/biolinnean/blx161

Daufresne M, Lengfellner K, Sommer U. 2009. Global warming benefits the small in aquatic ecosystems. Proceedings of the National Academy of Sciences of the United States of America 106(31):12788–12793. https://doi.org/10.1073/pnas.0902080106

Gardner JL, Peters A, Kearney MR, Joseph L, Heinsohn R. 2011. Declining body size: a third universal response to warming? Trends in Ecology & Evolution 26(6):285–291. https://doi.org/10.1016/j.tree.2011.03.005

Gaynor KM, Hojnowski CE, Carter NH, Brashares JS. 2018. The influence of human disturbance on wildlife nocturnality. Science 360(6394):1232–1235. https://doi.org/10.1126/science.aar7121

Gilbert NA, McGinn KA, Nunes LA, Shipley AA, Bernath-Plaisted J, Clare JDJ, Murphy PW, Keyser SR, Thompson KL, Maresh Nelson SB *et al.* 2023. Daily activity timing in the Anthropocene. Trends in Ecology & Evolution 38(4):324–336. https://doi.org/10.1016/j.tree.2022.10.008

Guralnick R, Hantak MM, Li D, McLean BS. 2020. Body size trends in response to climate and urbanization in the widespread North American deer mouse, *Peromyscus maniculatus*. Scientific Reports 10(1):8882. https://doi.org/10.1038/s41598-020-65755-x

Habibullah MS, Din BH, Tan S-H, Zahid H. 2022. Impact of climate change on biodiversity loss: global evidence. Environmental Science and Pollution Research 29(1):1073–1086. https://doi.org/10.1007/s11356-021-15702-8

Hantak MM, McLean BS, Li D, Guralnick RP. 2021. Mammalian body size is determined by interactions between climate, urbanization, and ecological traits. Communications Biology 4(1). https://doi.org/10.1038/s42003-021-02505-3

Hays GC, Rusli MU, Booth D, Laloë J. 2025. Global decline in the size of sea turtles. Global Change Biology 31(5):e70225. https://doi.org/10.1111/gcb.70225

Huston MA, Wolverton S. 2011. Regulation of animal size by eNPP, Bergmann's rule, and related phenomena. Ecological Monographs 81(3):349–405. https://doi.org/10.1890/10-1523.1

Jantz SM, Barker B, Brooks TM, Chini LP, Huang Q, Moore RM, Noel J, Hurtt GC. 2015. Future habitat loss and extinctions driven by land-use change in biodiversity hotspots under four scenarios of climate-change mitigation. Conservation Biology 29(4):1122–1131. https://doi.org/10.1111/cobi.12549

Jirinec V, Burner RC, Amaral BR, Bierregaard RO, Fernández-Arellano G, Hernández-Palma A, Johnson EI, Lovejoy TE, Powell LL, Rutt CL *et al.* 2021. Morphological consequences of climate change for resident birds in intact Amazonian rainforest. Science Advances 7(46):eabk1743. https://doi.org/10.1126/sciadv.abk1743

Kaspari M, Welti EAR. 2024. Nutrient dilution and the future of herbivore populations. Trends in Ecology & Evolution 39(9):809–820. https://doi.org/10.1016/j.tree.2024.05.001

Keesing F, Belden LK, Daszak P, Dobson A, Harvell CD, Holt RD, Hudson P, Jolles A, Jones KE, Mitchell CE *et al.* 2010. Impacts of biodiversity on the emergence and transmission of infectious diseases. Nature 468(7324):647–652. https://doi.org/10.1038/nature09575

Kruuk LEB. 2017. A new explanation for unexpected evolution in body size. PLOS Biology 15(2):e2001832. https://doi.org/10.1371/journal.pbio.2001832

LeBauer DS, Treseder KK. 2008. Nitrogen limitation of net primary productivity in terrestrial ecosystems is globally distributed. Ecology 89(2):371–379. https://doi.org/10.1890/06-2057.1

Lendemer J, Thiers B, Monfils AK, Zaspel J, Ellwood ER, Bentley A, LeVan K, Bates J, Jennings D, Contreras D *et al.* 2020. The extended specimen network: A strategy to enhance US biodiversity collections, promote research and education. BioScience 70(1):23–30. https://doi.org/10.1093/biosci/biz140

Lewis SL, Maslin MA. 2015. Defining the Anthropocene. Nature 519(7542):171–180. https://doi.org/10.1038/nature14258

Linderholm HW. 2006. Growing season changes in the last century. Agricultural and Forest Meteorology 137(1–2):1–14. https://doi.org/10.1016/j.agrformet.2006.03.006

Liow LH, Fortelius M, Lintulaakso K, Mannila H, Stenseth NChr. 2009. Lower extinction risk in sleep-or-hide mammals. The American Naturalist 173(2):264–272. https://doi.org/10.1086/595756

Lomolino MV, Perault DR. 2007. Body size variation of mammals in a fragmented, temperate rainforest. Conservation Biology 21(4):1059–1069. https://doi.org/10.1111/j.1523-1739.2007.00727.x

Ma D, Abrahms B, Allgeier J, Newbold T, Weeks BC, Carter NH. 2024. Global expansion of human-wildlife overlap in the 21st century. Science Advances 10(34):eadp7706. https://doi.org/10.1126/sciadv.adp7706

MacLean SA, Beissinger SR. 2017. Species' traits as predictors of range shifts under contemporary climate change: A review and meta-analysis. Global Change Biology 23(10):4094–4105. https://doi.org/10.1111/gcb.13736

Manishin KA, Cunningham CJ, Westley PAH, Seitz AC. 2021. Can late stage marine mortality explain observed shifts in age structure of Chinook salmon? PLOS ONE 16(2):e0247370. https://doi.org/10.1371/journal.pone.0247370

McCain CM, King SRB. 2014. Body size and activity times mediate mammalian responses to climate change. Global Change Biology 20(6):1760–1769. https://doi.org/10.1111/gcb.12499

McNab BK. 1971. On the ecological significance of Bergmann's rule. Ecology 52(5):845–854. https://doi.org/10.2307/1936032

McNab BK. 2010. Geographic and temporal correlations of mammalian size reconsidered: a resource rule. Oecologia 164(1):13–23. https://doi.org/10.1007/s00442-010-1621-5

Meiri S, Guy D, Dayan T, Simberloff D. 2009. Global change and carnivore body size: data are stasis. Global Ecology and Biogeography 18(2):240–247. https://doi.org/10.1111/j.1466-8238.2008.00437.x

Nakahama N. 2021. Museum specimens: An overlooked and valuable material for conservation genetics. Ecological Research 36(1):13–23. https://doi.org/10.1111/1440-1703.12181

Names GR, Grindstaff JL, Westneat DF, Heidinger BJ. 2024. Climate change and its effects on body size and shape: the role of endocrine mechanisms. Philosophical Transactions of the

Royal Society B: Biological Sciences 379(1898):20220509. https://doi.org/10.1098/rstb.2022.0509

Oke KB, Cunningham CJ, Westley PAH, Baskett ML, Carlson SM, Clark J, Hendry AP, Karatayev VA, Kendall NW, Kibele J *et al.* 2020. Recent declines in salmon body size impact ecosystems and fisheries. Nature Communications 11(1):4155. https://doi.org/10.1038/s41467-020-17726-z

Paniw M, James TD, Ruth Archer C, Römer G, Levin S, Compagnoni A, Che-Castaldo J, Bennett JM, Mooney A, Childs DZ *et al.* 2021. The myriad of complex demographic responses of terrestrial mammals to climate change and gaps of knowledge: A global analysis. Journal of Animal Ecology 90(6):1398–1407. https://doi.org/10.1111/1365-2656.13467

Paniw M, Maag N, Cozzi G, Clutton-Brock T, Ozgul A. 2019. Life history responses of meerkats to seasonal changes in extreme environments. Science 363(6427):631–635. https://doi.org/10.1126/science.aau5905

Parmesan C. 2006. Ecological and evolutionary responses to recent climate change. Annual Review of Ecology, Evolution, and Systematics 37(1):637–669. https://doi.org/10.1146/annurev.ecolsys.37.091305.110100

Pauli JN, Zuckerberg B, Whiteman JP, Porter W. 2013. The subnivium: a deteriorating seasonal refugium. Frontiers in Ecology and the Environment 11(5):260–267. https://doi.org/10.1890/120222

Peters RH. 1983. The ecological implications of body size. Cambridge, UK: Cambridge University Press.

Rodriguez-Dominguez A, Connell SD, Leung JYS, Nagelkerken I. 2019. Adaptive responses of fishes to climate change: Feedback between physiology and behaviour. Science of The Total Environment 692:1242–1249. https://doi.org/10.1016/j.scitotenv.2019.07.226

Rouyer T, Sadykov A, Ohlberger J, Stenseth NChr. 2012. Does increasing mortality change the response of fish populations to environmental fluctuations? Ecology Letters 15(7):658–665. https://doi.org/10.1111/j.1461-0248.2012.01781.x

Sanders NJ, Cooper N, Davis Rabosky AR, Gibson DJ. 2023. Leveraging natural history collections to understand the impacts of global change. Journal of Animal Ecology 92(2):232–236. https://doi.org/10.1111/1365-2656.13882

Scheele BC, Hunter DA, Banks SC, Pierson JC, Skerratt LF, Webb R, Driscoll DA. 2016. High adult mortality in disease-challenged frog populations increases vulnerability to drought. Journal of Animal Ecology 85(6):1453–1460. https://doi.org/10.1111/1365-2656.12569

Schmidt NM, Jensen PM. 2003. Changes in mammalian body length over 175 years—adaptations to a fragmented landscape? Conservation Ecology 7(2):6. https://doi.org/10.5751/ES-00520-070206

Schmidt NM, Jensen PM. 2005. Concomitant patterns in avian and mammalian body length changes in Denmark. Ecology and Society 10(2):5. https://doi.org/10.5751/ES-01372-100205

Sepp T, McGraw KJ, Kaasik A, Giraudeau M. 2018. A review of urban impacts on avian life-history evolution: Does city living lead to slower pace of life? Global Change Biology 24(4):1452–1469. https://doi.org/10.1111/gcb.13969

Teplitsky C, Mills JA, Alho JS, Yarrall JW, Merilä J. 2008. Bergmann's rule and climate change revisited: Disentangling environmental and genetic responses in a wild bird population. Proceedings of the National Academy of Sciences of the United States of America 105(36):13492–13496. https://doi.org/10.1073/pnas.0800999105

Ter Haar SF, Van Bodegom PM, Scherer L. 2025. CO_2 Rise Directly Impairs Crop Nutritional Quality. Global Change Biology 31(11):e70568. https://doi.org/10.1111/gcb.70568

Thackeray SJ, Henrys PA, Hemming D, Bell JR, Botham MS, Burthe S, Helaouet P, Johns DG, Jones ID, Leech DI *et al.* 2016. Phenological sensitivity to climate across taxa and trophic levels. Nature 535(7611):241–245. https://doi.org/10.1038/nature18608

Theriot MK, Olson LE, Lanier HC. 2024. Accounting for age: uncovering the nuanced drivers of mammal body-size responses to climate change. Journal of Mammalogy 105(3):512–523. https://doi.org/10.1093/jmammal/gyae005

Thomas CD, Cameron A, Green RE, Bakkenes M, Beaumont LJ, Collingham YC, Erasmus BFN, de Siqueira MF, Grainger A, Hannah L *et al.* 2004. Extinction risk from climate change. Nature 427:145–148.

Urban MC. 2015. Accelerating extinction risk from climate change. Science 348(6234):571–573. https://doi.org/10.1126/science.aaa4984

Van Vliet J. 2019. Direct and indirect loss of natural area from urban expansion. Nature Sustainability 2(8):755–763. https://doi.org/10.1038/s41893-019-0340-0

Vitousek PM, Aber JD, Howarth RW, Likens GE, Matson PA, Schindler DW, Schlesinger WH, Tilman DG. 1997. Human alterations of the global nitrogen cycle: Sources and consequences. Ecological Applications 7(3):737–750. https://doi.org/10.1890/1051-0761(1997)007%255B0737:HAOTGN%255D2.0.CO;2

Watt C, Mitchell S, Salewski V. 2010. Bergmann's rule; a concept cluster? Oikos 119(1):89–100. https://doi.org/10.1111/j.1600-0706.2009.17959.x

Webster MS. 2017. The extended specimen. In: Webster MS, editor. *The extended specimen: emerging frontiers in collections-based ornithological research*. Studies in Avian Biology. Boca Raton, FL: CRC Press; p. 1–9.

Welti EAR, Roeder KA, de Beurs KM, Joern A, Kaspari M. 2020. Nutrient dilution and climate cycles underlie declines in a dominant insect herbivore. Proceedings of the National Academy of Sciences 117(13):7271–7275. https://doi.org/10.1073/pnas.1920012117

Williams CM, Henry HAL, Sinclair BJ. 2015. Cold truths: how winter drives responses of terrestrial organisms to climate change. Biological Reviews 90(1):214–235. https://doi.org/10.1111/brv.12105